

Journal of Materials Chemistry A

Materials for energy and sustainability

Accepted Manuscript

This article can be cited before page numbers have been issued, to do this please use: F. Sher, A. Hayward, A. El Guerraf, I. Ziani, H. Hrnji, E. Boškailo, B. Wang, A. Chupin and M. R. Nemanu, *J. Mater. Chem. A*, 2024, DOI: 10.1039/D4TA03877K.



This is an Accepted Manuscript, which has been through the Royal Society of Chemistry peer review process and has been accepted for publication.

Accepted Manuscripts are published online shortly after acceptance, before technical editing, formatting and proof reading. Using this free service, authors can make their results available to the community, in citable form, before we publish the edited article. We will replace this Accepted Manuscript with the edited and formatted Advance Article as soon as it is available.

You can find more information about Accepted Manuscripts in the [Information for Authors](#).

Please note that technical editing may introduce minor changes to the text and/or graphics, which may alter content. The journal's standard [Terms & Conditions](#) and the [Ethical guidelines](#) still apply. In no event shall the Royal Society of Chemistry be held responsible for any errors or omissions in this Accepted Manuscript or any consequences arising from the use of any information it contains.

Advanced metal-organic frameworks for superior carbon capture, high-performance energy storage and environmental photocatalysis – A critical review

Farooq Sher^{1,*}, Anna Hayward², Abdelqader El Guerraf^{3,4}, Bohong Wang⁵, Imane Ziani^{4,6},

Harun Hrnjić^{4,7}, Emina Boškailo^{4,7}, Alexander Chupin⁸, Monica R. Nemțanu⁹

¹*Department of Engineering, School of Science and Technology, Nottingham Trent University,
Nottingham NG11 8NS, United Kingdom*

²*School of Mechanical, Aerospace and Automotive Engineering, Coventry University, Coventry
CV1 5FB, United Kingdom*

³*Laboratory of Applied Chemistry and Environment, Faculty of Sciences and Technologies,
Hassan First University, Settat 26002, Morocco*

⁴*International Society of Engineering Science and Technology, Nottingham, United Kingdom*

⁵*National and Local Joint Engineering Research Center of Harbor Oil and Gas Storage and
Transportation Technology, Zhejiang Key Laboratory of Petrochemical Environmental
Pollution Control, Zhejiang Ocean University, No. 1 Haida South Road, 316022, Zhoushan,
P.R. China*

⁶*Physical Chemistry of Natural Substances and Process Research Team, Laboratory of Applied
Chemistry and Environment (LCAE-CPSUNAP), Faculty of Sciences, Mohammed Ist
University, Oujda 60000, Morocco*

⁷*Department of Chemistry, Faculty of Science, University of Sarajevo, Sarajevo 71000, Bosnia
and Herzegovina*

⁸*Peoples' Friendship University of Russia (RUDN University), Moscow 117198, Russia*

⁹*Electron Accelerators Laboratory, National Institute for Laser, Plasma and Radiation Physics,
409 Atomistilor Street, Bucharest-Măgurele, Romania*

*Corresponding author:

Dr. F. Sher

Assistant Professor

Department of Engineering, School of Science and Technology
Nottingham Trent University

Nottingham

NG11 8NS

UK

E-mail address: Farooq.Sher@ntu.ac.uk

Tel.: +44 (0) 115 84 86679



38	Contents	
		View Article Online DOI: 10.1039/D4TA03877K
39	Abstract	3
40	1. Introduction	4
41	2. Porous MOF and conventional materials for carbon capture	10
42	2.1 Conventional liquid alkanolamine in carbon capture	10
43	2.2 Metal organic frameworks in carbon capture	16
44	2.2.1 Performance and challenges	16
45	2.2.2 Manufacturability, stability and cost.....	23
46	3. Energy storage devices	29
47	3.1 Porous carbonaceous materials for supercapacitors	32
48	3.1.1 Performance and properties	33
49	3.1.2 Environmental impact.....	38
50	3.1.3 Recent developments in AC electrodes	40
51	3.2 Metal organic frameworks as supercapacitors.....	42
52	3.2.1 Pristine MOFs and their composites.....	44
53	3.2.2 Nanocrystalline MOFs.....	50
54	3.2.3 Environmental impacts	52
55	3.3 Metal-organic frameworks for battery technologies.....	55
56	3.4 MOF metal nodes, ligand architecture, and synthesis strategies	58
57	4. Photocatalysis	62
58	4.1 Conventional photocatalytic materials.....	62
59	4.2 Metal organic frameworks as photocatalysts.....	70
60	5. Evaluation and comparison	76
61	5.1 Carbon capture	78
62	5.2 Photocatalysis	83
63	5.3 Supercapacitors.....	86
64	6. Limitations and future research directions	91
65	6.1 Limitations of current MOF technologies.....	91
66	6.2 Future research directions.....	93
67	7. Conclusion.....	95
68	Acknowledgement	97
69	Reference	98
70		
71		



72 **Abstract**

73 Metal-organic frameworks (MOFs) have emerged as a transformative class of materials,
74 offering unprecedented versatility in applications ranging from energy storage to environmental
75 remediation and photocatalysis. This groundbreaking review navigates the recent
76 advancements in MOFs, positioning them against traditional materials to underscore their
77 unique strength and potential drawbacks. In the context of energy storage, particularly within
78 the realm of supercapacitors (SCs), MOF-based electrodes are evaluated for their superior
79 specific capacitance (exceeding 1000 F/g), although these benefits are tempered by higher
80 production cost. A comparative analysis with conventional activated carbon (AC) electrodes
81 reveals MOFs' enhanced performance but also highlights cost as a significant barrier to
82 widespread adoption. In carbon capture and storage (CCS), MOFs are contrasted with
83 established liquid-amine technologies, with MOFs demonstrating environmental benefits,
84 including the ability to achieve high-purity CO₂ collection (>99%), despite higher expenses.
85 Similarly, in photocatalysis, while titanium dioxide remains dominant, MOFs are shown to
86 offer competitive performance with a reduced environmental footprint, though cost
87 considerations again play a decisive role. This review not only consolidates the current state of
88 MOF research but also identifies critical gaps, particularly in cost-effectiveness, that must be
89 addressed to enable broader application. The findings advocate for continued innovation in
90 MOF synthesis and production, with an emphasis on achieving a balance between performance
91 and affordability. In summary, this review highlights the pivotal role of MOFs in advancing
92 material science and underscores the need for holistic approaches in material selection, with a
93 forward-looking perspective on sustainable and economical production methods.

94
95 **Keywords:** Metal-organic frameworks; Activated carbon; Energy storage; Environmental
96 remediation; Carbon capture and Photocatalysis.



97 1. Introduction

View Article Online
DOI: 10.1039/D4TA03877K

98 The dawn of the 21st century marked the emergence of metal-organic frameworks (MOFs);
99 porous structures consisting of metal ions and organic linkers. Prior to MOFs, zeolites
100 (aluminium silicate crystals) were the world's most porous materials ¹. However, MOFs have
101 overcome zeolites' surface area by more than 100% in some cases. In addition to that, the
102 structure of the cavities and the size of the pore in MOFs can be tailored as a function of metal
103 ions, organic ligands, and synthesis conditions, and hence are thus amenable to engineering for
104 targeted applications ², which catalyses exponential growth in research on their applications ³.
105 Due to their unique architectures and chemical or physicochemical properties, MOFs remain in
106 a class apart, with a wide reach of applications. Metal-containing nodes (SBUs) and organic
107 linkers are used to create very porous structures, which typically have surface areas greater than
108 7000 m²/g ⁴. Control over topology, dimensionality, and stability can be achieved by selecting
109 the right metal centers and organic ligands. For example, functional groups high in nitrogen can
110 enhance CO₂ absorption; certain MOFs can attain up to 40 cc/g ⁵.

111
112 On the other hand, sensitivity to humidity and thermal instability create practical problems, as
113 illustrated by ZIF-8, which swells at low pressure but phase transitions at higher pressures ⁶.
114 Synthesis conditions and metal-organic coordination bonds are key to the chemical stability and
115 reactivity of MOFs; high-throughput computational screenings have identified MOFs with high
116 gas adsorption capacities, such as methane storage up to 200 cm³/cm³ ⁴. However, theoretical
117 predictions do not often match real-world performance, suggesting that somehow models and
118 real applications are detached from one another. It typically focuses on crystallinity and leaves
119 out the other forms, such as amorphous or semi-crystalline forms, which might also hold special
120 properties ⁷. All this proves that there is a need to develop better characterization techniques
121 and insight into structure-function interplay to further advance the application of MOFs in



122 carbon capture, energy storage, and environmental remediation. The historical development of
123 MOFs shows the huge progress made in material science from exclusively inorganic or organic
124 structures to hybrid systems possessing new properties ⁸. The necessity of material that shows
125 high porosity but custom architecture of the material developed during the late twentieth
126 century marked the starting point for the development of MOF ⁹. Early studies, and mostly
127 those related to Prussian blue analogues, were the basis for the fast-growing interest in MOF
128 research in the late 1980s ¹⁰. The "node-and-spacer" approach, proposed by Richard Robson,
129 enabled design of frameworks with well-defined coordination geometries and complex
130 structures. MOFs, like HKUST-1 and MOF-5, developed in the late 1990s and early 2000s,
131 represent advances in synthesizing large surface area materials that have high porosity and good
132 crystallinity ¹¹.

133
134 In response to escalating energy demands and intensifying environmental challenges, the
135 development of advanced materials has become increasingly critical ¹². MOFs have emerged as
136 a highly versatile class of materials, offering exceptional properties that hold the potential to
137 revolutionize energy storage, environmental remediation, and photocatalysis ¹³. As the global
138 population continues to grow and conventional energy sources dwindle, innovative approaches
139 to sustainable energy generation and environmental restoration are urgently needed. MOFs
140 present a promising solution due to their structural flexibility, large surface area, and tunable
141 properties. Energy storage, environmental remediation, and photocatalysis are key areas where
142 advanced materials have the potential to drive transformative change. Traditional materials,
143 such as metals, semiconductors, and polymers have historically played significant roles in these
144 applications. However, these materials often face in efficiency, stability, and versatility. MOFs,
145 with their exceptional characteristics, offer a promising alternative that could overcome these
146 limitations. While MOFs are very promising, there are several serious technological problems



147 to be overcome. Their structural stability is the first and foremost problem. Such interactions of
148 the proton and metal ion can result in degradation, and therefore most MOFs cannot be used
149 for an extended period of time in these environments ¹⁴. Improvement of stability includes high-
150 valent metal ions and proper organic linkers, which generally decrease the diversity of possible
151 MOFs. On the other hand, most MOFs require comparatively high temperature and pressure for
152 synthesis and, therefore, are energy-consuming and expensive. In this regard, the search for
153 alternative synthesis techniques, including the solvothermal and microwave methods, or
154 recently mechanochemical methods, assumes the leading role among researchers to decrease
155 the price of synthesis and increase scalability ¹⁵.

156
157 Moreover, their generally low electrical conductivity limits the broad use of MOFs in
158 electrochemical applications. Strategies to enhance conductivity include embedding conductive
159 material carbon-based compounds or using highly conjugated organic linkers; however, these
160 add complexity and are more expensive to synthesize. For example, the MOF derivatives, such
161 as TMCs, have been designed to enhance conductivity and improve structural stability ¹⁶. One
162 such example of improvement is the hybrid ZnS/MXene, which was reported to demonstrate
163 improved electron transfer and ion adsorption capabilities due to uniform anchoring of ZnS
164 nanodots onto the MXene nanosheets. The incorporation of a few metals into one MOF
165 structure has also shown some bright prospects in enhancing electrochemical performance but
166 adds more complications in terms of synthesis and scalability. For instance, sequential chemical
167 etching and sulfurization in the preparation of Zn-Co-S rhombic dodecahedral cages showed
168 enhanced specific capacitance because they hold a double-shelled structure ¹⁷. Environmental
169 degradation stands as one of the foremost challenges of the 21st century. Increased awareness
170 of global warming, coupled with concerted efforts by governments and societies, is driving
171 research into environmental pollution mitigation. The United Nations has specified a series of



172 sustainable development goals, showcasing this assertion ¹⁸. Recent research suggests that
173 MOFs demonstrate tremendous potential in capturing and detoxifying environmental toxins
174 across various media, such as water, air, and soil ¹⁹. The increasing concentration of
175 atmospheric CO₂, primarily driven by the combustion of fossil fuels since the industrial
176 revolution, has been a major contributor to anthropogenic global warming ¹⁸. The atmospheric
177 concentration of CO₂ has increased from 280 ppm in 1962 to 400 ppm in 2015 ²⁰, a concerning
178 trend due to its links to global warming and associated environmental degradation, as well as
179 potential adverse health effects ¹⁹. MOFs have shown significant potential in this regard,
180 particularly in carbon capture and storage (CCS) technologies. Their ability to selectively
181 adsorb CO₂ from the atmosphere makes them a viable candidate for reducing greenhouse gas
182 emissions ²¹.

183
184 In the realm of energy storage, MOFs' are being explored for their application in both
185 supercapacitors (SCs) and metal-ion batteries. MOFs can serve two main roles in these energy
186 storage devices: Primarily, they can function as direct electrode materials with modifiable
187 particle and pore dimensions. Secondly, they can serve as templates and precursors for
188 producing porous carbons and metal oxides. The resulting porous carbons and metal oxides
189 maintain the extensive surface area and highly porous structure of the MOF precursors, making
190 them ideal for implementation in electrical double-layer supercapacitors (EDLCs) and
191 pseudocapacitors ²². Moreover, MOFs have garnered attention in photocatalysis owing to their
192 distinctive properties. Photocatalysis entails harnessing light energy to propel chemical
193 reactions ²³, and MOFs' extensive surface area and porosity provide numerous active sites for
194 catalytic reactions. Researchers have incorporated various photocatalytic components, such as
195 metal nanoparticles or organic dyes, into MOF structures to enhance their photocatalytic
196 performance. MOFs can serve as photocatalysts themselves or as platforms to support other



197 catalytic materials. The tunable nature of MOFs allows researchers to modify their electronic
198 and optical properties, influencing their efficiency in light absorption and charge separation
199 critical factors in photocatalytic processes.

200

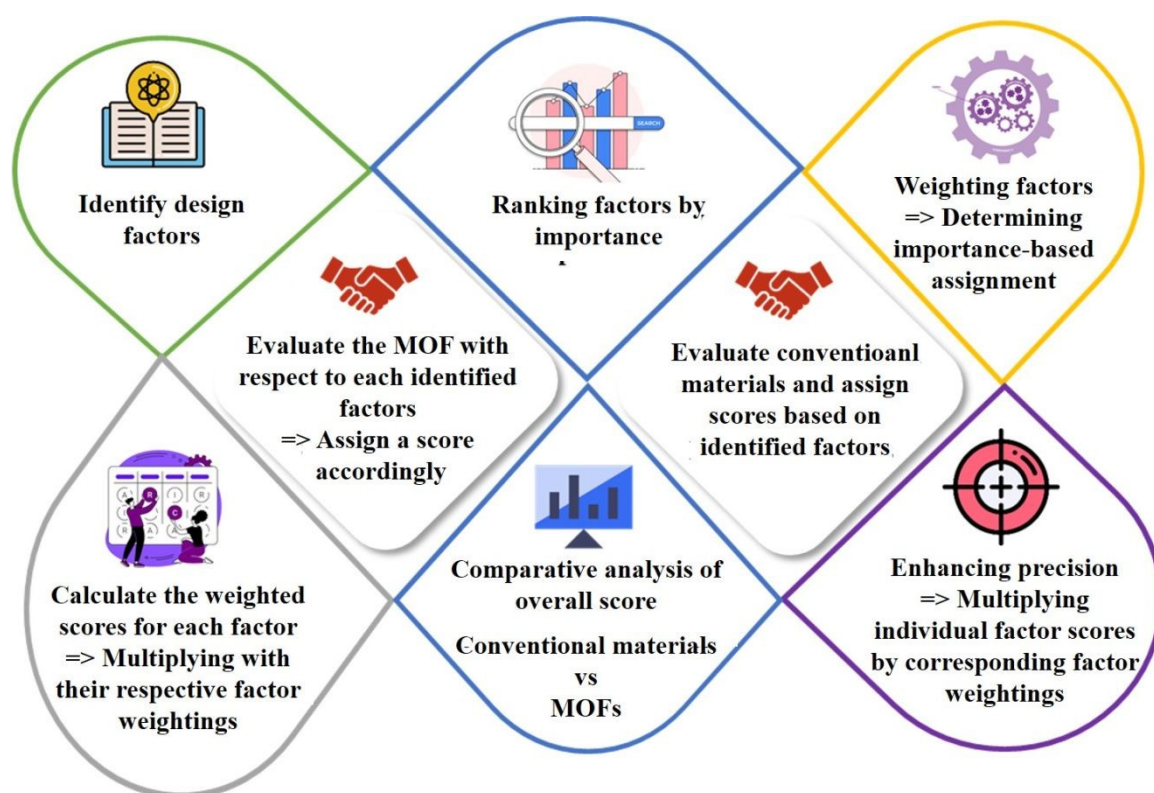
201 In this comprehensive and groundbreaking review, the report embarks on a pioneering journey
202 to assess the comparative advantages of MOFs over conventional materials. Delving into the
203 realm of energy storage, it investigates how MOFs can potentially revolutionize energy storage
204 technologies, including supercapacitors and metal-ion batteries, due to their exceptionally high
205 surface area, tunable electronic properties, and facile ion diffusion pathways. This new
206 approach to energy storage could enable previously unattainable levels of efficiency and
207 performance to be achieved. In the context of environmental challenges, the exploration focuses
208 on a remarkable novelty, namely the way MOFs display an unprecedented affinity for carbon
209 dioxide capture. This discovery offers a compelling and revolutionary alternative to
210 conventional adsorbents, with the potential to significantly mitigate greenhouse gas emissions.
211 Furthermore, in the domain of photocatalysis, MOFs have showcased a transformative capacity
212 to harness solar energy for driving chemical reactions with unmatched efficiency, representing
213 a major leap forward in sustainable energy conversion technologies.

214

215 This review tackles these issues by providing an in-depth analysis of case studies, experimental
216 results, and theoretical insights to illuminate the merits and limitations of MOFs compared to
217 conventional materials across three key applications: energy storage, carbon capture, and
218 photocatalysis. Tables summarizing the advantages and disadvantages of both conventional and
219 MOF materials are presented for each application, with a focus on performance, environmental
220 impact, and cost-effectiveness. Each broad factor receives a relative percentage weighting
221 based on importance, with the most critical factor assigned the highest percentage. Sub-factors



222 within each category are also identified based on the literature, assigning them scores out of 3
 223 (3 correlating to high importance). After determining the weightings, both materials are
 224 evaluated using a comparison matrix for each factor, using a scale of 1 to 5 (1 very bad, 2 bad,
 225 3 suitable, 4 good, and 5 very good). The resulting scores allow a comparison of MOFs and
 226 conventional materials for each of the three applications, helping identify which material offers
 227 the most benefits based on the identified factors. Such a systematic approach will ensure that
 228 all aspects are covered and that clear, actionable insights into practical benefits of MOFs in
 229 addressing technological challenges in energy storage, carbon capture, and photocatalysis are
 230 delivered. **Fig. 1** summarizes the methodology followed throughout this groundbreaking
 231 literature review.



232
 233 **Fig. 1.** Diagram explaining the adopted methodology for the present literature review. A
 234 systematic comparison matrix is employed to assess the relative benefits of MOFs, offering
 235 clear, actionable insights into their potential as a transformative material in critical fields.



236 **2. Porous MOF and conventional materials for carbon capture**

View Article Online

DOI: 10.1039/D4TA03877K

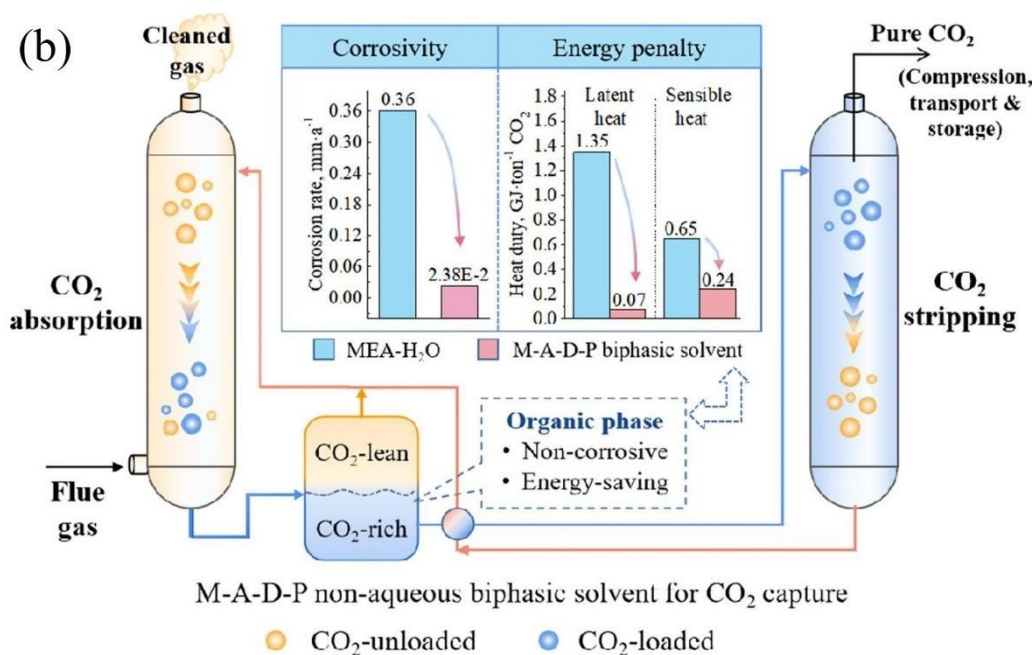
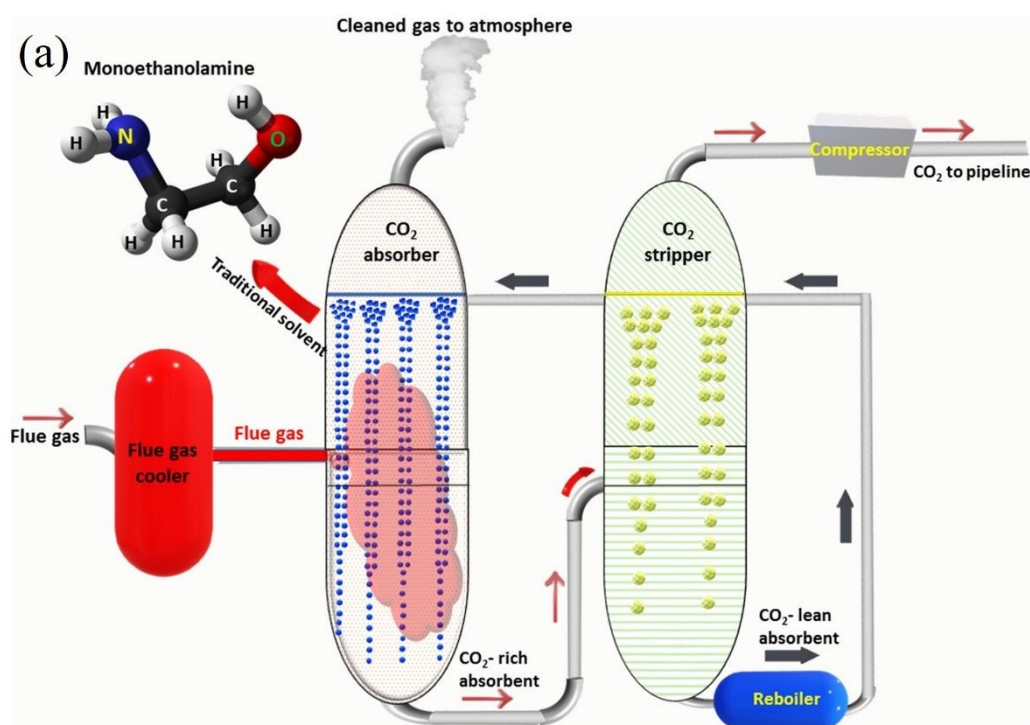
237 The argument presented by Mukherjee et al.¹⁸ emphasizes humanity's reliance on gas as a
238 critical component of energy and industrial processes. They contend that liquid fuels and
239 feedstocks in the chemical industry have been largely replaced by gases. However, this
240 viewpoint is challenged by the research conducted by Furukawa et al.²⁴ which shows a steady
241 increase in all fossil fuels, both sources agree on the general trend of increasing CO₂ levels and
242 their contribution to global warming and consequential environmental degradation. A sorbent's
243 CO₂ selectivity is determined by comparing how much CO₂ it can absorb to another gas while
244 meeting certain predetermined parameters¹⁸. In the examination of a sorbent employed for
245 post-combustion carbon capture, selectivity versus nitrogen (SCN) holds significant relevance.
246 Selectivity is crucial as it impacts both the purity of the captured CO₂ and the concentration of
247 CO₂ in the effluent gas discharged into the atmosphere. Mukherjee and colleagues¹⁸ also
248 suggest that increasing the SCN of a sorbent by five-fold could significantly reduce the cost of
249 C-capture. Other important factors that influence sorbent selection for C-capture include
250 stability, working capacity, regenerability and feasibility of scale-up.

251 **2.1 Conventional liquid alkanolamine in carbon capture**

252 For over half a century, liquid amine technology has remained at the forefront of carbon capture
253 and storage (CCS) technologies¹⁸. This method of bulk-scale carbon capture operates through
254 chemisorption, involving chemical reactions between CO₂ and the sorbent material. Originating
255 in the 1930s, these processes were initially developed, and since the 1950s, they have been
256 employed by gas-treating plants for the removal of acid gases like CO₂ and H₂S
257^{19,25} Consequently, liquid amine processes are frequently recognized as the most mature CCS
258 method and boast a high Technology Readiness Level (TRL) of 9^{25,26}. In two commercial-scale
259 facilities housed within coal-fired power plants, post-combustion liquid amine CCS technology
260 had been successfully installed as of 2018²⁶. The post-combustion liquid-amine CCS process



261 (Fig. 2(a)) involves exposing the flue gas stream to an aqueous amine solution, commonly a
 262 member of the alkanolamine class, typically a 20–30 wt% aqueous monoethanolamine (MEA)
 263 ²⁷. Subsequently, the amine undergoes a reaction with CO₂ in the flue gases, resulting in the
 264 formation of carbamates or bicarbonate products, which can then be separated and removed.
 265 The utilization of liquid amines is based on their capacity to achieve significant levels of
 266 purification and separation through the chemisorption process ¹⁸.



267



268 **Fig. 2.** (a) Post-combustion technology involves cooling hot flue gas before directing it to an
269 absorber unit that typically contains a monoethanolamine solvent as the traditional sorbent. The
270 CO₂-rich absorbent is then sent to a stripper unit to release the CO₂ gas, while the CO₂-lean
271 absorbent is recycled back to the absorber unit. Finally, the pure CO₂ is compressed and
272 dehydrated for transport via pipelines and for storage purposes. Adopted from Ref. ²⁸ with
273 permission. (b) A schematic illustration of a reactor containing a nonaqueous
274 monoethanolamine-based biphasic solvent for reduced energy penalty and corrosion of carbon
275 dioxide capture. Adopted from Ref. ²⁹ with permission.

276

277 Monoethanolamine (MEA) offers several advantages, such as a substantial CO₂-carrying
278 capacity, biodegradability, and rapid adsorption rates ^{26,27}. Additionally, it is well-suited for
279 carbon capture applications with low CO₂ partial pressures. Because of this, MEA has become
280 the industry standard for carbon capture amines despite having modest degrees of toxicity and
281 oxidative and thermal degradation ²⁶. In the context of standard post-combustion flue gas CO₂
282 separation, employing a 30 wt% MEA solution at pressures ranging from 10–15 kPa, a
283 temperature of 40 °C, and targeting a 90% CO₂ removal rate, it is typically estimated that a
284 reboiler would necessitate approximately 3.6–4.0 GJ per tonne of captured CO₂ ²⁶. This value
285 has been verified by a number of small- and medium-sized pilot studies ³⁰. While it's important
286 to acknowledge that reducing reboiler energy is just one of several performance considerations,
287 it is often regarded as a primary focus in the realm of chemical sorbent research. Liquid amines
288 offer a notable advantage for CCS due to their often-high selectivity. Liquid amine CCS
289 technology does have several disadvantages, though. Chemisorbents form strong covalent
290 connections, in contrast to physisorbents, which work through van der Waals interactions ¹⁸.
291 Consequently, the regeneration of sorbents in the case of chemisorbents demands more energy,
292 resulting in a larger energy footprint. Furthermore, in situations with low CO₂ concentrations,
293 the kinetics of the chemisorption process are likely to be sluggish, which is less than ideal for
294 CCS.

295



296 In a study conducted by Li et al.²⁹, a novel approach to advance CO₂ capture technology aims
297 to reduce energy penalties and mitigate equipment corrosion simultaneously (**Fig. 2(b)**). A new
298 biphasic solvent system was developed for carbon dioxide (CO₂) capture, comprising
299 monoethanolamine (MEA), 2-amino-2-methyl-1-propanol (AMP), dimethyl sulfoxide
300 (DMSO), and N,N,N',N'',N'''-pentamethyldiethylenetriamine (PMDETA). Performance
301 evaluation revealed that the optimized solvent achieved a high CO₂ loading of 0.88 mol/mol,
302 with 95.3% of absorbed CO₂ stored in the rich phase, occupying only 56.8% of the total volume.
303 Both MEA and AMP could absorb CO₂ to generate mostly carbamic acid species, according to
304 ¹³C nuclear magnetic resonance (NMR) studies and quantum chemical calculations. Sufficient
305 mutual solubility was guaranteed by hydrogen bonding with the polar DMSO. Only the CO₂-
306 rich phase needed to regenerate since the less polar PMDETA remained isolated and caused
307 phase separation. The M-A-D-P biphasic solvent dramatically reduced sensible heat and
308 vaporisation heat by 63.1% and 94.8%, respectively, when compared to the MEA benchmark.
309 Corrosion tests demonstrated that M-A-D-P exhibited virtually no corrosion to carbon steel,
310 outperforming the MEA solution. Although liquid-amine technologies have proven effective as
311 "wet scrubbers", their industrial-scale deployment has been hindered by several drawbacks.
312 Grande et al.³¹, in their report, emphasize the need to advance CCS technology beyond liquid
313 amine approaches to ensure sustainability, primarily due to the substantial regeneration energy
314 requirements associated with liquid amine-based wet scrubbers, which can exceed 140 °C. The
315 increased energy requirements result from the high stability of the carbamate/bicarbonate
316 species generated during the amine-CO₂ reaction³². It is worth noting that the energy required
317 to reverse an amine-CO₂ reaction varies depending on the specific amine used. Ghosh et al.¹⁹
318 elucidate that this discrepancy is a consequence of bicarbonates demanding less energy
319 compared to carbamates when regenerating the constituent amine.

320



321 Various additional drawbacks associated with liquid-amine technologies have been also
322 highlighted³¹. Equipment requirements pose limitations as it is prone to corrosion over time,
323 and retrofitting can prove challenging due to its substantial size. This perspective is
324 substantiated by Vega et al.²⁵, who propose a potential solution to mitigate equipment corrosion
325 through the use of corrosion-resistant materials and inhibitors, albeit at an added cost. Vericella
326 et al.²⁷ suggest an alternative approach by proposing the microencapsulation of the amine. This
327 approach seeks to avoid direct contact between the amine and the equipment, as well as effluent
328 gases, potentially mitigating equipment corrosion and decreasing evaporative losses. Moreover,
329 it has been reported by several sources that liquid amines are susceptible to deterioration and
330 breakdown when they come into contact with dust, HCL, HF, SO_x, NO_x, and oxygen, among
331 other contaminants²⁵. Concerns have been expressed regarding the elevated volatility and
332 limited stability of liquid amines. As per the findings of Williams and their research team³³,
333 conducting multiple capture-release cycles leads to notable losses of amine sorbent,
334 subsequently causing a decrease in efficiency and performance. The collective impact of these
335 factors can also negatively affect the overall efficiency of a power plant utilizing post-
336 combustion liquid amine carbon capture and storage technology. A recent report attributed a
337 30–40% reduction in the overall efficiency of power plants to the difficulties associated with
338 implementing CCS technology¹⁹.

339
340 Furthermore, an associated cost was estimated to range from €70 to €100 per ton for this
341 reduction in efficiency. Concerns have been also raised regarding the industrial scalability of
342 liquid-amine technology, with certain publications questioning its suitability for large-scale
343 implementation. Vega et al.²⁵ contend that, until the CO₂ capacity can be expanded from its
344 present 800 tons per day to the necessary 8000 tons per day, the technology may not be suitable
345 for large-scale CO₂ emission mitigation on an industrial level. Additionally, one of the most



346 significant challenges associated with liquid-amine processes is their restricted scope for
347 performance enhancement¹⁸. Much of the existing literature underscores the significance of
348 creating novel technologies with enhanced capabilities to supplant current liquid-amine
349 processes. Conversely, the Energy Technologies Institute (ETI) argues that liquid-amine
350 technologies still offer opportunities for future advancements³⁴. They cite the development
351 progress of bi-phasic systems as evidence of this potential.

352
353 Moreover, the environmental impact of amines has raised significant concerns. Williams et al.
354³³ argue that, owing to their highly toxic nature, amines are unsuitable for direct air capture
355 (DAC) applications and could potentially pose an environmental threat if employed in such
356 contexts. Vericella et al.²⁷ corroborate this viewpoint, noting that the commonly used amine
357 for CCS, monoethanolamine (MEA), generates toxic degradation byproducts. Furthermore,
358 there are apprehensions that the decrease in power plant efficiency resulting from the presence
359 of liquid-amine post-combustion technologies may partially offset the technology's advantages
360¹⁸. Another foremost issue with liquid-amine CCS is the high cost; with some sources claiming
361 the capture of 1 ton of CO₂ costs around 50–100 USD (as a conservative estimate)¹⁸.
362 Contrarily, an earlier report from 2015 provided an estimate of the maximum cost of post-
363 combustion amine CCS as \$110/tCO₂³⁵. As a result, numerous sources contend that the
364 technology is not yet commercially feasible for widespread use. Another problem is the extra
365 expense associated with the post-combustion C-capture system because it needs electricity to
366 operate. Liquid-amine CCS (L-A CCS) technology typically causes a large rise in capital costs
367 along with a decrease in power plant efficiency³⁴.

368
369 There are indications that beyond 2030, continuous technological advancements may lead to
370 cost reductions in liquid-amine technology, ultimately enhancing its viability for large-scale
371 implementation. Developers in the US, Canada, and the UK have committed to sharing publicly



372 all knowledge, data, and designs related to CCS technology, which should foster innovation.
373 According to the ETI, larger projects will enable the exploitation of economies of scale, which
374 will lead to additional cost reductions ³⁴. One recommended approach is the sequential
375 deployment of existing C-capture technologies in 3 or more full-scale power plants. The ETI
376 suggests that sequential deployments will result in a reduction in risk ³⁴. Reduced finance costs,
377 larger scale, and infrastructure sharing all work together to potentially cut the cost of output
378 energy by about 45%. Because it might result in more affordable financing solutions, risk
379 minimisation reduces financing costs.

380 **2.2 Metal-organic frameworks in carbon capture**

381 **2.2.1 Performance and challenges**

382 Solid sorbents such as MOFs are exciting candidates for low-temperature C-capture ³². Their
383 intrinsic properties such as their high porosity and their customizable chemistry provide the
384 potential to tune MOFs for improved CO₂ uptake capacity and selectivity ²⁶. Despite their
385 benefits, MOF sorbents face several hurdles. It is generally agreed that the thermal conductivity
386 of sorbents affects the C-capture operation and regeneration process's cost and cycle time ³⁶.
387 MOFs, however, tend to have poor thermal conductivities (at T = 25 °C, the thermal
388 conductivity of MOF-5 single crystal stands at a mere 0.32 W/m K) ³⁷. The enhancement of
389 MOFs' thermal conductivity is presently the subject of relatively few studies, thus perhaps more
390 research in this field is warranted. Opt-UiO-66(Zr)-(OH)₂ (2.50 mmol/g) is one of the best-
391 performing pristine MOFs ³⁸. This MOF is both water-stable and shows a CO₂ uptake higher
392 than that of MEA ³⁸. Based on their functional characteristics, modified metal oxide fragments
393 (MOFs) for C-capture can be broadly categorised into three groups: MOFs with amine-
394 functionalized sites (AFSs), unsaturated metal centres (UMCs), and saturated metal centres
395 (SMCs)¹⁸. Reports suggest that, while able to provide a significantly improved working
396 capacity, the UMC-rich MOFs with the highest capacities suffer from modest selectivity versus



397 nitrogen (SCN)¹⁸. UMCs can be generated by removing the solvent molecules responsible for
398 the partially coordinated metal atoms in some MOFs. This can be done through heating the
399 material or vacuuming. These UMCs exhibit an excellent CO₂ affinity, and can therefore be
400 used to enhance the capture capacity of a MOF at low pressures³⁹.

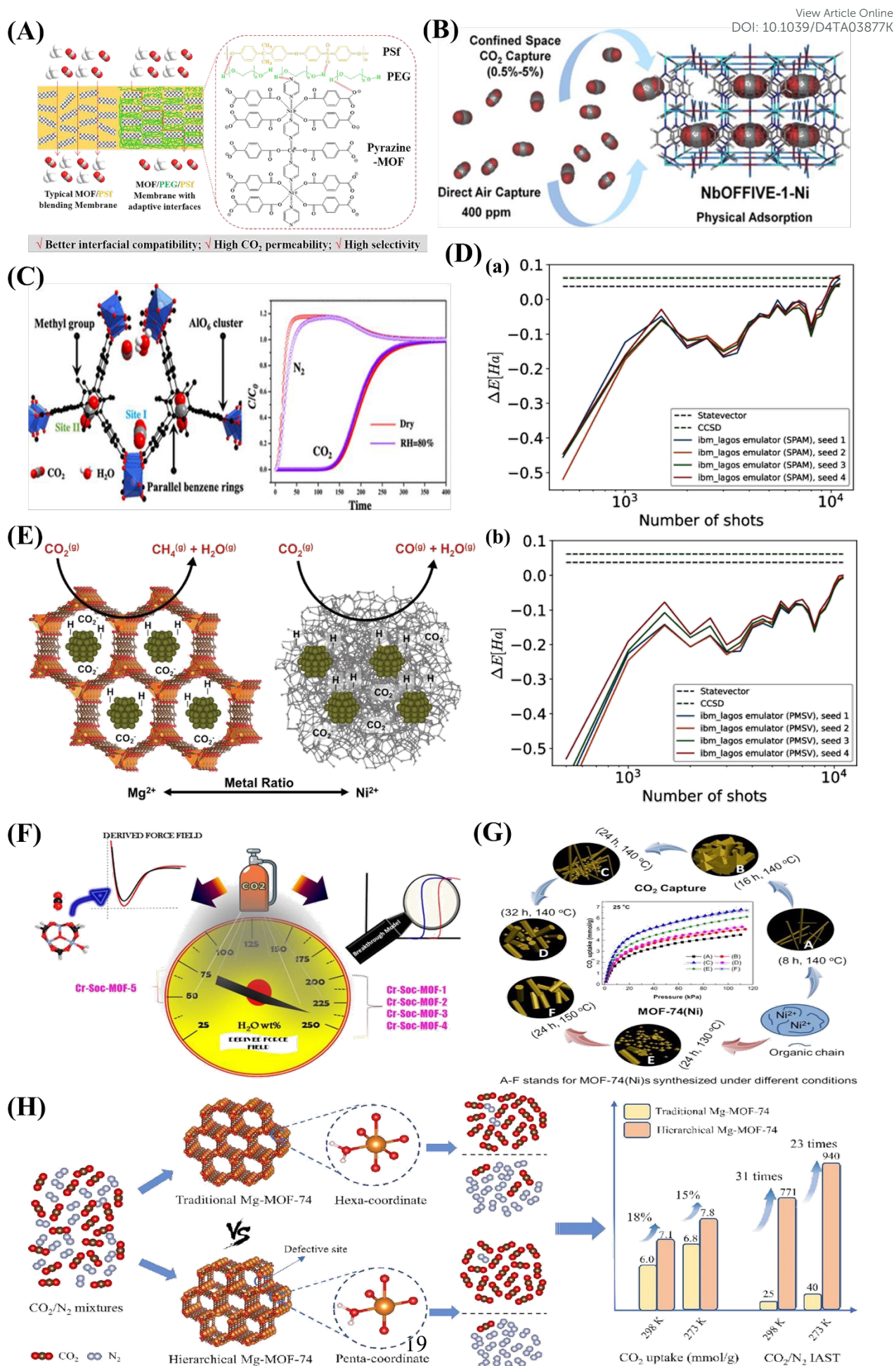
401
402 A new bimetallic MOF, functionalized with pyrazine and used in combination with polysulfone
403 (PSf), was employed to create a mixed matrix membrane (**Fig. 3(A)**)⁴⁰. This innovative
404 membrane demonstrated adaptable interfaces facilitated by the incorporation of the interfacial
405 plasticizer, polyethylene glycol (PEG). The inclusion of the MOF filler notably boosted the
406 CO₂ capture capacity of both pristine PSf membranes and PSf/PEG blend membranes.
407 Specifically, with the PSf/PEG/Pyrazine-MOF membrane, the CO₂ permeability rose
408 dramatically from 6.82 Barrer for the pure PSf membrane to 17.13 Barrer⁴⁰. Bhatt et al.⁴¹
409 detailed the development of a hydrolytically stable fluorinated metal-organic framework
410 (MOF) referred to as NbOFFIVE-1-Ni. Remarkably, this synthesized MOF exhibits significant
411 CO₂ adsorption capacities, measuring approximately 1.3 mmol/g gravimetrically and 51.4 cm³
412 (STP) cm³ volumetrically when exposed to 400 ppm of CO₂ at 298 K (**Fig. 3(B)**). Furthermore,
413 a methyl-functionalized aluminium-based MOF (ZJU-620(Al)) with remarkable chemical-
414 thermal stability and a high specific surface area of 1347 m²/g has been recently developed⁴².
415 This MOF has emerged as a highly promising candidate for CO₂ capture due to its exceptional
416 recyclability and impressive capacity, reaching up to 4.25 mmol/g at 298 K and 1 atm. CO₂
417 molecules are primarily captured within two distinct sites. The first site (I) is situated in close
418 proximity to the AlO₆ clusters, while the second site (II) is positioned between two parallel
419 benzene rings, separated by a distance of 6.64 Å (**Fig. 3(C)**). While MOF technology has held
420 great promise to date, the performance data from **Fig. 3(D)** raises some deeply troubling
421 questions about realistic applicability⁴³. Specifically, it constructs bond dissociation energy



422 from the noisy-prone measurements of emulated hardware under two error mitigation schemes.
423 state preparation and measurement (SPAM) error mitigation and post-measurement symmetry
424 verification (PMSV). A variational outcome of up to ± 1 mHa based on noise alone illustrates
425 the practical challenges in reliably predicting MOF performance under more realistic conditions
426 ⁴³.
427

View Article Online
DOI: 10.1039/D4TA03877K





429 **Fig. 3.** (A) An illustration of the interactions and interfacial structure of the PEG/PSf mixed
430 matrix membrane with pyrazine-MOF incorporation for the separation of CO₂ from CH₄.
431 Adopted from Ref. ⁴⁰ with permission. (B) Fluorinated MOF, NbOFFIVE-1-Ni, for trace CO₂
432 removal and air capture. Adopted from Ref. ⁴¹ with permission. (C) Methyl-functionalized Al-
433 based MOF ZJU-620(Al) for CO₂ capture. The two main types of sites where CO₂ molecules
434 are adsorbed are Site I, which is close to the AlO₆ clusters, and Site II, which is between two
435 parallel benzene rings. Adopted from Ref. ⁴² with permission. (D) Calculate bond dissociation
436 energy using noisy emulated hardware data for 2 noise rates. Demonstrating two error
437 mitigation approaches: (a) state preparation and measurement (SPAM) error mitigation, and (b)
438 post-measurement symmetry verification (PMSV). Both approaches use the same set of 4
439 randomization seeds results in order of the number of measurement shots. Adopted from Ref.
440 ⁴³ with permission. (E) Catalysts with MOF-74 templating comprising mixed metals for
441 effective carbon dioxide capture and methanation. The resultant support material influences a
442 qualitative CO₂ hydrogenation reaction pathway involving the reverse water-gas shift and
443 Sabatier reactions. Adopted from Ref. ⁴⁴ with permission. (F) Coordinatively unsaturated MOF
444 with square octahedral (Soc) topology (Cr-Soc-MOF) for super-adsorption of CO₂ under humid
445 conditions. Adopted from Ref. ⁴⁵ with permission. (G) MOF-74(Ni) synthesized under different
446 conditions for carbon capture and storage. Adopted from Ref. ⁴⁶ with permission. (H) A
447 schematic diagram showing how defect-rich hierarchical porous Mg-MOF-74 and conventional
448 Mg-MOF-74 are prepared differently and their application in CO₂ adsorption. Adopted from
449 Ref. ⁴⁷ with permission.

451 Mg-MOF-74 is often used as a benchmark for other physisorbents, as it has an excellent CO₂
452 adsorption capacity in dry conditions at low pressures (5.5 mmol/g at 0.15 bar, 313 K ^{18,48} and
453 up to 8 mmol/g at 1 bar and 298 K ³⁹). The high density of UMCs is largely responsible for the
454 remarkable CO₂ uptake values. It is created by reacting 2,5-dihydroxyterephthalic acid with
455 magnesium metal salts, which produces a large amount of UMCs within the MOFs framework.
456 Bahamon and associates compare a number of MOFs to zeolites in their report ⁴⁹. Because Mg-
457 MOF-74 performs well in TSA operating settings, they present it as having good potential for
458 TSA separation. According to their findings, Mg-MOF-74 outperformed zeolite 13X, a zeolite
459 that is frequently utilised ⁴⁹. In the same context, a mixed-metal metal-organic framework
460 (MOF) referred to as NiMg-MOF-74 was utilized as a template to achieve the even distribution
461 of small nickel nanoclusters within the native MOF framework ⁴⁴. Through the adjustment of
462 the Ni-to-Mg ratio within the initial MOF, it is possible to modulate both the available surface
463 area and crystallinity after thermal treatment (**Fig. 3(E)**). This, in turn, has an impact on the
464 capacity for CO₂ adsorption and the selectivity of hydrogenation.



465
466 On the other hand, critics have often pointed out the poor performance of MOFs in gas
467 separation, particularly under humid conditions. Palakkal et al.⁴⁵ examined coordinatively
468 unsaturated MOF (CUS-MOF) with square octahedral (Soc) topology. The research
469 encompassed examinations of both co-adsorption (CO₂/N₂) and single-component (CO₂, N₂)
470 adsorption with moisture at 298 K and pressures between 0 and 10 bar. The authors focused on
471 five different Cr-Soc-MOFs, which exhibited experimentally established iso-structural
472 topologies but differed in polynuclear aromatic ring size and N-heteroatom content within their
473 pore walls (**Fig. 3(F)**). Remarkably, Cr-Soc-MOFs with larger pore volumes exhibited CO₂
474 uptake ranging from 23 to 35% by weight, with selectivity levels ranging from 20 to 50%, even
475 up to 70% relative humidity (RH)⁴⁵. A Ni-based metal–organic framework, MOF-74(Ni), was
476 synthesized using a straightforward condensation reflux method⁴⁶. By adjusting the synthesis
477 duration at different temperatures, both the structure and CO₂ adsorption isosteric heat of MOF-
478 74(Ni) could be customized (**Fig. 3(G)**). After being produced at 140 °C for 24 hours, the
479 optimised MOF-74(Ni)-24-140 demonstrated remarkable CO₂ adsorption capacity, attaining
480 8.29/6.61 mmol/g at 273/298 K with a pressure of 1 bar. This capacity surpassed that of
481 previously reported MOF-74-Ni, UTSA-16, and DA-CMP-1 under similar conditions by
482 factors of 2.0/2.1, 1.5/1.6, and 3.6/4.9, respectively. An et al.⁴⁷ reported the synthesis of a
483 defect-rich hierarchical porous Mg-MOF-74 (**Fig. 3(H)**). The defect-rich hierarchical porous
484 Mg-MOF-74 exhibits an increased adsorption enthalpy of CO₂ at zero load, rising from 36 to
485 46 kJ/mol compared to conventional Mg-MOF-74. Moreover, the saturated CO₂ adsorption
486 capacity under ambient pressure has seen a significant improvement of 15%.
487
488 Despite high performance of Mg-MOF-74, their application is hindered by several factors
489 including its relatively poor CO₂ selectivity over other gases such as O₂, N₂, and CH₄ (all of



490 which are abundant in the flue gas mixture)¹⁸. Additionally, whereas CO₂ molecules are
491 strongly attracted to UMCs, H₂O molecules would preferentially occupy the open metal sites
492 ⁵⁰. As a result, Mg-MOF-74 absorbs substantially less CO₂ when it is exposed to moisture. This
493 is troublesome since there is a significant amount of H₂O(g) (5–7%) in flue gases ⁵⁰. Hence, it's
494 crucial to explore and devise methodologies for enhancing the selectivity over nitrogen of the
495 MOF, particularly in the presence of water. An example of the ongoing research into this issue
496 includes the introduction of amines into MOFs in an effort to emulate the chemisorption of CO₂
497 used by conventional liquid-amine technologies ⁵¹. In a recent study conducted by Kim et al.
498 ⁵², MOFs modified with diamines (nitrogen compounds) were investigated. The modified
499 MOFs can capture and release CO₂ at lower temperatures than those used by existing carbon
500 capture materials ⁵². As a result, the CCS process requires far less energy than it does with
501 existing technology, which lowers the process's cost ⁵². Amine-modified MOFs are produced
502 by grafting amine functional groups onto MOFs ¹⁸. This can improve the MOF's SCN and
503 operating capacity, but regrettably, there is frequently a significant regeneration energy penalty
504 ⁵³. Nonetheless, under capture conditions, some alkylamine-modified MOFs have good CO₂
505 working capabilities, SCN, and moderate regeneration ³⁹. There have been successful reports
506 of functionalizing Mg₂(dobpdc) with N,N'-dimethylethylenediamine (mmen). Coordination
507 bonds form between the amine groups and the unsaturated metal centers (UMCs) on
508 Mg₂(dobpdc). The resultant MOF, mmen-Mg₂(dobpdc), boasts a high density of amine groups,
509 leading to enhanced selectivity versus nitrogen (SCN) even in the presence of water. At 313.15
510 K and 0.15 bar, the CO₂ adsorption capacity reaches 3.5 mmol/g. Moreover, this MOF
511 effectively mitigates the substantial energy requirements for regeneration, further bolstering its
512 potential for carbon capture applications ³⁹. **Table 1** summarizes adsorption data for a variety
513 of functionalized MOF sorbents at different pressures and temperatures.

514



515 **Table 1.** CO₂ adsorption data for a variety of functionalized MOFs at different experimental conditions.
 516

View Article Online
 DOI: 10.1039/D4TA03877K

Adsorbent	Functionality	CO ₂ uptake (mmol/g)			Temperature (K)	Selectivity (S _{CN})	References
		Low pressure (mbar)	0.15 bar	1bar			
Mg-MOF-74	UMC	NA	5.35	8.1	296	182 (IS) (15:85)	18
Mg ₂ (dobpdc)	UMC	NA	4.85	6.42	298	NA	53
UiO-66-(CH ₃) ₂	UMC	NA	1.3	4.01	293	58 (IS) (15:75)	54
UiO-66	UMC	NA	NA	1.8	298	23 (IAST) (14:57)	18
Co-MOF-74	UMC	NA	2.76	6.69	296	NA	18
mmen-Mg ₂ (dobpdc)	Amine-modified	2.05 at 0.4mbar	3.13	3.86	298	200 (IS) (15:75)	55
[Mg ₂ (dobdc)(N ₂ H ₄) _{1.8}]	Amine-modified	3.89 at 0.4mbar	5.18	5.51	298	NA	56
UiO-66-NH ₂	Amine-modified	NA	1.15	2.6	298	32 (IS)	18
MOF-5	Pristine MOF	NA	NA	2.1	298	10.1 (IS)	57
MOF-505	Pristine MOF	NA	0.4	1.5	304	NA	18

517

518 2.2.2 Manufacturability, stability and cost

519 Mukherjee et al.¹⁸ emphasize the importance of the industrial-scale production of candidate
 520 sorbents to meet the quantity demands of later-stage pilot-scale testing and wide-scale rollout.

521 Most MOFs are not yet manufactured on a large scale, and the few that can be, are synthesized
 522 as powders²⁶. MOFs need to be structured sorbents to be incorporated into the C-capture
 523 procedure. Therefore, it is necessary to look for ways to turn MOFs into pellets, beads, fibres,
 524 or monoliths. The absence of methods for transforming microcrystalline MOF powders into
 525 devices has given rise to numerous problems¹⁸. Some studies explore the incorporation of



526 MOFs into support structures (monoliths or pellets) but these are still in the early development
527 stages⁵⁸. Generally, research into the pelletizing MOFs without binders has shown a reduction
528 of approximately 5% in the MOF's CO₂ uptake capacity⁵⁹. Research conducted by Peterson et
529 al.⁶⁰ employed octane adsorption experiments to investigate the effect of pelletization pressure
530 on the properties of UiO-66. Results showed that pelletization at 68.94 bar led to an 8%
531 reduction in octane adsorption and pelletization at 689.5 bar led to a larger reduction of 16%.
532 However, results for the pelletization of HKUST-1 reported by Asadi et al.⁶¹ show a 20%
533 decrease in CO₂ uptake capacity. This suggests that sorbents may have varying uptake capacity
534 responses to pelletization. Hu et al.⁶² argue that, given the complexity of pelletization, an
535 empirical approach involving practical investigations is necessary.

536
537 The current synthesis of MOF powders is typically done via solvothermal batch processes.
538 These processes are time-consuming, require the use of expensive organic solvents, and involve
539 complex purification methods⁶². These problems lead to high manufacturing costs, which may
540 reduce their attractiveness as possible sorbents from an economic standpoint. Although more
541 work needs to be done, some progress has been made recently, such as the utilisation of twin-
542 screw extrusion (TSE) kg per hour-scale MOF synthesis without the use of ore-reduced
543 solvents. When suggesting uses for newly created materials, a variety of considerations,
544 including toxicity, life-cycle assessment studies, and economic implications, must be taken into
545 account in addition to the previously mentioned concerns. On the other hand, one prominent
546 drawback that has hampered the applicability of MOFs in this domain is their stability under
547 the conditions of CCS operation, with many MOFs exhibiting poor hydrolytic stability¹⁸. This
548 means that when MOFs are exposed to moisture, they are prone to decompose. There have been
549 developments in the field to address this issue and recent research shows promise of progress.
550 Investigated strategies include doping MOFs with alkyl amines (or other chemical functions)

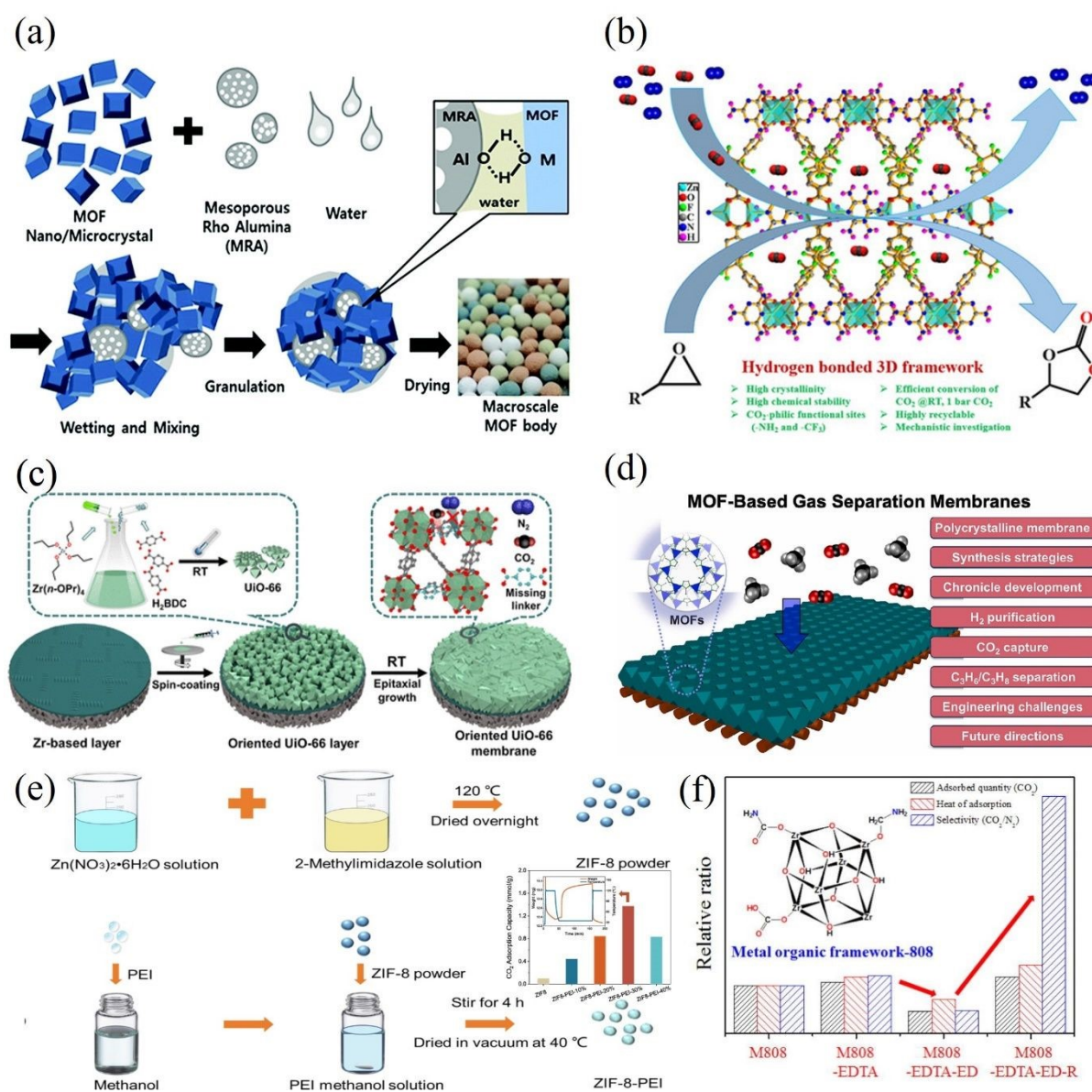


551 and improving the MOF's hydrophobicity ⁶². Studies on doping MOFs with N,N,N',N'-tetraalkylethylenediamine, hydrazine (N₂H₄), and 2,2-dimethyl-1,3-diaminopropane (dmpn) New Article Online
DOI: 10.1039/D4TA03877K
552 dimethylethylenediamine, hydrazine (N₂H₄), and 2,2-dimethyl-1,3-diaminopropane (dmpn)
553 have shown that the CO₂ absorption capability is nearly entirely retained when there is moisture
554 present ⁶³. However, it is important to note that doped MOFs may still struggle with poor
555 chemical, mechanical, and thermal stability ⁵³. Research by Dalvi and Rossky ⁶⁴ showed a
556 marked improvement in hydrophobicity from MOFs decorated with fluoro or alkyl groups,
557 suggesting this could be an alternative solution.

558
559 Another method of preparation that has been explored is wet granulation. This method,
560 proposed by Chang and colleagues ⁶⁵, mixes the MOF with a mesoporous γ -alumina (MRA)
561 binder to produce millimeter-scale spheres (**Fig. 4(a)**). Numerous MOFs, including MIL-
562 101(Cr), UiO-66(Zr)-NH₂, MIL-100(Fe), and UiO-66(Zr), have shown effectiveness with this
563 strategy. After shape, the MOF's natural characteristics are preserved with the aid of a binder.
564 Furthermore, tiny businesses like Mosaic Materials and NuMat are making a concerted effort
565 to satisfy these needs ²⁶. In the research conducted by Das et al. ⁶⁶, the authors detailed formation
566 of a hydrogen-bonded three-dimensional (3D) framework involves a zinc (II) center, a partially
567 fluorinated elongated dicarboxylate ligand, and an amine-rich melamine co-ligand (**Fig. 4(b)**).
568 Notably, this framework exhibits two distinct types of 1D channels adorned with CO₂-attractive
569 (–NH₂ and –CF₃) groups that facilitate the framework's exceptional selectivity for CO₂
570 adsorption (uptake of 49.88 and 31.16 cm³/g at 273 and 298 K, respectively) ⁶⁶. Furthermore, a
571 straightforward and comprehensive room-temperature procedure has been established for the
572 fabrication of (111)-oriented UiO-66 membranes ⁶⁷. This method utilizes a ZrO₂ buffer layer-
573 modified porous α -Al₂O₃ substrate and a Zr(n-OPr)₄ source (**Fig. 4(c)**). Experimental findings
574 revealed that conducting the reaction at room temperature (RT) increased the number of missing
575 linkers within the UiO-66 framework (1.5 per Zr₆ formula unit). Consequently, this resulted in



576 enhanced CO₂/N₂ adsorption selectivity due to a stronger affinity interaction between CO₂ and
 577 the defective sites in the Zr₆-oxo cluster nodes⁶⁷.



578
 579 **Fig. 4.** (a) Creating MOF granules or spheres via the wet granulation process by aggregating
 580 MOF and MRA particles. Adopted from Ref.⁶⁵ with permission. (b) The rational design of a
 581 porous Zn(II)-MOF with several functional sites that can be used, under moderate conditions,
 582 for extremely effective CO₂ fixation with internal and terminal epoxides. Adopted from Ref.⁶⁶
 583 with permission. (c) A schematic diagram depicting the entire room temperature preparation
 584 process for defect-engineered (111)-oriented UiO-66 membranes. A higher CO₂/N₂ adsorption
 585 selectivity was demonstrated and attributed to the stronger affinity interactions between CO₂
 586 molecules and the defective sites in the Zr₆-oxo cluster nodes. Adopted from Ref.⁶⁷ with
 587 permission. (d) Diagram showing the in-situ growth process for homochiral MOF membrane
 588 production on nickel net and its use for molecular separations. Adopted from Ref.⁶⁸ with
 589 permission. (e) A synthesis process of unmodified and PEI-modified ZIF-8 and the
 590 corresponding adsorption capacity at different PEI loadings. Adopted from Ref.⁶⁹ with
 591 permission. (f) Zr-based MOF functionalized with ethylenediaminetetraacetic acid (MOF-808-



592 EDTA), ethylenediamine (MOF-808-EDTA-ED), and lithium aluminium hydride (MOF-808-
593 EDTA-ED-R) for selective CO₂ adsorption. Adopted from Ref. ⁷⁰ with permission.

594

595 Conversely, many research endeavours have focused on MOF-based gas separation
596 membranes, with particular attention to ZIF-8 ⁶⁸ (**Fig. 4(d)**). The exploration of MOF
597 membranes for gas separation traces back to 2009 ⁷¹, with the milestone achievement of the
598 first continuous MOF-5 membrane via an in-situ growth method. This milestone marked the
599 beginning of MOF membrane development for gas separations. Other methods include layer-
600 by-layer growth, electrochemical synthesis, vapour phase synthesis, seeding and secondary
601 growth, and contra-diffusion also appeared in the ensuing ten years. Particularly noteworthy is
602 the considerable focus on ZIF-8 in MOF membrane research due to its exceptional C₃H₆/C₃H₈
603 separation capabilities, straightforward synthesis, and the potential for producing high-quality
604 membranes. A recent study involved the synthesis and characterization of ZIF-8 with varying
605 weights of polyethyleneimine (PEI) ⁶⁹. The results indicated that ZIF-8 with 30 wt.% PEI
606 achieved the highest CO₂ uptake of 1.4 mmol/g under dry conditions and demonstrated
607 remarkable CO₂/N₂ separation performance (**Fig. 4(e)**). The CO₂ adsorption capacity of ZIF-8-
608 PEI30% notably rose to 1.7 mmol/g when exposed to humid flue gas with 50% relative
609 humidity (RH). Furthermore, even after undergoing 50 adsorption/desorption cycles, only a
610 slight decrease in adsorption capacity was observed. Park et al. ⁷⁰ have directed their efforts
611 towards improving the efficiency of Zr-based metal-organic framework (MOF-808) for CO₂
612 capture by introducing various functional groups onto the MOF surface. Notably, reducing the
613 MOF-808-EDTA-ED compound with lithium aluminium hydride (LAH) led to a significant
614 enhancement in performance, including higher CO₂ adsorption capacity, CO₂/N₂ selectivity,
615 and isosteric heat of adsorption. For example, under conditions of 298 K and 1 atm, MOF-808,
616 MOF-808-EDTA, MOF-808-EDTA-ED, and MOF-808-EDTA-ED-R demonstrated CO₂/N₂
617 selectivity of 40, 48, 19, and 197, respectively (**Fig. 4(f)**). This significant enhancement is



618 attributed to the contribution of functional groups and porosity. The introduction of amides
619 during the reaction with ED resulted in decreased MOF porosity, negatively impacting CO₂
620 capture. However, subsequent reduction of amides to amines improved adsorption effectiveness
621 ⁷⁰.

622
623 Regarding the cost, it can vary widely depending on several factors, including the specific MOF
624 composition, synthesis method, scale of production, and market demand. Generally, MOFs are
625 more expensive to produce compared to traditional adsorbents like activated carbon due to their
626 complex synthesis processes and sometimes costly precursor materials. At present, the
627 production of MOFs typically involves expensive starting materials and specialized synthesis
628 techniques, which contribute to higher production costs. Additionally, the purity and quality of
629 MOF materials also affect their cost, with higher-purity MOFs often commanding a premium
630 price. As was previously said, the creation of MOFs that require less temperature to absorb and
631 release CO₂ will probably lead to lower process costs over time ⁵². However, MOF sorbent costs
632 are still considered the limiting factor for their commercial application ⁶². Since MOF sorbents
633 for post-combustion C-capture have not been subjected to real-world trials, prices can be
634 estimated in part by considering the price of the substrates or raw sorbent utilised in the
635 preparation ¹⁸. The metal ions or clusters are often inexpensive, consequently, the main factor
636 affecting the cost of a MOF sorbent is the linker cost. Whilst most sorbents use polycarboxylate
637 ligands, there is a variety of inexpensive and commercially available ligands, for example, one
638 of the most common ligands, 4,4'-bipyridine (bipy) ⁷². Commercial MOF vendors still charge
639 significantly more than more conventional porous materials like zeolites, even though MOFs
640 are synthesised from comparatively cheap ingredients ⁶². This is often attributed to high
641 manufacturing costs which are the result of a shortfall in large-scale production methods.



642 3. Energy storage devices

643 Currently, supercapacitors (SCs) are among the most popular energy-storage devices ⁷³, which
644 have already found applications in consumer electronics, memory backup systems as well as
645 industrial-scale power and energy management devices ⁷⁴. Although conventional capacitors
646 have a larger energy density, SCs are seen to be better because of their many benefits, including
647 flexible packaging, low weight, minimal heating, and strong device stability ⁷⁵. Furthermore,
648 SCs have proven to be both safe and reliable, as Sundriyal et al. ⁷⁴ highlight in their recent
649 application in the emergency doors of the Airbus A380. In addition, one of the most intriguing
650 uses of SCs is in contemporary transportation systems like electric cars. The sales ban on
651 internal combustion engines (IC) engines will be accelerated from 2040 to 2035 as a result of
652 growing social and governmental pressure to reduce fossil fuel consumption. As a result, the
653 electrical energy storage (EES) devices used in these transportation systems must be able to
654 provide a high enough power density to expedite vehicle charging times ⁷⁴. SCs' high-power
655 densities (up to 15 kW/kg) give them the ability to charge and discharge rapidly, which would
656 enable fast charging of electric vehicles and their good cyclic stability would ensure that their
657 performance wouldn't degrade significantly over time. However, their largescale usage is
658 hindered by low energy densities meaning that they are unable to hold large amounts of energy
659 ⁷⁵.

660
661 In the same context, electrodes play a critical role in SC performance, therefore selecting an
662 electrode design and material is key to ensuring effective energy storage. Sundriyal et al. ⁷⁴
663 suggest several critical electrode parameters that determine the performance of the SC including
664 specific capacitance, power and energy densities, cycle life, and stability in bending. Forse et
665 al. ⁷⁶ also offer a range of critical electrode material properties that require consideration,
666 including a large specific surface area, good stability at high temperatures, pores size and
667 distribution, high corrosion resistance, high conductivity, and cost-effectiveness. Research by



668 Huang et al.⁷³ supports this but summarises the performance criteria under the broad umbrella
669 of material properties that allow for a short ion or charge transfer channel whilst also providing
670 many active sites.

671
672 Many sources discuss the relationship between the specific surface area (SSA) and capacitance
673 as though it were linear, with higher SSAs resulting in a higher capacitance⁷³. Whilst this is
674 true for certain SC electrodes, Wu and Cao⁷⁷, highlight that in some instances, a higher SSA
675 will not guarantee a greater capacitance. Effective surface area (ESA) is a surface area that is
676 directly utilised for charge absorption and is associated with the distribution of pore sizes. As
677 previously mentioned, the low energy density of SCs is currently impeding their practical
678 deployment⁷⁸. Energy density denotes the quantity of energy that a SC can store per unit
679 volume of SC⁷⁴. On the other hand, power density describes the amount of power transferred
680 per SC volume. The difference between SSA and the attained specific capacitance is a topic
681 covered in a number of studies. Some reports indicate that during charge storage, not all of the
682 pores are used⁷⁵. Consequently, Forouzandeh et al.⁷⁵ argue that while SSA is an important
683 performance parameter for EDLC design, other factors such as pore size distribution and ESA
684 will also influence the SC's electrochemical performance. In their research paper, Wu and Cao
685⁷⁷ state that the electrode surface area is the main influencer on the electrochemical properties
686 of the SC.

687
688 Phiri et al.⁷⁹ highlight the important role played by ion-transport kinetics in SC electrode
689 performance. According to their research, the material's surface area and pore structure affect
690 the electrode's ion kinetics. Consequently, the authors suggest a material that combines a high
691 SSA with a combination of micropores and mesopores (to raise the ESA) while thinking about
692 ways to improve the electrochemical performance of electrodes. They suggest that the



693 mesopores may serve as a quick pathway for the SC electrolyte to move, boosting the
694 capacitance of the SC and that the micropores offer a sizable SA for quick ion adsorption. Wu
695 and Cao ⁷⁷ also propose other factors for consideration such as the electrical conductivity of the
696 electrode material and the presence of surface functional groups. Overall, factors such as power
697 and energy densities, cyclability, specific capacitance and morphology require consideration
698 during the material selection process for SC electrode capacitors. Moreover, cyclability pertains
699 to the count of charge and discharge cycles a supercapacitor can undergo before experiencing
700 electrode degradation and notable performance decline. ⁷⁷. Often, degradation only becomes
701 evident after prolonged cycling. Consequently, estimating the cyclability can be difficult.
702 Weinstein and Dash ⁸⁰ warn that laboratory-based testing of cyclability often relies on “beaker
703 tests”. During these tests, the SC electrodes are placed in a beaker and submerged in the
704 electrolyte. This kind of approach reduces the effect of contaminants on cyclability by allowing
705 them to diffuse into the huge volume of electrolyte that causes errors. On the other hand,
706 because of the device's real operating circumstances, there is minimal room for diffusion
707 because the electrolyte volume is rather tiny ⁸⁰. Therefore, the cycle life obtained through
708 laboratory tests is likely to be different from values obtained from testing the real fabricated
709 SC. Cyclability is an important factor for the assessment of both the performance and the
710 environmental impact of the design. If the electrode degrades quickly, more material will be
711 required over the lifetime of the device or the device will require replacing.

712
713 In another context, Forouzandeh et al. ⁷⁵ highlight a series of considerations for assessing the
714 environmental impact of an electrode including the toxicity, reusability (reformation prospects),
715 and energy requirements for the primary manufacturing (processing raw materials).
716 Furthermore, Weinstein and Dash ⁸⁰ postulate that, because SCs are often relatively small
717 compared to the device they power, there is little incentive to reduce the size and weight of the



718 SC if it results in higher costs. Manufacturers of SC are more concerned with controlling costs
719 than with making incremental performance advances. Price is acknowledged as significant, but
720 it is not given more weight than the other factors ⁷⁵. Contrarily to Weinstein and Dash,
721 Pongprayoon and Chaimanatsakun ⁸¹ argue that the two most important design requirements
722 for SCs are tuning the electrode material morphology (pore shape and size) to optimize the
723 transportation of electrolyte ions and a high SSA to increase the availability of
724 electrochemically active sites. Both are relevant for improving performance rather than
725 reducing cost.

726 **3.1 Porous carbonaceous materials for supercapacitors**

727 Porous carbonaceous materials stand out as highly versatile materials for supercapacitor
728 electrodes, particularly due to their diverse applications in various biomass sources. In recent
729 scientific research, there has been a notable emphasis on synthesizing carbonaceous materials
730 from biowaste, which produces a variety of morphologies and surface textures. The typical
731 synthesis process involves carbonization and activation steps, leading to activated carbon with
732 tunable pore sizes and exceptionally high specific surface area compared to other carbonaceous
733 materials. This renders activated carbon a preferred choice for supercapacitor electrodes. Prior
734 to the rise of MOFs, most studies on supercapacitor electrode materials were concentrated on
735 carbon-based materials ⁸². Activated carbon (AC) is used in almost all electrochemical
736 capacitors (ECs), and many producers of SC choose to use coconut shell AC as their active
737 electrode material ⁸⁰. Phiri et al. ⁷⁹ note that while graphene and carbon nanotubes (CNTs) are
738 also common material choices for SC electrodes, their wide-scale deployment has been
739 hindered by their high production costs and disposition to nanoparticle aggregation which limits
740 their effective SSA.

View Article Online
DOI: 10.1039/D4TA03877K



741 3.1.1 Performance and properties

742 Carbon SC electrodes usually work via charge adsorption, resulting in large power densities
743 and long cycle life ⁷³. In addition to this, carbon electrodes often present superb chemical
744 stability and electrical conductivity. An AC fabricated electrode in a study by Li et al. ⁸³
745 displayed a specific capacitance of 207.5 F/g and a cycle life of over 3000 cycles when tested
746 at a current density of 0.5 A/g. Another study reports an energy storage density of about 28
747 Wh/kg, but it also mentions that the device's charge supply rate limits the amount of power that
748 can be produced ⁸⁴. Research by Ajay and Dinesh ⁸⁵ yielded a specific capacitance of 107.6 F/g
749 for commercially available AC measured at a 5 mV/s scan rate. However, Phiri et al. ⁷⁹ argue
750 that biomass-derived ACs also have disadvantages, including discrepancies in the structures of
751 the biomass sources. Because of this, the ideal circumstances for the synthesis of AC from one
752 biomass source might not be appropriate for another. According to their studies, this can also
753 apply to a single biomass source that is used intermittently. As a result, a biomass source needs
754 to have a predictable and consistent structure to be taken into consideration for large-scale
755 practical applications.

756
757 AC-based SC electrodes are well suited for this purpose, not only do they have a high thermal
758 and electrochemical stability, but they also benefit from a large SSA. Available values of AC
759 SSA vary with most papers agreeing on a value within the range of 1000–3000 m²/g ^{86,87}.
760 Conversely, a study by Weinstein and Dash ⁸⁰ suggests a theoretical maximum SSA of 2000
761 m²/g. Carbon materials have a high SSA in addition to being relatively simple to produce,
762 modify, and optimise ⁸⁷. The premium-grade AC utilised for SC electrodes has been refined to
763 guarantee that the ash level is less than 1% and the halogen and iron impurities are fewer than
764 100 ppm ⁸⁰. This purification helps to improve the cycle life of the electrode. Despite this, ACs
765 are still comparatively cheap. ACs also benefit from high pore volumes in the range of 0.5–2



766 cm^3/g ⁸⁷. As previously stated, other literature suggests that the SSA is not as important as the
767 pore size and its impact on the effective specific surface area (ESSA)⁷⁵. Research by Arenillas
768 et al.⁸⁸ supports this, suggesting that for AC electrodes, the whole SSA is not used for charge
769 storage as the larger electrolyte ions are unable to enter the small micropores. The largest
770 obtainable SSA for AC is estimated at $3000 \text{ m}^2/\text{g}$, whilst the obtainable ESSA ranges from 1000
771 to $2000 \text{ m}^2/\text{g}$ ⁷⁵. Forouzandeh et al.⁷⁵ also examine the potential drawbacks associated with
772 large specific surface areas (SSAs), noting in their report that, in some scenarios, augmenting
773 the SSA can induce electrolyte decomposition and create dangling bond positions. Additionally,
774 a high pore volume may arise from attempts to raise the SSA through excessive activation. Poor
775 conductivity and low material density, which resulted in low energy and power densities, were
776 among the effects of these huge pore volumes that were investigated⁸⁹. The impact of various
777 electrolytes on the obtained capacitance of AC electrodes has also been studied. It was shown
778 that the capacitive performance of AC electrodes was enhanced when an aqueous electrolyte
779 was used instead of an organic electrolyte.

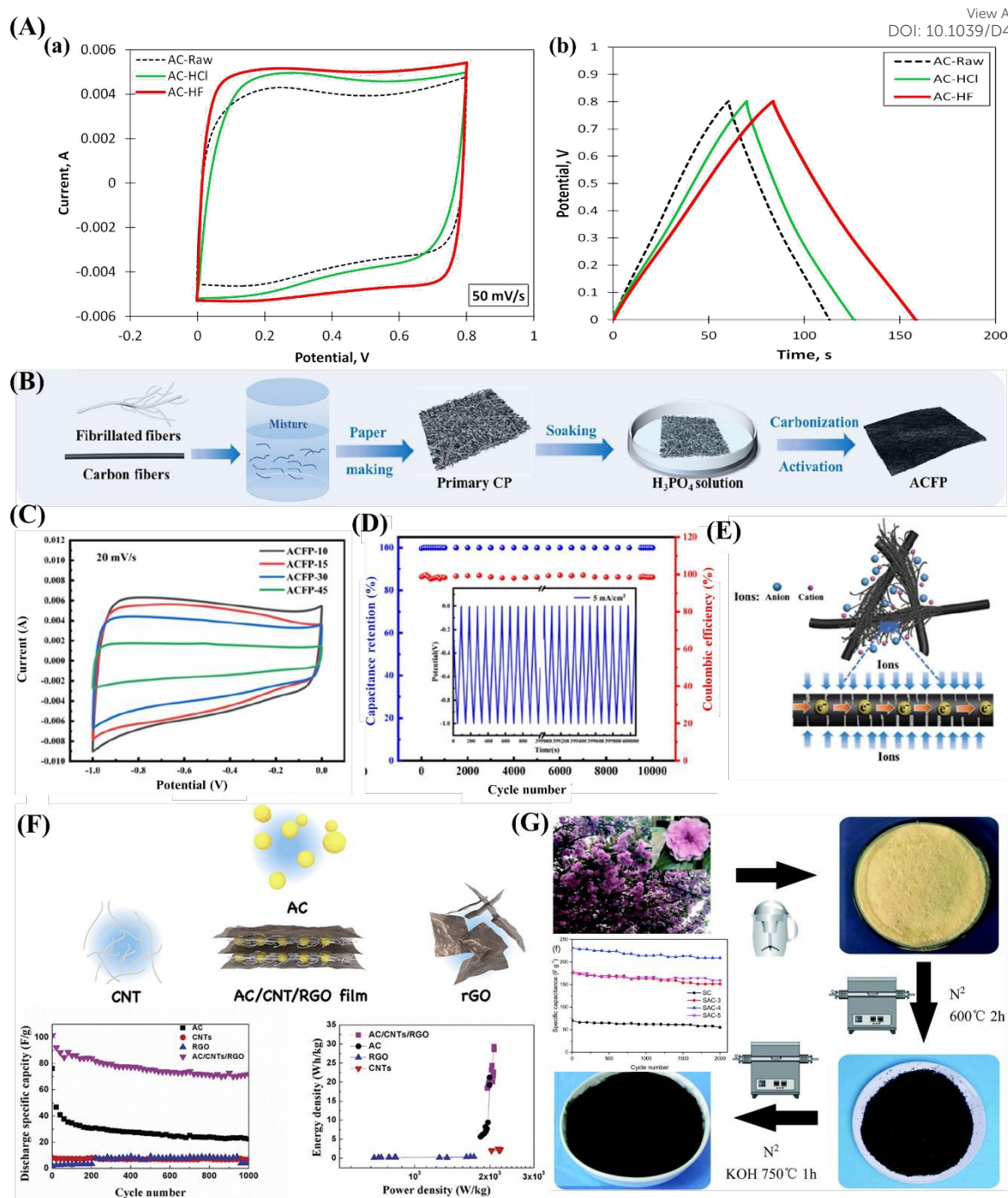
780
781 The performance and characteristics of activated carbon as electrode materials for
782 supercapacitors are very well presented in **Fig. 5A (a, b)**. The latter presents the CV curves of
783 the electrodes at a scan rate of 50 mV/s and gives an idea about their capacitive behaviour and
784 electrochemical performance. That nearly rectangular shape of the CV curve indicates ideal
785 capacitive properties; among them, better performance is obtained for the AC-HF sample⁹⁰.
786 **Fig. 5A(b)** shows the galvanostatic charge-discharge curves of the electrodes at a current
787 density of 1.5 mA/cm^2 , which provides the potential for energy storage. The GCD curves are
788 overlapping linearly and symmetrically, which further testifies to the high reversibility and
789 efficiency of the activated carbon electrodes, especially AC-HF, with the longest charging time
790 and discharge time and thus indicative of higher energy storage capacity⁹⁰. A recent



791 breakthrough introduced a straightforward and cost-effective technique for producing high-
792 performance cellulose-based activated carbon fibre papers (ACFPs), capable of serving as self-
793 supporting supercapacitor electrodes without the need for binders ⁹¹. This innovative approach
794 combines wet papermaking, thermal carbonization, and double activation processes, enabling
795 the on-site conversion of fibrillated pulp fibres into cellulose-derived activated carbon,
796 seamlessly integrated with carbon fibres (CFs) (**Fig. 5(B)**). The electrochemical evaluations
797 demonstrated that the ACFPs exhibited outstanding electric double-layer capacitive behaviour
798 (**Fig. 5(C)**), with coulombic efficiency and capacity retention remaining at 98.58% and 100%,
799 respectively, even after 10,000 cycles (**Fig. 5(D)**). The authors further elucidated the schematic
800 representation of charge transfer and electrolyte ion transfer within ACFP ⁹¹. The configuration
801 presented in **Fig. 5(E)** demonstrates a stable three-dimensional conductive network structure
802 through the close interweaving of CFs within the ACF matrix. This arrangement facilitated
803 swift electron migration along the CFs and enhanced the adsorption of electrolyte ions by the
804 ACFs ⁹¹.

View Article Online
DOI: 10.1039/D4TA03877K





805

806 **Fig. 5.** (A) (a) Cyclic voltammetry curves measured at a scan rate of 50 mV/s; (b) galvanostatic
 807 charge discharge curves measured at a current density of 1.5 mA/cm². Adopted from Ref. ⁹⁰
 808 with permission. (B) Illustration depicting the production process of cellulose-based activated
 809 carbon fibre papers (ACEPs), (C) Cyclic voltammetry curves recorded for ACFPs with varying
 810 CFs content using a 20 mV/s scan rate, (D) Retention of capacitance and coulombic efficiency
 811 measured at a current density of 5 mA/cm², and (E) Schematic diagram illustrating the charge
 812 transfer and electrolyte ion transfer within the conductive networks in ACFP. Adopted from
 813 Ref. ⁹¹ with permission. (F) A flexible electrode consisting of self-supporting activated carbon,
 814 carbon nanotube, and reduced graphene oxide and its SCs performances show a high specific
 815 capacitance of 101 F/g at the current density of 0.2 A/g. Adopted from Ref. ⁹² with permission.
 816 (G) Schematic representation illustrating the production process of porous carbon derived from



817 sakura, along with its corresponding long-term cycling performances. Adopted from Ref. 93
818 with permission. View Article Online
DOI: 10.1039/D4TA03877K

819

820 In the work of Li et al. ⁹², a deliberately engineered self-supporting and flexible film composed
821 of activated carbon, carbon nanotubes, and reduced graphene oxide (AC/CNT/RGO) has been
822 developed (**Fig. 5(F)**). The AC/CNT/RGO electrode demonstrates an impressive specific
823 capacitance of 101 F/g when operated at a current density of 0.2 A/g, resulting in a remarkable
824 maximum energy density of 30 Wh/kg. Conversely, three-dimensional porous carbon materials
825 were synthesized by utilizing sakura petals as the source material and employing a combination
826 of pre-carbonization and KOH activation techniques (**Fig. 5(G)**) ⁹³. The synthesized porous
827 material exhibited a high specific surface area (up to 1785.41 m²/g), leading to a maximum
828 specific capacitance of 265.8 F/g at a current density of 0.2 A/g. Additionally, under continuous
829 cycling for 2000 cycles, the capacitance retention rate remains excellent, reaching an impressive
830 90.2%, demonstrating outstanding cycling stability ⁹³. Recently, AC was prepared using biochar
831 derived from date seeds via pyrolysis and activated with H₂SO₄ ⁹⁴. The elaborated samples
832 demonstrated a specific capacitance of 487.5 F/g at a current density of 1 A/g. Additionally,
833 galvanic charge and discharge trends indicated a higher charge storage capacity with reduced
834 discharge. Another study focuses on converting inexpensive Cilantro plants (*C. sativum*) into
835 AC aiming to produce a cost-effective AC material that shows promise in supercapacitors for
836 energy storage ⁹⁵. The material that was synthesised at 700 °C showed ideal specific surface
837 area (SSA) and surface functionalities, which promoted surface redox processes, electrode
838 wetting, and ion diffusion-induced pseudo-capacitance. At 1 A/g, its specific capacitance was
839 162.4 F/g. Particularly noteworthy is the remarkable performance of the activated carbon (AC)
840 symmetric supercapacitor, delivering a high-power density of 243.94 W/kg and maintaining
841 minimal capacitance loss over 5000 cycles at 10 A/g, indicative of excellent cycling stability.



842 3.1.2 Environmental impact

View Article Online
DOI: 10.1039/D4TA03877K

843 Numerous commercially available ACs are produced from precursors such as coal and
844 polymers, which are fossil fuel-based, making them both expensive and environmentally
845 unfriendly ⁷⁹. However, ACs derived from biomass are still promising candidates for SC
846 electrode materials ⁸⁶. Large pore volume and surface area (which can surpass graphene's), ease
847 of preparation, and a customised architecture that has been deemed feasible for commercial
848 usage are some of their potential qualities. Gao et al. ⁹⁶ also draw attention to the other
849 environmental benefits of bio-mass-derived ACs including the renewability and abundance of
850 raw materials that can be used to make ACs. Furthermore, AC-based electrodes show good
851 potential for recyclability. The recycling process for activated carbon was investigated by Jiang
852 and Pickering ⁹⁷. The recycling procedure is assumed to be capable of recovering 90% of the
853 electrode's active materials ⁸⁴. The measured surface area of the AC that was recovered by this
854 technique is only 95% of its original, pristine value. This indicates a little decline in the content's
855 quality ⁹⁷.

856
857 Considering the environmental impact of recycling/recovering materials, Cossutta et al. ⁸⁴
858 suggest using the substitution model. This model's underlying idea is that material recovery
859 reduces the need to generate additional virgin material, which benefits the environment. The
860 quality of the recycled product determines how much virgin material may be substituted (0.95
861 g of virgin AC can be replaced by 1 g of recovered material) ⁸⁴. This is not a 1:1 substitution
862 due to the degradation of material quality/properties. Research by Ke and Wang ⁹⁸ provides a
863 value for the theoretical specific capacitance for used AC as 200 F/g (this value is based on
864 results for maximum actual SSA). Cossutta et al. ⁸⁴ highlight that, while the production of AC
865 requires energy, it is not as greenhouse gas (GHG) intensive as other electrode materials (such
866 as graphene). AC production produces around 5 g CO₂ eq./g (compared to ~80 g CO₂ eq./g).
867 Furthermore, since the emissions from the recycling process are lower than the emissions



868 connected to the sourcing and initial production of ACs, recycling AC supercapacitors can
869 result in a net reduction in GHG emissions. Research by Ntuli and Hapazari ⁹⁹, also suggests
870 that the use of agricultural by-products or lignocellulosic materials (such as coconut shells) as
871 feedstocks for AC production would further reduce GHG emissions as processing would avoid
872 the emission of GHGs when they rot or burn. However, the lifecycle analysis (LCA) of the AC
873 as electrode materials for supercapacitors manifests a fundamental environmental performance.
874 From here, it is observed that following the ISO framework, 1 kg of AC from coconut shells
875 contains 34.4 MJ of energy use and 5.68 kg of CO₂, char production and activation account for
876 86% of the CO₂ emissions at 97% ¹⁰⁰. New AC electrodes exhibit competitive environmental
877 performance in comparison with coal-derived AC, reduced graphene oxide, and algae-derived
878 biochar aerogel electrodes, though they have larger impacts on land and water use as a function
879 of the agricultural intensity of coconut production. They have lower impacts in regard to
880 terrestrial ecotoxicity and freshwater eutrophication ¹⁰¹.

881

882 The AC production process involves high temperatures and activation agents such as potassium
883 hydroxide, hence is highly energy-intensive with chemical wastes as by-products. The specific
884 surface area for mesophase-derived AC, for example, is 2000 m²/g, reducing to 1600 m²/g when
885 treated thermally but improving its stability by 99% ¹⁰². During usage, AC-based
886 supercapacitors show excellent performance, with thermally treated AC (AC-1000) exhibiting
887 only a 5% reduction in specific capacitance after 10,000 cycles, compared to untreated AC's
888 reductions of 12% and 17% ¹⁰³. An asymmetric capacitor using AC and AC-1000 shows a
889 capacitance decrease from 220 F/g to 210 F/g after 10,000 cycles, and to 198 F/g after 20,000
890 cycles ¹⁰⁴. These efficiencies translate into reduced energy losses and extended lifetimes for
891 devices. However, some of the challenges are in disposal and recycling, wherein exposure to
892 residual chemicals from AC materials may contaminate the environment. Overall, AC materials

View Article Online
DOI: 10.1039/D4TA03877K



893 enjoy huge technical advantages, but their lifecycle environmental impact implores that the
894 production methods used should be as clean and green as possible, the usage as efficient as can
895 be, and the disposable or recyclable end-of-life-time processes as innocuous as can be to avoid
896 adverse impacts on the environment.

897 3.1.3 Recent developments in AC electrodes

898 Recent literature provides a range of strategies for the improvement of AC electrochemical
899 performance. In their 2020 research paper, Grishchenko and colleagues¹⁰⁵ explored modifying
900 the surface of the AC electrodes through oxidation, and while there was a significant reduction
901 in the SSA of oxidized material, they achieved a 1.4 times higher specific capacitance in a
902 symmetric SC electrode compared to a pure AC electrode. Another example of the continuing
903 improvement of AC electrodes can be seen in the work by Cheng et al.¹⁰⁶. To create a new
904 class of nanocomposite electrodes, the scientists examined the synergistic effects of combining
905 ACs and carbon black (CB) with other species such as carbon nanofibers (CNFs) and carbon
906 nanotubes (CNTs). The study demonstrated that, in comparison to pure AC electrodes, the
907 electrochemical performance was significantly improved by mixing the species employed in
908 the SC electrode. The weight percentage composition of the optimised nanocomposite electrode
909 was 1.25% CB, 3.75% CNT, 1.25% CNF, and 88.75% AC. The completed SC demonstrated
910 good cyclability (capacitance retention of 91.4% over 30000 cycles) and volumetric
911 performance (high capacitance of 66.1 F/cm³, power density of 101.7 kW/L, and energy density
912 of 29.6 W h/L).

913
914 The improved performance is the result of the obtained morphology, as the added CB particles
915 fit into the voids between AC particles and it was found that the flexible CNTs wrap tightly and
916 uniformly around the AC particles. The CNFs were added, which helped to lessen the CB
917 particles' tendency to aggregate. By acting as a bridge between CB and CNT-wrapped AC



918 particles, CNFs' relative stiffness (as compared to CNTs) enhances the structural stability of the
919 nanocomposite. The final electrode featured a three-dimensional electrical conduction network
920 that enhanced capacitive behaviour and packing density. Furthermore, the nanocompositing
921 approach employed by Cheng et al.¹⁰⁶ utilizes readily available materials to synthesize the
922 nanocomposites. These can then be used to mass-produce large-scale high-performance SC
923 electrodes via the cost-effective industrial slurry process. A recent study focuses on
924 synthesizing graphene oxide (GO) using a modified version of the Hummers' method¹⁰⁷. The
925 produced GO is then incorporated into an activated carbon slurry to create electrodes for
926 supercapacitors. The addition of an appropriate amount of graphene oxide (GO) into the
927 electrode renders it hydrophilic, thereby enhancing the interfacial contact between the electrode
928 and the hydrogel electrolyte. The oxygen-containing functional groups present on GO attract
929 cations and facilitate ion dissociation, thereby improving ion mobility. However, as an insulator,
930 GO affects electrode conductivity. Remarkably, utilizing GO with weight ratios of 5% achieves
931 a balance, providing a sufficient free ion ratio for good ion conductivity while maintaining
932 acceptable electronic conductivity. Supercapacitors incorporating GO5 exhibit minimal
933 equivalent series resistance (ESR) of 4 Ω and a maximum specific capacitance of 117.7 F/g. In
934 a similar context, biowaste from litchi seeds was utilized to synthesize 3D activated carbon
935 (3D-AC), which was further combined with reduced graphene oxide (rGO) and multi-walled
936 carbon nanotubes (MWCNT) to create a multidimensional carbonaceous material¹⁰⁸. This
937 composite exhibited a specific capacitance of 320 F/g at 1 A/g. Additionally, 3D-AC served as
938 a supporting matrix for the growth of zinc cobalt sulfide nanoparticles, leading to promising
939 electrochemical performance in both asymmetric and symmetric devices.

940

941 Other recently explored strategies include using ultrasonic radiation for Fermi-level position
942 modification of the activated carbon¹⁰⁹, sulphur and oxygen functionality doping of the porous

View Article Online
DOI: 10.1039/D4TA03877K



943 AC¹¹⁰, and the formation of composite electrodes via the insertion of polymers into the AC
944 substrate¹¹¹. The price of AC has decreased dramatically over time, and this has been ascribed
945 to the SC carbon market's strong price sensitivity relative to performance. Suppliers such as
946 Kuraray, whose prices have dropped from \$150–200 USD per kilogramme to \$15 USD per kg,
947 are an example of this price reduction⁸⁰. More recent works provide a lower value of \$4.15
948 USD per kg and also emphasize the manufacturing economic benefits of coconut shell AC by
949 highlighting their abundant supply^{87,112}. Activated carbon, while a popular material in
950 supercapacitors, has several limitations that impact its performance. One of the main issues is
951 its broad and irregular pore size distribution that is predominantly microporous (<2 nm). These
952 small pores can limit the accessibility of electrolyte ions, particularly larger ions in organic
953 electrolytes, resulting in reduced capacitance and inefficient ion transport. Despite its high
954 surface area, activated carbon often exhibits low specific capacitance because not all of its
955 surface area is effectively utilized due to the presence of micropores that are too small for ion
956 penetration. Additionally, the properties of activated carbon are less tuneable compared to
957 materials MOFs. This lack of tunability restricts the ability to optimize its surface chemistry,
958 pore structure, and functional groups for specific applications.

959 **3.2 Metal organic frameworks as supercapacitors**

960 **Table 2** presents a selection of functionalized MOFs investigated for their suitability as
961 supercapacitor electrodes and compared to activated carbon. The table demonstrates a wide
962 range of potential specific capacitances, with some MOFs showing values higher than those of
963 AC, indicated at the bottom of the table. Additionally, MOFs exhibit the potential for enhanced
964 cyclability compared to ACs, highlighting their promise for supercapacitor applications.

965

966 **Table 2.** Supercapacitor's performance of functionalized MOF compared to AC electrodes.



Electrode material	Cycle life	Specific surface area m ² /g	Current density /scan rate	Specific capacitance F/g	Reference
ZIF-8 (HNC) MOF derived porous carbon	20000	1215	536 mA/hg 1 mV/s	253.6	73
ZIF-8 (NPCF) MOF derived porous carbon	5000	NA	1 mV/s (rate)	332	22
ZIF-8 (NCF) MOF derived porous carbon	10000	NA	5 mV/s (rate)	264	22
Co-MOF MOF directly used	NA	2900	0.6 A/g	206.76	74
Zr-MOF (1) MOF directly used	NA	1047	5 mV/s	1144	22
ZIF-8 (NPC) MOF derived porous carbon	NA	1523	5 mV/s	251	22
MOF-5 (NPC) MOF derived porous carbon	NA	2872	1 mV/s	312	22
Ni-MOF	49.1% (5000)	295.7	1 A/g	1024.4	74
NiOx@NP 3-electrode system. From waste PET	(91.5% retention after 5000 cycles)	1523	5 mV/s	581.30	113
3D) Ni-MOF	5000	NA	1 A/g	2150	114



Fe-MOF@AC	10000	180.7	1 A/g 1 mV/s	470.05	115
NiO@Ni-MOF	3000	433	1 A/g 1 mA/cm ²	144	116
Cu-MOF and Co-MOF	1000	NA	3 mV/s	451 and 103 C/g	117
Activated carbon	> 3000	NA	0.5 A/g	207.5	83

967

968 **3.2.1 Pristine MOFs and their composites**

969 From the available literature, it can be observed that the use of pristine MOFs for
 970 electrochemical applications, such as SC electrodes, is rare ¹¹⁸. As previously mentioned, this
 971 is predominantly due to their inherent insulating properties which result in low capacitance,
 972 often regarded as insufficient for most electrochemical applications ¹¹⁹. One report explores the
 973 use of Fe-MOF and its variants (MIL-88B, MIL100, and MIL-53) as SC electrodes coupled
 974 with an aqueous and neutral electrolyte ¹²⁰. The device's performance is significantly impacted
 975 by the material properties of the electrode, such as the size of the pellet and the pore diameters.
 976 Using an aqueous 0.1M Na₂SO₄ electrolyte, it was discovered that the MIL-100 sample only
 977 produced a specific capacitance of 34 F/g. The irritating nature of the Fe-MOF and insufficient
 978 mixing between the conductive and non-conductive phases of the Fe metal centres were the
 979 authors' explanations for this very low specific capacitance. This stops the material's electrons
 980 from moving through it in the best possible way when the iron centre is being reduced or



981 oxidised. The Fe-MOF was deemed unsuitable for use as an electrode due to the limited quantity
982 of redox-active Fe ions in the structure. The use of bare Fe-MOF electrodes has also proven
983 problematic, as experiments have shown that during the reduction cycle, the electrode is subject
984 to some degree of dissolution.

985
986 Despite their limitations, MOFs exhibit a rapid diffusion of electrolyte ions into the pores of
987 electrode materials. Consequently, research into utilizing pristine MOFs as SC electrodes has
988 experienced a noticeable uptick. These MOFs often work as pseudocapacitors via faradaic
989 redox reactions between the electrodes and the electrolyte. As the work by Wang et al.¹²¹ shows,
990 these fabricated electrodes yield theoretical values for capacitance as high as 2000 F/g¹²¹.
991 However, Ramachandran et al.¹²² argue that these benefits come at the cost of the electrode's
992 cycle life. In their investigation, they discovered that the cyclic stability of pseudocapacitive
993 MOFs was weakened by frequent charging and discharging cycles. This results from the
994 occasional dissolving of MOF electrode material during the reduction reactions, as well as
995 incompatibility between the electrode and electrolyte. A prominent example of the use of
996 pristine MOFs as SC electrodes is the work done by Lee et al.¹²³ in their paper. During their
997 experiments with a Co-based MOF electrode in an aqueous electrolyte of 1 M LiOH, the authors
998 were able to achieve a specific capacitance of 206.76 F/g with a current density of 0.6 A/g.
999 After the electrode's cycle life was examined, it was discovered that, after 1000 cycles of testing,
1000 its capacitance retention could reach 98.5%. However, the Co-based MOF electrode's
1001 performance significantly decreased and was ultimately declared unsatisfactory when tested in
1002 different electrolytes (such as KOH and KCl). An investigation was conducted into how the
1003 temperature of the synthesis reaction affected the performance, degree of crystallisation, and
1004 particle size of a zirconium-based MOF (UiO-66)¹²⁴. It was observed that a sample with the
1005 smallest particle size and a synthesis reaction temperature of 50 °C achieved the highest specific

View Article Online
DOI: 10.1039/D4TA03877K



1006 capacitance (1144 F/g at a 5 mV/s scan rate). However, the cost may prove to be a limiting
1007 factor as 1 kg of UiO-66 has been priced at around \$25000 USD ¹²⁵.

1008
1009 Other research into altering MOF morphology to improve SC performance includes the
1010 synthesis of a superstructure electrode from “accordion-like Ni-MOF” ¹²⁶. Whilst being tested
1011 at current densities of 1.4 and 7 A/g, the electrode achieved enhanced specific capacitances
1012 (988 F/g and 823 F/g respectively). Additionally, after 5000 cycles, the capacitance retention
1013 was 96.5%, which was a respectable retention rate. Highly elevated specific capacitances have
1014 also been seen with Ni-MOF electrodes in combination with a 6 M aqueous KOH electrolyte.
1015 Yang et al. ¹²⁷ report that, with current densities of 0.5 A/g and 10 A/g, specific capacitances of
1016 1127 F/g and 668 F/g respectively could be achieved. The high specific capacitances were
1017 explained by the authors as the result of the electrode's pseudocapacitive nature. Additionally,
1018 it was discovered that this electrode had improved cyclic stability, demonstrating 90% after
1019 3000 cycles. The MOF's layered structure and sizable open facets were both credited with its
1020 cyclic stability and quick surface redox reactions.

1021
1022 Rahmanifar et al. ¹²⁸ reported a one-pot co-synthesis method for creating a novel, water-stable
1023 Ni-MOF in combination with a Co-MOF. They also developed a dual Ni/Co-MOF-reduced
1024 graphene oxide (rGO) nanocomposite (**Fig. 6(a)**). The asymmetric device comprising activated
1025 carbon//Ni/Co-MOF-rGO demonstrated impressive performance, delivering a specific energy
1026 of 72.8 Wh/kg at 850 W/kg and maintaining a capacity of 15.1 Wh/kg even under the high
1027 specific power of 42.5 kW/kg. Furthermore, it exhibited exceptional cycle life, retaining 91.6%
1028 capacitance after 6000 charge-discharge cycles at 1 A/g ¹²⁸. In the work of Li et al. ¹²⁹, a
1029 controlled and straightforward two-step method was introduced for cultivating Ni-MOF arrays
1030 on the surface of NiCo₂O₄ nanowires by regulating the MOFs' formation reaction (**Fig. 6(b)**).

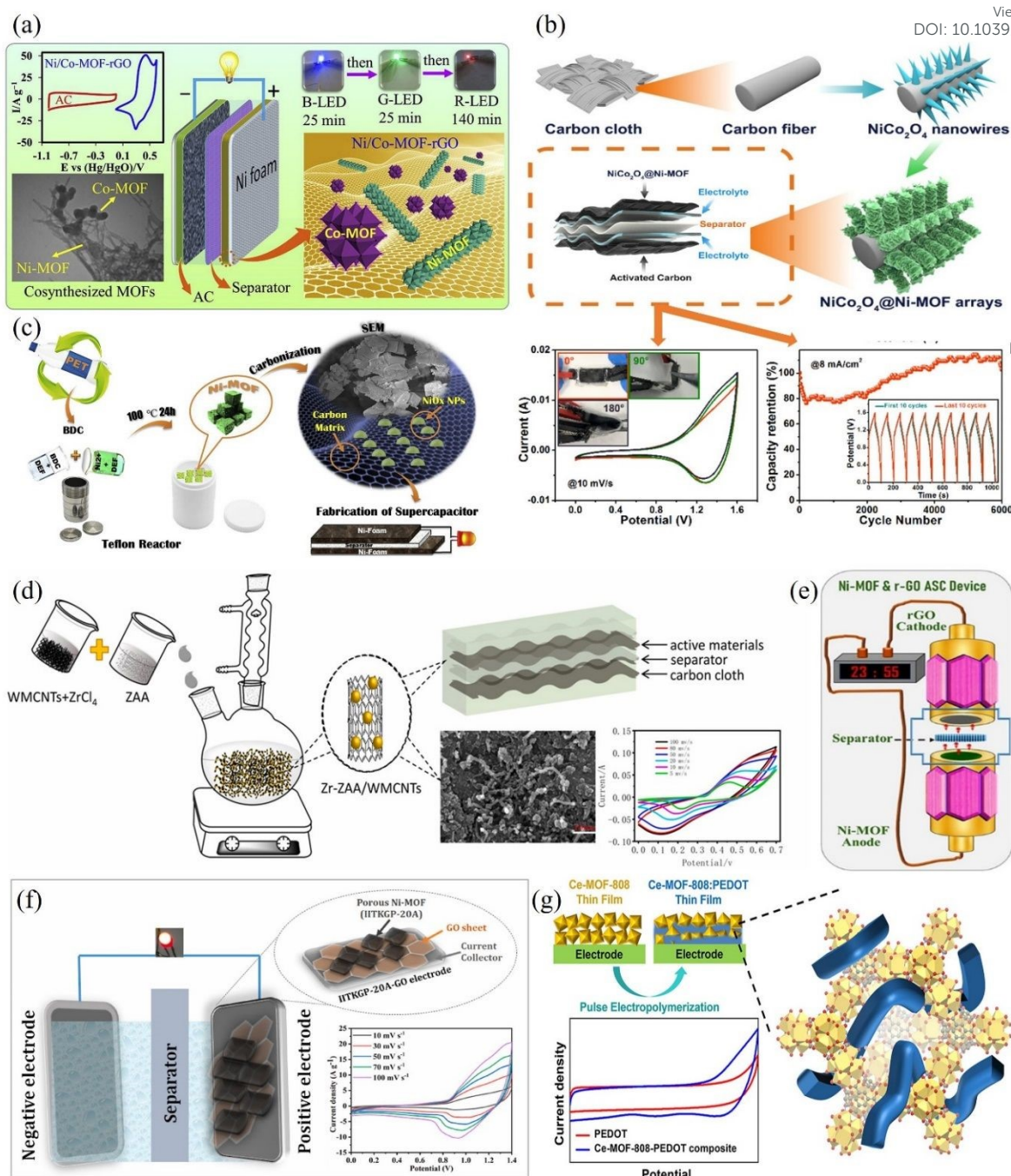


1031 The NiCo₂O₄@Ni-MOF hybrid electrode, after optimization, demonstrates improved
1032 electrochemical performance. It presents a notable specific capacity of 208.8 mA h/g at a
1033 current density of 2 mA/cm², alongside exceptional rate capability ¹²⁹.

1034
1035 Recent research focused also on the potential of using waste polyethylene terephthalate (PET)
1036 derived Ni-MOFs in the synthesis of NiOx@NPC nanocomposite (NiOx nanoparticles with
1037 nitrogenous porous carbon) ¹¹³. The simple solvothermal route used to synthesize this porous
1038 carbon composite has been described as cost-efficient. A schematic of the process can be seen
1039 in **Fig. 6(c)**. The BDC (benzene-1,4-dicarboxylic acid) utilised in this report's synthesis of the
1040 NiOx@NPC came from discarded PET bottles. The final product showed good specific
1041 capacitance, cyclic stability, and a high specific surface area (1523 m²/g). But nothing about
1042 whether it's appropriate for widespread implementation is mentioned ¹¹³. In another context, a
1043 novel electrode material comprising MOFs (Zr-TAA, where TAA stands for trans-aconitic acid)
1044 and multi-walled carbon nanotubes (MWCNTs) was easily synthesized using a one-pot reflux
1045 method and subsequently employed in a high-performance supercapacitor (**Fig. 6(d)**). Due to
1046 its improved conductivity and even distribution of pore sizes, this composite material exhibits
1047 outstanding electrochemical performance, achieving a specific capacitance of 562.06 F/g.
1048 Moreover, it retains nearly all of its initial capacitance even after undergoing 1000 cycles of
1049 testing with a 6 M KOH electrolyte ¹³⁰.

1050





1051

1052 **Fig. 6.** (a) An asymmetric AC//Ni/Co-MOF-rGO device showing a capacitance of
 1053 860 F/g@1.0 A/g in a 3E cell setup. Adopted from Ref. ¹²⁸ with permission. (b) A schematic
 1054 depiction of the synthetic method employed to create core/shell hybrid arrays of NiCo₂O₄@Ni-
 1055 MOF on a carbon cloth substrate and the corresponding CV curves, and cycling stability tested
 1056 at 8 mA/cm². Adopted from Ref. ¹²⁹ with permission. (c) Schematic diagram of the proposed
 1057 method of synthesizing NiO_x@NPC nanocomposites using waste PET with enhanced electrical
 1058 conductivity and stability and improved charge relocation operation for a better performance of
 1059 supercapacitor devices. Adopted from Ref. ¹¹³ with permission. (d) A novel electrode material,
 1060 composed of MOFs (Zr-TAA, where TAA is trans-acetic acid) and MWCNTs synthesized
 1061 using a simple one-pot reflux method and applied to high-performance supercapacitors.
 1062 Adopted from Ref. ¹³⁰ with permission. (e) A three-dimensional Ni-MOF used as an anode
 1063 electrode in a two-electrode asymmetric supercapacitor device setup. Adopted from Ref. ¹¹⁴



1064 with permission. (f) Highly scalable and pH stable 2D Ni-MOF-based composites (IITKGP
1065 20A-GO) for high-performance supercapacitors exhibiting a specific capacitance of ~ 840 F/g
1066 at 2 A/g current density. Adopted from Ref. ¹³¹ with permission. (g) A cerium-based
1067 MOF@conducting polymer (PEDOT) nanocomposites for supercapacitors. Adopted from Ref.
1068 ¹³² with permission.

1069

1070 A recent study has concentrated on developing a 3D Ni-MOF with an outstanding capacitance
1071 of 2150 F/g at a current density of 1A/g ¹¹⁴. Subsequently, the synthesized Ni-MOF and reduced
1072 graphene oxide were utilized as the anode and cathode electrode materials, respectively, in a
1073 two-electrode asymmetric supercapacitor device (ASC) setup (**Fig. 6(e)**). This ASC manifested
1074 a specific capacitance of 125 F/g (at 0.2 A/g) and showcased a high energy density of 50.17
1075 Wh/kg at a power density of 335.1 W/kg. Furthermore, the ASC demonstrated excellent
1076 reversibility (97.9% Coulombic efficiency) and cyclic stability (94%) after 5000 constant
1077 charge-discharge cycles. In the investigation by Sahoo et al. ¹³¹, a microporous 2D Ni-MOF
1078 was elaborated, demonstrating high scalability and thermodynamic stability across a wide pH
1079 range (2–10). Upon introducing GO with a weight percentage of 3%, a specific capacitance
1080 value of approximately 840 F/g at 2 A/g was achieved, ranking among the highest within the
1081 category of bare MOFs and their composites/derived materials. Subsequently, when used as the
1082 electrode material in an asymmetric supercapacitor (**Fig. 6(f)**), it displayed a specific
1083 capacitance of 111.4 F/g at a current density of 2 A/g and exhibited excellent retention of 84%
1084 cycle life over 7000 cycles ¹³¹.

1085

1086 The study by Wechsler et al. ¹³³ reported the fabrication of supercapacitor electrodes using
1087 pristine nickel hexaaminobenzene ($\text{Ni}_3(\text{HAB})_2$) metal-organic framework (MOF) via
1088 electrophoretic deposition (EPD). The symmetric supercapacitor employing the MOF
1089 showcases remarkable electrochemical capacitive performance within a potential range of 0–1
1090 V, demonstrating an areal capacitance of 13.64 mF/cm² and exceptional ultra-high cycling



1091 stability, maintaining 81% of its capacity over 50,000 cycles. The superior performance of the
1092 supercapacitor is attributed to the binder-free electrophoretic deposition (EPD) process and the
1093 distinctive structure of 2D MOF nanosheets, which promote ion diffusion throughout the
1094 electrodes. Additionally, the literature review explored the utilization of a combination of
1095 MOFs and conducting polymers. Nanocomposites were fabricated by combining a cerium-
1096 based MOF (Ce-MOF-808) with poly(3,4-ethylene dioxythiophene) (PEDOT) through pulse
1097 electrodeposition of PEDOT within thin films of Ce-MOF-808¹³². The highly porous Ce-MOF-
1098 808 displays reversible electrochemical reactivity, offering pseudocapacitance, while
1099 electronically conducting PEDOT contributes to a notable double-layer capacitance and
1100 enhances electronic conduction between the redox-active cerium sites in the MOF (**Fig. 6(g)**).
1101 As a result, the composite demonstrates superior performance compared to both pristine MOF
1102 and pristine electrodeposited PEDOT as active materials for supercapacitors¹³².

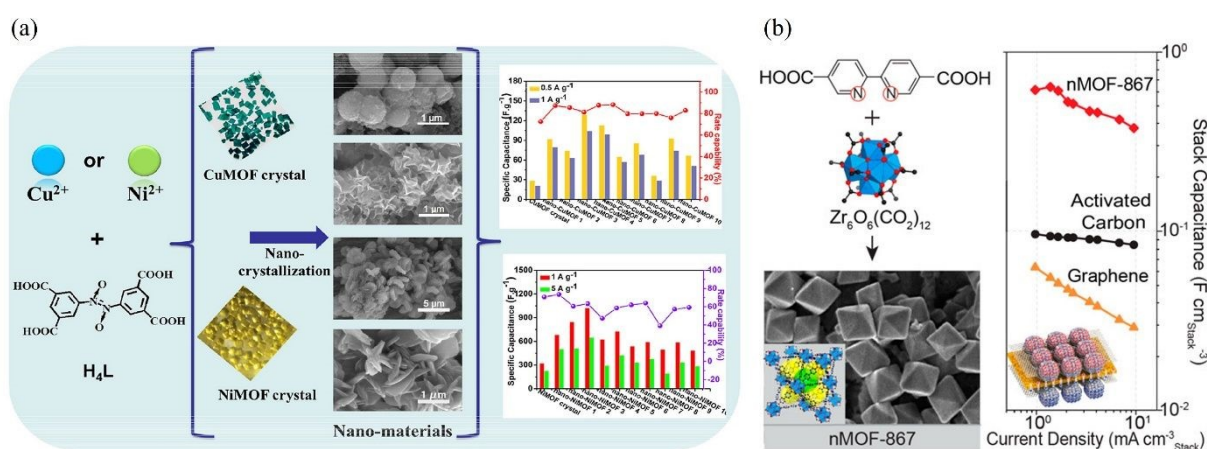
1103 3.2.2 Nanocrystalline MOFs

1104 Research has also advanced in the field of nanocrystalline MOFs (nMOFs) and coin-type cell
1105 SCs, this is another example of altering the morphologies of pristine MOFs to enhance their
1106 supercapacitive properties. Gu et al.¹¹⁹ posit that decreasing the particle size of MOFs into
1107 nanometre dimensions is an effective method for increasing their achievable capacitance.
1108 Particle size reduction improves the material's electrochemical performance significantly by
1109 lowering the electrolyte ion diffusion distance and raising the material's ESA¹³⁴. These nMOFs
1110 were not commonly reported until recently. Only a few well-known MOFs, like MOF-5, ZIF-
1111 8, and ZIF-67, attracted attention because of their composition, which made downscaling
1112 simple. A variety of brand-new nMOFs have been developed and tested as part of recent
1113 research. Gu et al.¹¹⁹ begin by synthesizing two MOF crystals via the adoption of the redox-
1114 organic linker from 3,3',5,5'-oxybenzobenzene tetracarboxylic acid (H₄L) and metal centres
1115 of Ni²⁺/Cu²⁺ (**Fig. 7(a)**). An in-situ solvothermal procedure was used in a single step to obtain



1116 the appropriate nanomaterials. One significant finding was that, with careful choice of solvent
 1117 and surfactant, the different morphologies attained during material production could be
 1118 efficiently controlled. When evaluated at current densities of 1 A/g and 5 A/g, respectively, one
 1119 sample of the as-synthesised nano-NiMOF electrode produced capacitances of 1024.4 F/g and
 1120 648.9 F/g, demonstrating exceptional SC performance ¹¹⁹.

1121
 1122 Work by Choi et al. ¹³⁵ explores the synthesis of a range of nMOF structures including HKUST-
 1123 1, Zr-MOF, nMOF-867, and MOF-5. The nMOF-867 sample exhibited very good
 1124 supercapacitive behaviour, achieving a capacitance of 5.085 mF/cm², almost 6 times higher
 1125 than the achievable capacitance from a fabricated electrode using commercially available AC
 1126 (**Fig. 7(b)**). After 10,000 charge-discharge cycles, the nMOF-867 electrode continued to show
 1127 exceptionally good cyclic stability, with a retention of over 90%. With a capacitance of 5.085
 1128 mF/cm², the Zr-MOF sample under evaluation demonstrated exceptional supercapacitive
 1129 qualities. This is nearly a 6-fold increase above the capacitance provided by an AC electrode
 1130 made from commercially available AC. Additionally, the Zr-MOF electrode demonstrated
 1131 exceptionally high cyclic stability (greater than 90%, which is considered ultrahigh) even after
 1132 10,000 cycles ¹³⁵.



1133
 1134 **Fig. 7.** (a) *In-situ* solvothermal synthesis of nanoscale CuMOF and NiMOF crystals and their
 1135 specific capacitance (1024.44 F/g and 128.82 F/g for nano-NiMOF and nano-CuMOF
 1136 respectively) and rate capacitance. Adopted from Ref. ¹¹⁹ with permission. (b) Nanocrystals



1137 nMOF-867 with exceptionally high capacitance showing a stack and areal capacitance of 0.64
1138 and 5.09 mF cm², respectively, with performance maintained over at least 10,000
1139 charge/discharge cycles. Adopted from Ref. ¹³⁵ with permission.

1140
1141 Some 2-dimensional (2D) MOFs with a high SSA and tuneable porosity have been discovered
1142 recently. In their pure state, these MOFs can give sufficiently high electrical conductivity for
1143 SC applications ¹³⁶. Charge delocalisation inside the material's planes and prolonged pi-
1144 conjugation provide this electrical conductivity ¹³⁷. Sheberla et al. ¹³⁶ observed MOF
1145 Ni₃(HITP)₂'s high bulk electrical conductivity (over 5000 S/m), a value that exceeds those
1146 achieved by AC and porous graphite. The first non-carbon-based EDLC symmetric SC was
1147 fabricated using Ni₃(HITP)₂ electrodes after this discovery. After 10,000 cycles, the
1148 supercapacitor showed an extremely high areal capacitance of 18 mF/cm², and 90% capacity
1149 retention ¹³⁶. Another 2D MOF that has been investigated for high-performing SC electrodes is
1150 hexaaminobenzene (HAB)-derived MOF. Feng et al. ¹³⁸ reported both a high volumetric and
1151 areal capacitance (760 F/cm³ and 20 F/cm² respectively). The cycle life data were similarly
1152 encouraging, demonstrating that capacitance retention could only be increased by a factor of 10
1153 after 12000 charging-discharging cycles. Research indicates that selecting the right electrolyte
1154 is essential for optimal SC performance. In one experiment, a 1 M LiOH aqueous electrolyte
1155 and a Co-based MOF electrode operated at a current density of 0.6 A/g produced a specific
1156 capacitance of 206.76 F/g ¹²³. Furthermore, retention of this capacitance was good (up to 98.5%)
1157 over 1000 test cycles. Although, when the electrolyte was changed to KCl or KOH, the
1158 performance of the electrode was not satisfactory.

1159 3.2.3 Environmental impacts

1160 Literature focusing on MOF toxicity is limited, and the topic is generally poorly understood ¹²⁵.
1161 If a MOF is toxic, this is likely the result of the organic ligand metal ions or functional groups
1162 ¹³⁹. The metal ions in MOFs are in the form of nanoparticles that are nonbiodegradable ¹²⁵.



1163 Kumar et al.¹²⁵, have suggested that out of the most common metal ions in MOFs, zinc and
1164 iron are likely to be the least toxic as they are used in the human body. While the toxicity of
1165 MOFs may not be fully known, some sources suggest that when MOFs decompose, they may
1166 exhibit the same toxicity levels as constituent raw materials from which they are generated. In
1167 summary, when considering the environmental impact of MOFs, several factors come into play:
1168 (1) Synthesis process: The synthesis of MOFs often involves solvents and energy-intensive
1169 processes. Depending on the specific synthesis route, this could contribute to environmental
1170 impacts such as greenhouse gas emissions and resource depletion. However, efforts are being
1171 made to develop more sustainable synthesis methods, such as using green solvents or employing
1172 energy-efficient techniques. (2) Resource utilization: The materials used in MOF synthesis,
1173 such as metal ions and organic ligands, can have environmental implications depending on their
1174 sources and extraction methods. For example, if the extraction of metal ions involves
1175 environmentally damaging processes or if rare or toxic elements are used, it could pose
1176 environmental concerns. (3) End-of-life disposal: Consideration should be given to the disposal
1177 of MOF-based supercapacitors at the end of their lifespan. While MOFs themselves are
1178 generally stable materials, the electrodes and other components of supercapacitors may contain
1179 metals or other materials that could pose environmental risks if not properly managed through
1180 recycling or safe disposal methods. (4) Performance and durability are key considerations for
1181 MOF-based supercapacitors. These devices have inherent advantages such as high surface area
1182 and customizable pore structures, which can significantly improve their performance. If MOFs
1183 can facilitate the development of supercapacitors with greater energy density and prolonged
1184 cycle life compared to conventional materials, it could have a positive impact on the
1185 environment. By extending the lifespan of electronic devices and minimizing the frequency of
1186 replacements, this advancement has the potential to reduce environmental impacts. (5) Scale of
1187 production: As with any technology, the environmental impact of MOF-based supercapacitors

View Article Online
DOI: 10.1039/D4TA03877K



1188 will depend on the scale of production and deployment. Large-scale production could lead to
1189 increased energy consumption, waste generation, and resource depletion if not managed
1190 properly. The environmental impact and sustainability of Metal-Organic Frameworks (MOFs)
1191 used in supercapacitors necessitate a thorough examination, particularly when compared to
1192 traditional materials. MOFs like nMOF-867 exhibit superior electrochemical properties, with a
1193 stack capacitance of 0.644 F cm^3 and an areal capacitance of 5.085 mF cm^2 , far surpassing
1194 commercial activated carbon supercapacitors ¹⁴⁰.

1195 However, most of the methods for MOF synthesis incorporate eco-toxic solvents, such as N,N-
1196 dimethylformamide, coupled with high energy requirements, which may pose a serious
1197 environmental impact. Therefore, an in-depth LCA is needed in estimating these materials. For
1198 instance, high carbon footprint and energy use can be associated with the production of MOFs;
1199 for instance, nMOF-867 is associated with high environmental cost despite its high performance
1200 and long lifetime, maintaining activity beyond 10,000 cycles ¹⁴¹. Moreover, the environmental
1201 advantages of MOFs like UiO-66-NH₂, which can be synthesized using aqueous methods
1202 reducing environmental impacts by up to 91%, must be weighed against challenges such as
1203 degradation and scalability. These methods yield a cradle-to-gate carbon footprint of 43 kg CO_2
1204 eq/kg and a lower production cost of $\$15.8/\text{kg}$ compared to solvothermal processes ¹⁴². On the
1205 long-term sustainability front, MOFs still hold much promise because green synthesis methods
1206 using either water or ethanol as solvents have already been developed, and biodegradable MOFs
1207 that can minimize their impact on the environment are under construction. Although this might
1208 be the case, there is a clear lack of long-term data relating to MOF recyclability and degradation,
1209 and their high initial production costs underline the necessity for performing holistic LCA with
1210 respect to end-of-life disposal and possible environmental release to make such next-generation
1211 materials more environmentally and economically feasible against traditional ones ¹⁴³.



1213 3.3 Metal-organic frameworks for battery technologies

1214 MOFs and their derivatives have accommodated much interest and proved rather promising to
1215 improve sodium-ion batteries (SIBs), and lithium-ion batteries (LIBs) performance. The work
1216 by Zhao et al.¹⁴⁴ proved the potential of Prussian blue analogues (PBAs) as SIB cathode
1217 material through effective etching. Specifically, etching $\text{Na}_2\text{NiFe}(\text{CN})_6$ (NaNiHCF) into a dice
1218 shape increased its specific surface area, enhancing sodium storage sites and accelerating Na^+
1219 diffusion. The etched NaNiHCF-3 showed a large reversible capacity of 83.5 mAh/g that
1220 accounted for about 98.2 % relative to the theoretical capacity, while the unetched counterpart
1221 precursor only delivered 76.8 mAh/g. Moreover, NaNiHCF-3 exhibited 71.2 mAh/g at 10 C
1222 with a rate capability far beyond that of other electrodes and maintained a very stable life with
1223 94% capacity retention over 1,000 cycles at 1 C. These results further underline the role of
1224 morphological control in the electrochemical performance of MOFs with respect to capacity
1225 use and cycling stability. Indeed, the tunable porosity and high surface area of MOFs enable
1226 theoretically improved ion transport and storage capabilities. For example, nitrogen-doped
1227 amorphous Zn-carbon multichannel fibers have exhibited a Coulombic efficiency above 99%
1228 for more than 500 cycles at current densities from 1 to 5 mA cm^2 , demonstrating major
1229 improvements in lithium metal anode performance. Symmetric cells based on these materials
1230 achieve stable cycling for over 2,000 hours, which is the potential for long-term applications
1231¹⁴⁵. However, the synthesis process is complex due to electrospinning and MOF coating, and
1232 this complicates large-scale production. The specific capacity of 104 mAh/g during the high
1233 rate of 5 C in the full-cell tests with LiFePO_4 cathodes is quite encouraging, but its broader
1234 compatibility with various cathode materials remains to be explored. While these MOF-derived
1235 materials could effectively reduce dendrite formation and issues regarding local current density,
1236 the long-term stability in a range of environmental conditions remains to be evaluated.

1237



1238 Always in the context of LIBs, the study of Du et al.¹⁴⁶ presents an efficient synthesis of 2D
1239 layered Mo-MOF@PPy via reflux heating and coating methods, aimed at improving the
1240 performance of anode materials in LIBs. Serving as a precursor during the electrochemical
1241 reaction, the high-valence Mo within the Mo-MOF effectively binds with Li⁺, thereby
1242 contributing to the superior electrochemical performance of the material. Additionally, the
1243 polypyrrole (PPy) coating significantly enhances the electrical conductivity of the composite
1244 by promoting electron transfer. As a result of these synergistic effects, Mo-MOF@ppy achieves
1245 a specific capacity of 930 mAh/g at a current density of 100 mA/g and retains a capacity of 750
1246 mAh/g at 500 mA/g after 200 cycles. In a similar study, Zhao et al.¹⁴⁷ utilized stannous sulfate
1247 (SnSO₄) and graphene to synthesize Sn-MOFs/G nanorods, which were evaluated as anode
1248 materials for LIBs. The resulting material exhibited a high specific capacity of 462 mAh/g after
1249 500 cycles at 1 A/g and demonstrated remarkable rate performance, achieving 265 mAh/g at 2
1250 A/g.

1251
1252 In detail, recent progress involving MOFs and MOF-derived materials has unveiled their huge
1253 potential towards enhancing the performance of batteries. For example, the synthesis of copper-
1254 substituted CoS₂@CuxS DSNBs by a multistep MOF-based templating strategy possessed very
1255 impressive electrochemical properties, such as high capacity (535 mAh/g at 0.1 A/g), better rate
1256 capability (333 mAh/g at 5 A/g), and extended cycling stability (76% capacity retention over
1257 300 cycles)¹⁴⁸. The improvements may be attributed to their complex nanostructure, which
1258 provided enhanced ionic and electronic conductivity, improved electrochemical reactivity, and
1259 mechanical stability. In this respect, this approach can overcome the poor conductivity and fast
1260 capacity fading of sulfur metal through the combination of different active materials with
1261 hierarchical hollow structures, which can reduce ion diffusion paths and strain accommodation
1262 during cycling. Rational design and controlled composition, as emphasized in the present work,
1263 are preliminary steps for the development of high-performance anode materials, and this work



1264 further confirms the bright application of MOF-derived materials in next-generation batteries.

View Article Online
DOI: 10.1039/D4TA03877K

1265 Although these results are very promising, problems like intrinsic instability of MOFs in
1266 electrolyte environments and scalability issues, coupled with generally low electrical
1267 conductivity, have to be resolved before their full potential is tapped. Therefore, future studies
1268 should address the issues of scalability and stability if the full potential of MOFs in battery
1269 applications is to be exploited, ensuring technological advancement with sustainability.

1270
1271 The main advantage of MOFs over activated carbon in energy storage devices lies in their
1272 highly tunable structure and functional versatility. MOFs are composed of metal nodes
1273 connected by organic linkers, allowing precise control over pore size, shape, and surface
1274 chemistry. This tunability enables the design of materials with optimized ion transport and
1275 storage, potentially leading to higher capacitance and energy density. Unlike activated carbon,
1276 which often has a broad and irregular pore size distribution, MOFs can be synthesized with
1277 uniform and well-defined pores, ensuring consistent ion diffusion and reducing resistance
1278 during charge-discharge cycles. Additionally, the organic linkers in MOFs can be chemically
1279 modified to introduce specific functional groups that enhance interactions with electrolyte ions,
1280 while the metal centers can be selected or doped to introduce redox activity, contributing
1281 additional pseudocapitance. MOFs can also encapsulate or host other functional materials,
1282 further enhancing their electrochemical performance by providing additional active sites or
1283 improving electrical conductivity. This versatility in synthesis and integration with conductive
1284 materials makes MOFs a promising material for next-generation supercapacitors, offering the
1285 potential for higher energy densities, improved ion transport, and customizable electrochemical
1286 properties. However, challenges such as low conductivity, stability, and cost still need to be
1287 addressed for MOFs to become a widely adopted alternative in commercial applications.



1288 **3.4 MOF metal nodes, ligand architecture and synthesis strategies**

View Article Online
DOI: 10.1039/D4TA03877K

1289 In MOFs, the metal nodes, also known as metal clusters or secondary building units (SBUs),
1290 play a pivotal role in determining the structure and properties of these materials. These nodes
1291 form the inorganic backbone of the MOF and are interconnected by organic ligands to create
1292 an extended porous network. The composition of these nodes can vary widely, ranging from
1293 simple single metal ions like Zn^{2+} , Cu^{2+} , or Fe^{3+} , which can coordinate with multiple ligands,
1294 to more complex metal clusters such as $Zr_6O_4(OH)_4$ or Cr_3O , which involve multiple metal ions
1295 linked together, contributing to the stability and diversity of the MOF structure ¹⁴⁹. The
1296 coordination environment of the metal nodes, defined by the number of ligands or atoms bonded
1297 to the metal ion, is crucial in determining the geometry of the node, which in turn influences
1298 the overall topology and dimensionality of the MOF. For example, a metal node with a high
1299 coordination number can lead to the formation of highly connected, three-dimensional
1300 frameworks, whereas lower coordination numbers might result in simpler, two-dimensional or
1301 even one-dimensional structures.

1302
1303 The metal nodes not only shape the structural framework but also impart distinct chemical
1304 properties to the MOF. The choice of metal can significantly influence attributes such as
1305 thermal stability, chemical reactivity, and catalytic activity. Transition metals like chromium
1306 (Cr), zirconium (Zr), or titanium (Ti) are known for imparting higher stability and robustness
1307 to the MOF, making them suitable for applications that require durability. On the other hand,
1308 metals like copper (Cu) or zinc (Zn) offer tunable reactivity, which can be advantageous in
1309 catalytic processes. Metal nodes also play a critical role in the functionality of MOFs. For
1310 instance, they can act as active sites for catalysis, with MOFs containing iron (Fe) or cobalt
1311 (Co) nodes being explored for oxidation reactions ^{150,151}. Additionally, the type of metal used
1312 in the nodes affects the adsorption characteristics of the MOF, particularly in gas adsorption



1313 applications. MOFs with unsaturated metal sites, such as those with open metal sites, can
1314 strongly adsorb gases like CO₂ or H₂, making them valuable for gas storage and separation
1315 technologies.

1316
1317 Moreover, the electrical properties of MOFs are influenced by the metal nodes, which is
1318 particularly important in applications such as supercapacitors and batteries, where conductivity
1319 is essential. Metal nodes can also be tuned through post-synthetic modifications, allowing for
1320 the enhancement or alteration of the MOF's properties. This can be achieved through metal
1321 exchange or doping, introducing new functionalities or improving stability. For example, in
1322 MOFs like HKUST-1, which utilizes Cu²⁺ ions as the metal node, the resulting structure is a
1323 robust three-dimensional framework that has been widely studied for gas storage ¹⁵². Similarly,
1324 MIL-101, which contains Cr³⁺ ions, is renowned for its exceptional thermal and chemical
1325 stability, making it suitable for various industrial applications ¹⁵³. Another notable example is
1326 UiO-66, where Zr⁴⁺ ions provide high stability, making it a popular choice for gas storage and
1327 separation ¹⁵⁴. Overall, metal nodes are a crucial design element in MOFs, as they not only
1328 determine the structural framework but also significantly influence the functional properties,
1329 making them central to the development of advanced materials for a wide range of applications.

1330
1331 On the other hand, ligand architecture in MOFs is a crucial determinant of their structural
1332 integrity, topology, and functional properties. Organic ligands, or linkers, connect metal nodes
1333 or clusters to form the extended porous networks characteristic of MOFs. The size and shape
1334 of these ligands significantly influence the MOF's pore dimensions and overall framework
1335 ^{155,156}. For instance, longer ligands typically create larger pores, which can be advantageous for
1336 applications like gas storage or catalysis, while the geometric arrangement of the ligands
1337 whether linear, angular, or branched affects the dimensionality and complexity of the MOF



1338 structure. Functional groups on the ligands, such as carboxylates, phosphonates, imidazolates,
1339 or sulfonates, play a pivotal role in determining the strength and nature of the coordination
1340 bonds with metal nodes, impacting the MOF's stability and reactivity. For example, carboxylate
1341 groups form strong bonds with metal ions, leading to highly stable frameworks like those in
1342 UiO-66, while functional groups such as amines or hydroxyls can enhance adsorption properties
1343 by introducing sites for hydrogen bonding ¹⁵⁴. The connectivity of the ligands how many
1344 coordination sites they offer affects the density of the network and the robustness of the
1345 resulting MOF. Ligands with higher connectivity can create more intricate and stable 3D
1346 frameworks, as seen in HKUST-1, where the bidentate trimesic acid ligand coordinates with
1347 multiple metal ions ¹⁵⁷. Additionally, the coordination mode of the ligand, whether
1348 monodentate, bidentate, or multidentate, influences the rigidity and stability of the framework.
1349 Ligand architecture can also be tuned through post-synthetic modifications, allowing for the
1350 introduction of new functionalities or enhancements, such as improved CO₂ capture capacities
1351 through the addition of amine groups. Examples of MOFs that showcase the importance of
1352 ligand architecture include the IRMOF series, which utilizes terephthalic acid ligands to form
1353 various frameworks with different properties, and ZIFs (Zeolitic Imidazolate Frameworks),
1354 where the imidazolate ligands create highly stable, zeolite-like structures ^{158,159}

1356 Regarding the synthesis of MOFs, it encompasses a variety of methods, each tailored to achieve
1357 specific structural, compositional, and functional characteristics in the final material ¹⁶⁰.
1358 Hydrothermal synthesis involves dissolving metal salts and organic ligands in water, followed
1359 by heating the solution in a sealed container under high temperature and pressure. This method,
1360 widely used for its simplicity, produces high-quality MOF crystals, as seen in the synthesis of
1361 UiO-66, where zirconium chloride reacts with terephthalic acid ¹⁶¹. Solvothermal synthesis, a
1362 variant that uses organic solvents instead of water, allows for the formation of MOFs that are



1363 sensitive to water or require particular solvents for solubility, such as HKUST-1, which is
1364 synthesized using a solvent system involving alcohols and acetic acid ¹⁶². Ligand-assisted
1365 synthesis leverages pre-formed metal-organic complexes to guide the growth of MOFs,
1366 enhancing uniformity and control over the final product's properties.

1367

1368 Microwave-assisted synthesis of MOFs is grounded in the principle of using electromagnetic
1369 radiation to interact with removable electronic components, such as electrons, ions, or polar
1370 molecules in solids, or ions and electrons in liquids. This method typically operates at
1371 temperatures above 100°C and within reaction times of no more than 60 minutes. Improvements
1372 in reaction conditions can be achieved by optimizing various factors, including the choice of
1373 solvent, duration of radiation exposure, temperature, intensity of microwave radiation, and the
1374 quantities of reactants. Adjusting these variables helps to enhance the efficiency and quality of
1375 the MOF synthesis process ¹⁶³. Electrochemical synthesis utilizes an electric current to drive
1376 the formation of MOFs from metal salts and ligands, allowing precise control and the creation
1377 of MOFs with unique properties, including thin films or coatings on conductive substrates.
1378 Moreover, solvothermal-hydrothermal hybrid synthesis combines aspects of both methods,
1379 using a solvent system that interacts with both water and organic components, useful for
1380 synthesizing MOFs with specific property balances. Post-synthetic modification, though not a
1381 primary synthesis method, involves altering the MOF framework after its initial formation
1382 through techniques like ligand exchange or metal ion substitution, tuning the MOF's
1383 functionality and stability for specialized applications. Direct synthesis from metal oxides uses
1384 metal oxides or salts directly to form MOFs in the presence of organic ligands under controlled
1385 conditions, advantageous for creating highly stable frameworks. Each of these methods offers
1386 unique advantages depending on the desired MOF properties, such as crystal size, pore



1387 structure, stability, and functional capabilities, making them crucial for tailoring MOFs to
1388 specific applications ^{164,165}.

1389 **4. Photocatalysis**

1390 In 1972, Fujishima and Honda's pioneering work saw the creation of the first photocatalytic
1391 system using TiO₂ and ultraviolet light irradiation ¹⁶⁶. Since then, a variety of materials have
1392 been investigated for photocatalysis applications. As noted by Djurišić et al. ¹⁶⁷, there have been
1393 few advancements or breakthroughs in photocatalyst concepts and designs. The majority of
1394 current research shows only modest advancements, and if photocatalytic technologies are to
1395 ever be used on an industrial scale, a significant amount of research and development will be
1396 needed. The standards for an effective photocatalyst are generally agreed upon in the literature.
1397 The material's characteristics should, in general, permit well-visible light absorption, sufficient
1398 degree of resistance to photo corrosion and ideally should inhibit the recombination of electron-
1399 hole pairs ¹⁶⁸. Work by Dhakshinamoorthy et al. ¹⁶⁹ further stresses the importance of
1400 responsiveness to visible light to ensure the efficient use of solar energy, by emphasizing that
1401 visible light makes up 43% of total solar energy. Shanmugham et al. ¹⁶⁸ provide a range of ideal
1402 photocatalyst material properties to help achieve these goals, including a high surface area,
1403 narrow band gap, and thermal stability. In addition, several papers agree on the importance of
1404 photocatalyst morphology and structure for performance as it influence the surface area and the
1405 availability of active sites.

1406 **4.1 Conventional photocatalytic materials**

1407 Photocatalysis is a transformative technology that leverages light to drive chemical reactions,
1408 offering innovative solutions in various fields including environmental remediation, energy
1409 production, and chemical synthesis. At the heart of this technology are photocatalyst materials,
1410 which absorb photons and use this energy to facilitate or accelerate chemical processes. Among



1411 conventional photocatalyst materials are titanium dioxide (TiO_2), zinc oxide (ZnO), and carbon-
1412 based materials such as graphene oxide (GO), and reduced graphene oxide (rGO). Each of these
1413 materials has its strengths and limitations, so the choice of photocatalyst often depends on the
1414 specific application and the desired properties. Pawar et al.¹⁷⁰ hail titanium dioxide (TiO_2)
1415 nanoparticles as being among the most promising photocatalyst materials for commercial use.
1416 This is due to their superb optical and electronic characteristics, excellent chemical stability,
1417 high photoactivity, low cost, and reusability. Various morphologies of titania photocatalysts,
1418 spanning from nano to macrostructures, have been documented in the literature¹⁷¹. These
1419 encompass spherical particles, rod-like structures, tubular forms, fibrous configurations, and
1420 sheet-like arrangements at the nanoscale (**Fig. 8(a)**). These diverse morphologies have been
1421 meticulously designed to achieve distinct photocatalytic capabilities by fine-tuning factors such
1422 as particle size, specific surface area, pore structure and volume¹⁷¹. Research by Zhao et al.¹⁷²,
1423 however, emphasizes the disadvantages of semiconductor nanoparticles (NPs) such as TiO_2
1424 including a complex separation process from reaction systems, and a high rate of recombination
1425 of photogenerated electron-hole pairs. TiO_2 is also prone to aggregation in reactions which
1426 reduces its effective surface area and therefore performance.

1427
1428 In their work, Moma and Baloyi¹⁷³ postulate that the main issue with TiO_2 photocatalysts is the
1429 bandgap (3.2 eV). As a result, only 5% of the solar spectrum of the UV light region can be used
1430 for photocatalysis. TiO_2 has a low photocatalytic efficiency as a result. Research by Zhao et al.
1431¹⁷² supports this view, by arguing that this disadvantage is the primary hindrance preventing the
1432 use of TiO_2 in isolation for photocatalysis. To increase TiO_2 's efficiency, current research also
1433 attempts to enhance its photocatalytic activity under visible light irradiation¹⁷⁴. One method
1434 investigated is nitrogen-doped TiO_2 , results of such studies show enhanced photocatalytic
1435 activity compared to pure TiO_2 ¹⁷³. Recent studies suggest also that modifying the defects in



1436 TiO₂ can expand the range of light absorption and enhance the efficiency of charge separation.
1437 Various methods, including hydrogenation, plasma treatment, chemical reduction,
1438 electrochemical reduction, and oxidation (**Fig. 8(b)**)¹⁷⁵, are employed to produce defective
1439 TiO₂ photocatalysts. These catalysts exhibit different types of defects, encompassing bulk and
1440 surface defects, and their relevance in photocatalytic applications is documented¹⁷⁵. Notably,
1441 oxygen vacancies and Ti³⁺ defects are identified as pivotal factors in augmenting photocatalytic
1442 performance.
1443
1444 Due to the wide band gap of TiO₂, its application in visible photocatalysis is limited. To address
1445 this issue, several studies propose introducing oxygen vacancies and carbon quantum dots
1446 (CQDs) with up-conversion properties to enhance photocatalytic activity. Li et al.¹⁷⁶ prepared
1447 various configurations, including one-dimensional TiO₂ nanotubes (TNs), TNs with oxygen
1448 vacancies (OVTNs), TNs embedded with composite CQDs (CQD-TNs), and OVTNs
1449 embedded with composite CQDs (CQD-OVTNs). The impact of oxygen vacancies and CQDs
1450 on NO_x removal through photocatalysis was investigated. Results show that CQD-OVTNs
1451 exhibit a significant synergistic effect between CQDs and oxygen vacancies, enhancing visible
1452 photocatalytic NO removal efficiency by approximately 12, 2, and 2.6 times compared to TNs,
1453 OVTNs, and CQD-TNs, respectively (**Fig. 8(c)**)¹⁷⁶. Similarly, nitrogen-doped carbon quantum
1454 dots (NCQDs) were utilized to enhance TiO₂ through a simple hydrothermal-calcination
1455 synthesis method¹⁷⁷. The incorporation of NCQDs enhances visible light absorption and
1456 facilitates electron transfer, thereby improving the separation of photo-generated electron-hole
1457 pairs. Even with a low NCQDs content of 3 wt%, the photodegradation rate for methylene blue
1458 was 2.25 times faster compared to pristine TiO₂.
1459
1460 A plausible mechanism for the photocatalytic degradation of methylene blue (MB) by

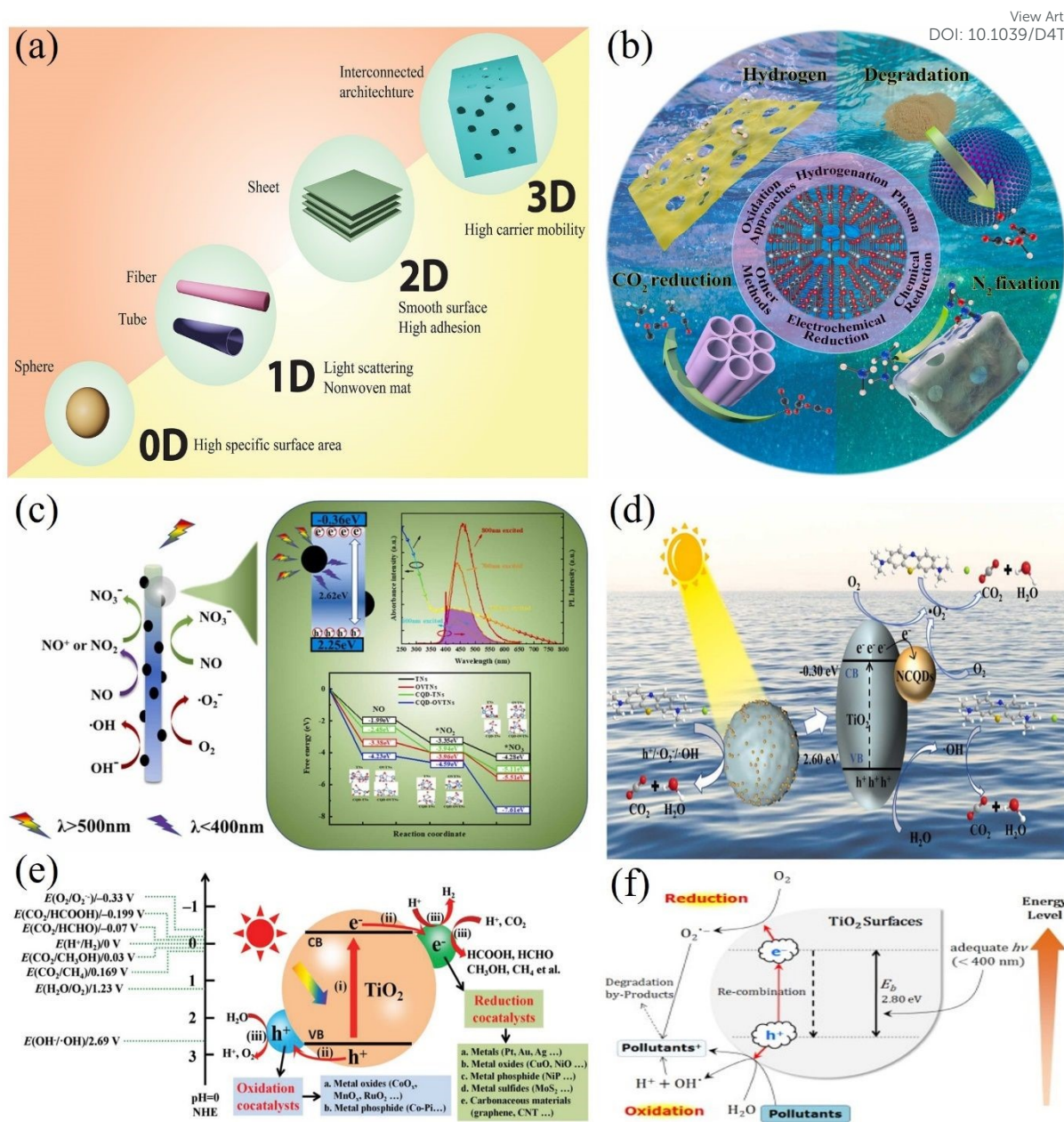


1461 NCQDs/TiO₂ is depicted in **Fig. 8(d)**¹⁷⁷. When exposed to sunlight, electrons within the
1462 valence band (VB) of TiO₂ absorb photon energy from solar radiation, generating electron (e⁻)
1463 hole (h⁺) pairs in the conduction band (CB) and VB, respectively. The e⁻ can readily combine
1464 with dissolved oxygen in water to form •O₂⁻. Furthermore, the h⁺ can oxidize OH⁻ and H₂O
1465 molecules adsorbed on the TiO₂ surface to produce •OH radicals. However, e⁻ and h⁺ often
1466 recombine with low efficiency, limiting photocatalytic activity. The introduction of nitrogen-
1467 doped carbon quantum dots (NCQDs) serves to enhance visible light absorption and promote
1468 charge transfer. Consequently, more photocarriers are generated, and their recombination is
1469 substantially suppressed, resulting in a notable increase in efficient active radicals.
1470 Consequently, with the combined action of h⁺, •O₂⁻, and •OH radicals, methylene blue (MB)
1471 molecules undergo mineralization to yield CO₂ and H₂O¹⁷⁷.

1472
1473 In a comprehensive photocatalytic process employing a TiO₂-based photocatalyst, three
1474 primary stages are involved: (1) absorption of light and the generation of photogenerated
1475 electron-hole pairs by TiO₂, (2) separation and transfer of these photogenerated electron-hole
1476 pairs, and (3) redox reactions occurring on the surface of TiO₂ and cocatalysts (as depicted in
1477 **Fig. 8(e)**). These consecutive steps collectively govern the overall photocatalytic effectiveness
1478 of TiO₂-based photocatalysts¹⁷⁸. On the other hand, to utilize semiconductor photocatalysts for
1479 water treatment, several requirements must be met: the process should be feasible at room
1480 temperature and pressure, ensuring complete mineralization without generating secondary
1481 pollution¹⁷⁹. In addition, it should enable repetitive cycles and maintain low operational costs.
1482 TiO₂ photocatalysis embodies a photo-induced charge separation process occurring on the TiO₂
1483 surface, which generates highly reactive oxygen species capable of microbial inactivation and
1484 organic mineralization without producing secondary pollutants.



1485



1486

1487 **Fig. 8.** (a) Various structural configurations of TiO_2 at both the nano and macro scales. Adopted
 1488 from Ref. ¹⁷¹ with permission. (b) A schematic diagram depicting the utilization of defective
 1489 TiO_2 materials in photocatalytic applications. TiO_2 photocatalysts are fabricated using various
 1490 methods such as hydrogenation, plasma treatment, chemical reduction, electrochemical reduction, and
 1491 oxidation. Adopted from Ref. ¹⁷⁵ with permission. (c) Oxygen vacancies and carbon quantum dots
 1492 (CQDs) with up-conversion properties for enhanced photocatalytic activity of TiO_2 for NO removal
 1493 under visible light irradiation. Adopted from Ref. ¹⁷⁶ with permission. (d) Mechanism for the degradation
 1494 of methylene blue using NCQDs/ TiO_2 under solar irradiation. Adopted from Ref. ¹⁷⁷ with permission.
 1495 (e) Illustration of the photocatalytic reactions occurring on TiO_2 -based photocatalysts, enhanced
 1496 with reduction and oxidation cocatalysts. The redox potentials of various species at pH = 0, referenced
 1497 to the NHE, are also depicted. Adopted from Ref. ¹⁷⁸ with permission. (f) Pollutant removal
 1498 through the generation of photoinduced charge carriers (e^-/h^+) on the surfaces of semiconductor
 1499 TiO_2 particles. Adopted from Ref. ¹⁷⁹ with permission.

1500



1501 The schematic representation depicted in **Fig. 8(f)**, illustrates the elimination of pollutants
1502 through the generation of photoinduced charge carriers (e^-/h^+) on the surfaces of
1503 semiconductor TiO_2 particles ¹⁷⁹. Upon exposure to UV light, the surface of TiO_2 catalysts
1504 suspended in water triggers photo-induced electrons in the conduction band to participate
1505 actively in reduction processes. Typically, they interact with dissolved oxygen in the air,
1506 resulting in the generation of superoxide radical anions. Meanwhile, the photo-induced holes in
1507 the valence band migrate to the surface of TiO_2 and react with adsorbed water molecules,
1508 leading to the formation of hydroxyl radicals ¹⁷⁹. It is worth noting that hydroxyl radicals ($\text{OH}\cdot$)
1509 play a crucial role as primary active species in the photocatalytic oxidation reaction.

1510
1511 Regarding the environmental impact, TiO_2 has been described as eco-friendly as not only is it
1512 reusable (for photocatalysis) but it is also non-toxic ^{170,180}, with Chen et al. ¹⁸¹ claiming it's "the
1513 most efficient and environmentally benign photocatalyst". However, there is concern over the
1514 potential effects of TiO_2 nanoparticles on humans and animals ¹⁸². Although the shape and
1515 magnitude of TiO_2 nanoparticle effects are mostly determined by the physical and chemical
1516 properties of the particles, research on the mechanistic toxicology of these particles indicates
1517 that they may induce genotoxicity, inflammation, and cell destruction. TiO_2 nanoparticles have
1518 been identified by the National Institute for Occupational Safety and Health as potentially
1519 carcinogenic to humans as a result ¹⁸². In their life cycle assessment (LCA), Wu et al. ¹⁸³
1520 evaluated the impact of nano- TiO_2 based on a range of synthesis routes. They discovered that
1521 physical synthesis approaches produced a greater environmental impact since they needed large
1522 amounts of supporting gas and substantial energy inputs. Chemical routes have a fair amount
1523 of impact, with upstream precursor production accounting for a large share of that impact.
1524 Because of the bacteria culture media utilised, biological channels also posed a significant
1525 environmental impact. Because organic precursors required large amounts of organic solvents,



1526 they performed especially poorly. The LCA model included a freshwater ecotoxicity evaluation
1527 factor to account for the possibility of nano-TiO₂ leakage into water sources. It is crucial to
1528 remember that while appropriate modelling assumptions have been made and some TiO₂
1529 production pathways are not covered by this LCA, total correctness cannot be guaranteed ¹⁸³.

1530
1531 On the other hand, TiO₂ is generally considered cost-effective for photocatalytic uses ¹⁸⁰.
1532 Furthermore, novel cost-effective production methods are still being developed. An example is
1533 the facile sequential calcination and ball milling strategy ¹⁸⁴. It was stated that a post-treatment
1534 procedure was developed for less expensive TiO₂ photocatalysts with lower photocatalytic
1535 activity. The straightforward and affordable method seeks to raise the less expensive TiO₂
1536 photocatalysts' photocatalytic activity to the same degree as more expensive commercial
1537 counterparts with higher photoactivities. This procedure about ninety-fold improves the
1538 performance of inexpensive KA100 in lab testing. In addition to TiO₂, zinc oxide (ZnO) and
1539 carbon-based materials have garnered significant attention as photocatalysts due to their
1540 excellent transport properties, affordability, and versatile morphological structures. In the work
1541 of Sansenya et al. ¹⁸⁵, photocatalyst based on ZnO with a specific surface area of about 10.6
1542 m²/g were prepared. The materials have demonstrated high photodegradation capacity of
1543 reactive red 141 (R141), Congo red (CR), and Ofloxacin after 20, 60, and 180 minutes of solar
1544 light irradiation, respectively. The stability of the photocatalyst was confirmed after three
1545 cycles of use, maintaining high performance even after the third cycle, indicating its promising
1546 reusability. In similar context, silver was incorporated into ZnO photocatalysts at varying
1547 concentrations, exhibited a hexagonal phase with notable performance under visible light and
1548 improved anti-photocorrosion properties ¹⁸⁶. Complete removal of reactive red dye and
1549 ofloxacin antibiotic was achieved after 25 and 80 minutes of irradiation, respectively. The
1550 enhanced photocatalytic activity is attributed to the efficient separation of electron-hole pairs



1551 at the photocatalyst interface. The introduction of metallic silver onto the ZnO photocatalyst
1552 creates a Schottky barrier at the silver/ZnO interface, which enhances quantum efficiency and
1553 photocatalytic activity.

1554
1555 Kim et al.¹⁸⁷ introduced a novel, high-efficiency catalyst based on a boron-doped C₃N₄/ZnO

1556 composite. This composite demonstrated a significantly enhanced photocatalytic hydrogen
1557 evolution rate, approximately 2.9 times greater than that of undoped C₃N₄/ZnO. This is a
1558 straightforward and effective approach for designing highly efficient heterojunction

1559 photocatalysts by utilizing charge transfer switching via doping. Recently, it has been found
1560 that decorating the Rh co-catalyst of the benchmark GaN–ZnO photocatalyst with Al₂O₃ species
1561 via atomic layer deposition significantly mitigates reverse reactions¹⁸⁸. This modification

1562 enhances photocatalytic oxygen water splitting (OWS) activity by more than an order of
1563 magnitude, with an apparent quantum efficiency increasing from 0.3 to 7.1% at 420 nm. The
1564 partial coverage of Rh surface sites with inert Al₂O₃ effectively suppresses reverse reactions by

1565 obstructing the reduction/oxidation cycle of Rh atoms during the photocatalytic OWS process.
1566 Moreover, combining ZnO with carbon-based materials, such as graphene oxide, can further
1567 enhance its photocatalytic properties. Indeed, an efficient photocatalyst was successfully

1568 synthesized using GO/ZnO nanocomposites with embedded metal nanoparticles through a
1569 simple one-pot method¹⁸⁹. A catalytic activity of 84% for the degradation of methylene blue
1570 (MB) dyes was achieved with a nanocomposite containing 3.125% GO after 90 minutes of

1571 sunlight irradiation. Thus, the GO–ZnO–Ag nanocomposite demonstrates significant potential
1572 as an efficient and adaptable photocatalyst for the photodegradation of organic dyes in industrial
1573 wastewater. In another work, the photocatalytic degradation of Rhodamine B (RhB) and MB

1574 by a material comprising sol-gel synthesized ZnO nanochips, GO and RGO was discussed¹⁹⁰.
1575 Results indicated that ZnO nanochips integrated onto graphene sheets exhibited enhanced



1576 photocatalytic activity, achieving approximately 76.5–98.9% degradation of RhB and MB
1577 within 90 minutes of visible light irradiation. Furthermore, ZnO@RGO demonstrated superior
1578 photocatalytic performance compared to ZnO@GO, with approximately 2.4 and 2 times higher
1579 kinetic rates for the removal of RhB and MB, respectively.

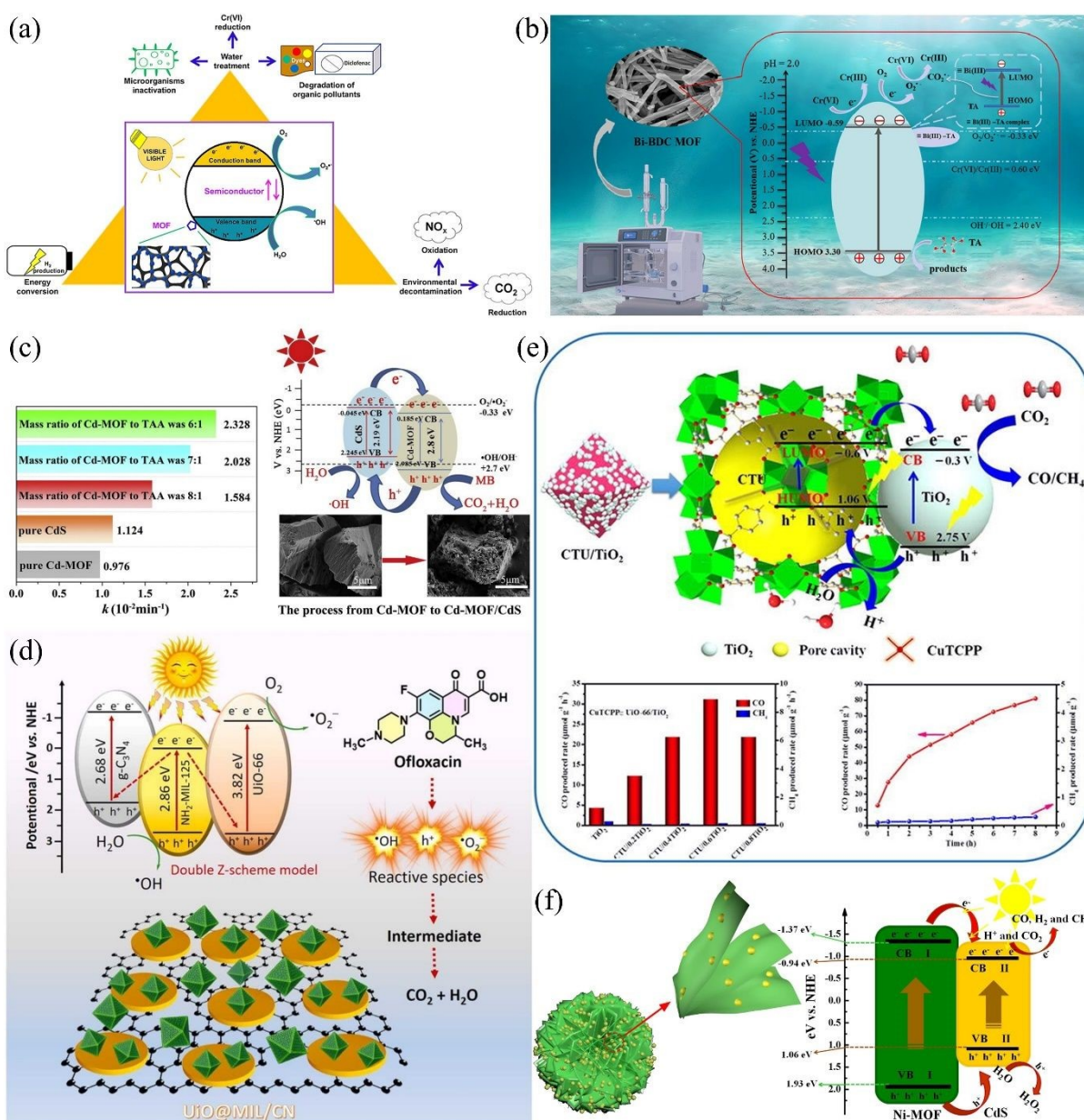
1580
1581 Common materials like TiO₂, ZnO, and GO are popular photocatalysts, but they have notable
1582 limitations compared. TiO₂ and ZnO both have wide band gaps (~3.0-3.2 eV and ~3.2 eV,
1583 respectively), restricting their activity to UV light, which limits their effectiveness under visible
1584 light. Both materials also suffer from rapid recombination of electron-hole pairs, reducing their
1585 photocatalytic efficiency. Additionally, TiO₂ and ZnO have lower surface areas, limiting the
1586 number of active sites, and ZnO is further hampered by photo corrosion under UV light. GO,
1587 while possessing a high surface area, offers limited photocatalytic activity on its own and
1588 primarily functions as a support material. Its variable band gap and the complexity of reducing
1589 GO to rGO for enhanced activity also pose challenges. In contrast, MOFs offer greater
1590 flexibility with tunable band gaps, higher surface areas, and versatile functionalization options,
1591 making them superior photocatalysts for a wide range of applications.

1592 4.2 Metal organic frameworks as photocatalysts

1593 Heterogeneous photocatalysis (HP) stands as an advanced oxidation method that has surfaced
1594 as a promising alternative with a broad spectrum of applications. These applications include
1595 treating effluents for decontamination and disinfection, addressing environmental challenges
1596 related to pollutants like CO₂ and NO_x in the atmosphere, and facilitating energy conversion.
1597 These are among the most prevalent and widespread uses of this technology. In this context,
1598 metal-organic frameworks (MOFs) have been developed to enhance the characteristics and
1599 photocatalytic capabilities of conventional semiconductors. MOFs have emerged as innovative
1600 photocatalysts due to their intrinsic structural features, which include vast surface area,



1601 organised porous structure, and structural diversity. This application is especially well-suited
 1602 for MOFs since they can combine photosensitiser and catalytic functions into a single structure
 1603 ¹⁹¹. The high porosity of MOFs (macropores larger than 50 nm in some cases) enables rapid
 1604 substrate and product transport/diffusion from the catalytic sites ²². Additionally, organic
 1605 ligands have the ability to absorb photons and transfer electrons from the ligand to the metal
 1606 centre, thereby generating an excited state in the process. Thus, the utilization of MOFs as
 1607 photocatalysts encompasses a diverse and extensive range of applications (Fig. 9(a)) ¹⁹².



1608

1609 **Fig. 9.** (a) Composite materials featuring metal-organic frameworks for heterogeneous
 1610 photocatalysis driven by visible light. MOF-based composites have potential applications in the



1611 degradation of organic compounds, reduction of Cr(VI), inactivation of microorganisms,
1612 oxidation of NO_x, reduction of CO₂, and production of H₂. Adopted from Ref. ¹⁹² with
1613 permission. (b) Microwave-assisted synthesis of Bi-BDC MOF photocatalyst and its efficient
1614 reduction of Cr(VI) within 6.0 min under low-power LED UV light. Adopted from Ref. ¹⁹³ with
1615 permission. (c) Visible light CdS/Cd-MOF photocatalyst with enhanced photodegradation of
1616 methylene blue (91.9% in 100 minutes under simulated sunlight irradiation). Adopted from Ref.
1617 ¹⁹⁴ with permission. (d) Double Z-scheme heterojunction based on UiO/MIL/CN for the
1618 photocatalytic degradation of ofloxacin under visible light irradiation. Adopted from Ref. ¹⁹⁵
1619 with permission. (e) CuTCPP-functionalized zirconium MOF and TiO₂ for photocatalytic CO₂
1620 reduction to CO under simulated solar illumination. The figure contains the dependence of total
1621 CO/CH₄ evolution on the amount of TiO₂ and various CTU/TiO₂ ratios under Xe lamp
1622 irradiation ($\lambda > 300$ nm) within 1 hour, total CO/CH₄ evolution amount produced by
1623 CTU/0.6TiO₂ under Xe lamp irradiation within 8 hours, and a proposed photocatalytic CO₂
1624 reduction pathway over CTU/TiO₂. Adopted from Ref. ¹⁹⁶ with permission. (f) 3D hierarchical
1625 structure of CdS/Ni-MOF and schematic diagram illustrating the electron transfer process and
1626 photocatalytic mechanism involved in the reduction of CO₂. Adopted from Ref. ¹⁹⁷ with
1627 permission.

1628
1629 Regarding the elimination of Cr(VI) from water, Gao et al. ¹⁹³ have synthesized a high-
1630 throughput MOF composed of Bi-benzene-1,4-dicarboxylic acid (Bi-BDC) and featuring a
1631 consistent rod-like structure using a microwave-assisted technique (**Fig. 9(b)**). This MOF
1632 demonstrated the capability to achieve a complete photocatalytic reduction of Cr(VI) in just 6.0
1633 minutes when exposed to low-power LED UV light ¹⁹³. Furthermore, the degradation of
1634 contaminant was also reported using MOFs photocatalyst. Jing et al. ¹⁹⁴ constructed a binary
1635 CdS-Cd-MOF nanocomposite by an *in-situ* sulfurization of Cd-MOF. When exposed to
1636 simulated sunlight, the degradation rate of methylene blue using 10 mg of the material reached
1637 91.9% within 100 minutes ¹⁹⁴. The mechanism of the photocatalytic degradation is described
1638 based on the difference in the band gap between the CdS (2.29 eV) and Cd-MOF (2.8 eV) (**Fig.**
1639 **9(c)**). In a similar context, a recent study investigates the photocatalytic degradation of
1640 ofloxacin using UiO/MIL/CN ¹⁹⁵. In this work, the synthesis involved growing UiO-66 on the
1641 surface of NH₂-MIL-125 using the solvothermal method to create MOF-on-MOF architectures.
1642 Following that, the authors achieved the successful deposition of g-C₃N₄ nanosheets onto the
1643 surface of UiO-66/NH₂-MIL-125, resulting in the development of a novel double Z-scheme
1644 heterojunction photocatalyst (**Fig. 9(d)**). When exposed to visible light, this double Z-scheme



1645 heterojunction serves as an exceptionally efficient photocatalyst for the degradation of
1646 ofloxacin, exhibiting a rate constant of 0.07 min^{-1} ¹⁹⁵.

1647
1648 Furthermore, the photocatalytic reduction of carbon dioxide into valuable chemicals stands as
1649 an appealing technique, addressing both environmental concerns and energy scarcity
1650 simultaneously. Interestingly, MOFs have garnered significant interest in this field due to their
1651 remarkable chemical and structural diversity. Wang et al. ¹⁹⁶ employed an in-situ hydrothermal
1652 process to combine TiO_2 nanoparticles with a mixed ligand-based MOF structure consisting of
1653 CuTCPP and BDC (CTU). This integration resulted in the formation of CTU/TiO_2
1654 nanocomposites, which effectively merge MOFs with inorganic semiconductors (**Fig. 9(e)**).
1655 When employed as photocatalysts for CO_2 conversion under simulated solar light ($\lambda > 300 \text{ nm}$),
1656 the optimized CTU/TiO_2 heterostructure demonstrated significantly enhanced performance ¹⁹⁶.
1657 The rate of CO_2 reduction into CO reached $31.32 \mu\text{mol/g h}$, approximately seven times higher
1658 than that achieved with bare TiO_2 . In another study conducted by Xu et al. ¹⁹⁷, they explored
1659 the development of 3D hierarchical CdS/Ni-MOF photocatalysts. These photocatalysts
1660 exhibited a notably CO yield, surpassing the yields achieved by both Ni-MOF and CdS
1661 individually by 16 and 7 times, respectively. The researchers proposed a preliminary
1662 mechanism for the CO_2 conversion process (**Fig. 9(f)**). Upon exposure to UV-Vis light, both
1663 Ni-MOF and CdS become excited, generating electrons (e^-) and holes (h^+). Their intimate
1664 interface facilitates the efficient transfer of excited electrons from Ni-MOF to CdS, which
1665 boasts a more positive conduction band ¹⁹⁷. Consequently, CdS, acting as the active site,
1666 proficiently reduces CO_2 to CO. Concurrently, the holes in the valence bands of Ni-MOF and
1667 CdS engage in oxidation reactions, yielding oxygen and hydrogen peroxide, effectively
1668 eliminating the holes. This well-coordinated charge separation and electron-hole pair transfer
1669 contribute to the enhanced photocatalytic activity of the system.



1670

View Article Online
DOI: 10.1039/D4TA03877K

1671 Because the careful selection of linkers/metal clusters or the addition of catalysts can
1672 significantly increase light adsorption, reactant adsorption, charge separation, and reactant
1673 activation, the modification of MOF elements is especially crucial for photocatalyst
1674 applications ²³. As a result, photocatalytic performance will be enhanced. Sensitiser addition is
1675 one example of modulating ligand and metal clusters. MOFs can incorporate sensitisers (metal
1676 complexes or organic dyes) to increase the amount of visible-light-driven photocatalysis ¹⁶⁷. In
1677 their study, Furukawa et al. ²⁴ successfully introduced dyes and encapsulated precious metals
1678 into a series of MOF photocatalysts, producing an enhanced photocatalytic performance for
1679 almost all MOFs tested as well as a slightly increased spectrum region for photoactivity. In a
1680 similar vein, Pt/ NH₂-MIL-125(Ti) was used in visible light for CO₂ reduction ²³. The results
1681 of this were also positive with the material showing an improvement in photocatalytic
1682 performance when compared to the plain NH₂-MIL-125(Ti). Pt/NH₂-MIL-125(Ti) exhibited a
1683 remarkable boost in its photocatalytic efficiency for CO₂ reduction into formate. Over the
1684 course of 8 hours of irradiation, Pt/NH₂-MIL-125(Ti) yielded approximately 12.96 mmol of
1685 formate, representing a notable 21% increase in activity when compared to the performance of
1686 pure NH₂-MIL-125(Ti). These experiments suggest that the use of precious metals in MOFs to
1687 improve photocatalytic behaviour has great potential.

1688

1689 Furthermore, studies indicate that MOFs' thermal and chemical stabilities are a bonus and
1690 contribute to their appeal as catalysts and catalytic hosts. Zhao et al. ²² posit that MOF
1691 photocatalysts should be stable under service conditions, including water. In addition to this,
1692 MOF photocatalysts have shown resistance to moderately acidic and basic solutions ²². An
1693 example of an aquatically stable MOF can be found in Drache et al. ¹⁹⁸ report in which they
1694 investigated a series of Zr-based MOFs and found they exhibited excellent stability in water.



1695 The authors suggest that this is a result of the strong coordination between the organic ligands
1696 and the Zr nodes. Howarth et al.¹⁹⁹ recommend another method to improve the stability of
1697 MOFs in water, involving decorating the MOF organic linkers with sulphonic, fluorinated, or
1698 phosphonate substituents. Metal oxide encapsulation within MOF photocatalysts is an
1699 additional line of inquiry. POMs, or polyoxometalates, have attracted a lot of interest because
1700 of their exceptional redox capacity, highly negative charges, and structural characteristics²².
1701 When POM [(PW₉O₃₄)₂Co₄(H₂O)₂] was encapsulated in MOF-545 the product was able to
1702 endure reversible electron transfer reactions with negligible structural degradation²⁰⁰. This
1703 material was also successfully used for water oxidation under visible light. As demonstrated,
1704 recent advancements have introduced numerous new MOFs and MOF-based composites
1705 specifically designed for the photocatalytic reduction of CO₂. MOFs are recognized as state-of-
1706 the-art photocatalysts due to their exceptional coordination between active metal centers and
1707 organic linkers. Their unique structural features such as vast surface areas, well-ordered
1708 frameworks, high porosity, and significant structural tunability contribute to their effectiveness
1709²⁰¹. Compared to traditional catalysts, MOF-based photocatalysts present several advantages,
1710 including ultra-high specific surface areas, adjustable pore structures that enhance CO₂
1711 adsorption and reduction and unlike homogenous photocatalysts, they are easily separated from
1712 the reaction products and can therefore be reused many times²². As such, MOF photocatalysts
1713 will have a longer lifetime, contributing to a decrease in waste, end-of-life process costs, and
1714 pollution. Additionally, the metal nodes and organic ligands in MOFs can be selectively
1715 functionalized, and the abundant pores allow for the accommodation of various functional guest
1716 substances.
1717
1718 Despite these benefits, challenges persist in the use of MOFs composites as photocatalysts.
1719 These include low visible light utilization efficiency, poor stability with rapid loss of activity

View Article Online
DOI: 10.1039/D4TA03877K



1720 and structural integrity after several cycles, and reliance on organic sacrificial reagents and
 1721 solvents that pose environmental concerns. Furthermore, not much research has been done on
 1722 how MOFs employed in photocatalytic applications affect the environment. An LCA could be
 1723 performed to more accurately assess the possible impact of MOF photocatalysts. On the other
 1724 hand, as previously noted, the synthesised MOFs continue to be costly because of the intricate
 1725 synthesis procedures and the absence of mass production processes, even though the component
 1726 linkers and ions are frequently quite affordable¹⁸. However, MOFs improved efficiency
 1727 compared to TiO₂ photocatalysts and their potential for an extended lifetime will likely reduce
 1728 their long-term costs.

1729 5. Evaluation and comparison

1730 Investigating potential MOF as sorbents, SCs electrodes or photocatalysts is a difficult
 1731 endeavour due to the vast number available, with over 90,000 synthesized MOFs in the public
 1732 domain²⁰². However, the creation of software with these capabilities is yet to be achieved³⁵.
 1733 To increase the TRL level of MOF sorbents, pilot-scale MOF production needs to be
 1734 investigated. Methods of bulk-producing structured MOFs are imperative if they are to be used
 1735 for industrial use. **Table 3** shows a summary of the advantages and disadvantages of MOFs,
 1736 liquid amine, activated carbon, as well as titanium dioxide for application in various
 1737 technologies identified from a review of recent literature.

1738 **Table 3.** Advantages and disadvantages of MOFs, liquid-amine, activated carbon, and TiO₂
 1739 technologies for uses in CCS, SCs electrodes and photocatalysis.
 1740

Advantages	Disadvantages
<ul style="list-style-type: none"> • Controllable morphology (pore size). • MOFs are used for CCS at lower temperatures compared to amines⁵². • CO₂ capture capacity \geq amine scrubber under the same dry working conditions³². • Solid sorbents have a much lower heat capacity compared to liquid-amine solutions³². • Suitable for DAC processes³³. 	<ul style="list-style-type: none"> • Still in early developmental stages – further research is required¹⁹¹. • Poor stability under CCS operational conditions¹⁸. • Prone to decompose when exposed to moisture¹⁸. • Poor thermal conductivity (leading to higher regeneration costs and slower regeneration processes)³⁶.



MOFs	<ul style="list-style-type: none"> • Some MOFs can provide a greater CO₂ uptake capacity, good SCN, and acceptable regeneration energy requirements⁵⁰. • Reduced effect on power plant efficiencies²⁰³. • High capacitance compared to ACs. • Some MOFs show exceptional cyclic stability²². • High power densities. • Possibility of using waste PET for production¹¹³. • Light harvesting range can be extended to include visible/NIR light through the inclusion of long-wavelength-light-responsive units within the MOF. • Can reduce recombination of the photogenerated electrons and holes. • Some MOFs have shown improved photocatalytic behaviour. • Reported successful application under mild conditions. 	<p>View Article Online DOI: 10.1039/D4TA03877K</p> <ul style="list-style-type: none"> • CO₂ capture capacity can be reduced in the presence of moisture¹⁸. • Lack of processes to convert MOF powders into devices¹⁸. • Low CO₂ capacity in the presence of water²⁷. • Reports of poor stability over multiple cycles of absorption/desorption²⁷. • Can have high production costs²⁷. • All the feasible methods to modify MOFs for DAC currently rely on amine doping⁶². • Little known about MOF toxicity. • Suitability for widescale deployment not well established • Comparatively complex synthesis process. • The stability of MOFs under photocatalytic reaction conditions requires more research – some reports of low stability.
Liquid amines	<ul style="list-style-type: none"> • Proven success in bulk scale CCS¹⁸. • The most developed method of CCS²⁵. • MEA has a high CO₂-carrying capacity²⁷. • MEA has a fast absorption rate²⁷. • Amines can provide high separation/purification performance¹⁸. • Some liquid amines like MEA are low-cost²⁶. • MEA is readily biodegradable²⁶. 	<ul style="list-style-type: none"> • Energy intensive - High solvent regeneration energies (>140 °C)³¹. • Requires large equipment³¹. • Prone to equipment corrosion and requires inhibitors to prevent it³¹. • Prone to degradation²⁵. • Can reduce the overall efficiency of a powerplant¹⁸. • Limited potential for performance improvement¹⁹. • High cost, and levels of sorbent loss^{33,35}. • Highly toxic and environmentally harmful, not suitable for DAC³³. • Insufficient CO₂ capacity for industrial-scale emissions mitigation²⁵.
Coconut shell activated carbon	<ul style="list-style-type: none"> • Low cost⁸⁰. • Raw material readily available⁸⁰. • High thermal and electrochemical stability²⁰⁴. • Renewable and non-toxic²⁰⁴. • Low net GHG emissions over the lifespan⁹⁶. 	<ul style="list-style-type: none"> • Low power densities. • Capacitive performance is not as high as that offered by some MOFs • Low specific capacitance⁸³.
Titanium dioxide	<ul style="list-style-type: none"> • Showed great promise for commercial use¹⁷⁰. • Non-toxic¹⁷⁰. • Environmentally benign¹⁸¹. • Suitably efficient photoactivity²⁰⁵. • High stability²⁰⁵. • Low cost²⁰⁵. 	<ul style="list-style-type: none"> • Complex separation process²⁰⁶. • Prone to aggregation²⁰⁶. • Rapid rate recombination of the photogenerated electron-hole pairs²⁰⁶.



• Photocatalytic activity is restricted to the UV region (low photocatalytic efficiency)²⁰⁷.

1741

1742 **5.1 Carbon capture**

1743 Metal-organic frameworks (MOFs) present numerous advantages over non-MOF materials for

1744 applications in carbon capture. MOFs such as MOF-5 and HKUST-1 exhibit exceptional

1745 surface areas and porosity, exceeding 1000 m²/g, which translates to higher CO₂ adsorption

1746 capacities up to 33.5 wt% and 31.0 wt% respectively under standard conditions²⁰⁸. This is

1747 significantly better than traditional materials like zeolites and activated carbons, which have

1748 lower surface areas and CO₂ adsorption capacities. The tunability of MOFs allows for precise

1749 control over pore size and functionality, enhancing selectivity towards CO₂, as demonstrated

1750 by ZIF-8's CO₂/N₂ selectivity of 25 at room temperature. However, MOFs generally show high

1751 sensitivity toward moisture and high structural degradation, such as MOF-5, which can lose as

1752 much as 90% of its CO₂ adsorption capacity under humid conditions. Moreover, high synthesis

1753 and processing costs, along with difficulties in the production of defect-free membranes, are of

1754 vital importance against scalability. Carbon capture performance metrics are important.

1755 Although MOFs showed an upper CO₂-carrying capacity compared to liquid amines in the

1756 laboratory tests, both materials showed a suitable level of CO₂ selectivity with excellent

1757 selectivity shown by MOFs doped with amines. MOFs doped with amine dopants also had

1758 lower regeneration energies compared to liquid amines. The possibility of development is

1759 higher for MOFs due to their tunable structure and number of available MOFs. While MOFs

1760 are under development, liquid amines find industrial applications. Both materials have stability

1761 problems under CCS conditions, and as far as reported there was no problem of corrosion

1762 observed with MOF, unlike liquid amines which in addition to being corrosive are volatile. On

1763 performance, MOF scores 128 against liquid amine's 93. The three broad factors were further

1764 allocated relative weightings based on the findings of the literature review and summed up to



1765 100. For C-capture, the weights were distributed as performance 34/100, environmental impact
 1766 25/100 and cost implications 41/100. The factors, along with weightings for the evaluation of
 1767 carbon capture materials, are shown in **Table 4**, and the comparison matrix showing the scoring
 1768 of liquid-amine and MOF-based materials against these factors is presented in **Table 5**.

1769 **Table 4.** C-capture factors and corresponding suggested weighting along with the justifications.
 1770

Subject	Factor	Weighting	Justification
Performance	CO ₂ -carrying capacity	3	This affects the efficiency of the material and influences the amount of sorbet required for a CCS application ¹⁸ .
	CO ₂ selectivity	3	This affects the purity of adsorbed CO ₂ and the concentration of CO ₂ in the emitted flue gases ¹⁸ .
	Regenerability	3	This affects the energy efficiency of the C-capture process ³¹ .
	Potential for development	1	All current technologies (both liquid amine and MOF sorbents) require further improvement before they can be deployed on an industrial scale. Therefore, the material must offer enough scope/potential for these changes ³¹ .
	Current successful application	2	CCS technology takes a considerable period of time to test and validate, very few materials make it to trials and even fewer are successful in reaching real-world applications ¹⁹ . Successful small-scale trials or real-world trials are good indications of the material's suitability.
	Stability under service conditions	3	The material used in CCS applications must be able to withstand the operating conditions and regeneration conditions to perform well.
	Corrosivity and volatility	2	Ideally, materials used should not be volatile as that can lead to high levels of sorbent loss and reduced levels of performance over time ³³ . Corrosive materials can also cause performance issues as they may damage equipment, thus reducing its efficiency ³³ .
	Material recyclability	3	For the technology to be "future-proof" it needs to be sustainable.
	Toxicity	2	A toxic material is detrimental to the environment, it can also result in



				View Article Online DOI: 10.1039/D4TA03877K
Environmental impact	Production methods	2		higher costs for disposal at the end of the products life.
	Functional requirements	energy	3	Energy-intensive production methods may negate some of the benefits of the technology use. Literature suggests that the application of post-combustion CCS can lead to an overall reduction of a power plant's efficiency ¹⁹ .
Cost	Raw material cost		2	Influences the overall cost of a material. It is also important to consider the likelihood of a significant change in the price of a material.
	Usage costs (equipment, temperature/pressure requirements)		3	If a technology is excessively expensive then it will likely never be suitable for wide-scale deployment. Furthermore, if the costs of using the technology outweigh the benefits then it is likely the technology will fail or be superseded and become obsolete.
	Synthesis/manufacturing costs		3	High production costs can act as a barrier to wide-scale technology deployment. It is also important to consider if the production costs are likely to reduce when the technology develops further/becomes more mainstream.

1771

1772

Table 5. Comparison matrix between liquid amines and MOFs for C-capture applications.

Factor	Weighting	Material score		Justification
		Liquid- amines	MOFs	
CO ₂ -carrying capacity	6	3	5	MOFs have shown higher CO ₂ -carrying capacities in laboratory tests ⁵² .
CO ₂ selectivity	5	3	3	Both materials have shown suitable levels of CO ₂ selectivity ⁵² . While pristine MOF sorbents have shown SCN values below those of liquid-amine sorbents, amine-doped MOF sorbents have shown excellent SCN values exceeding those of liquid-amine sorbents ¹⁸ .
Regenerability	5	3	4	While both materials have shown acceptable (albeit high) results for required regenerability energy, some amine-doped MOF sorbents have exhibited lower regeneration energies ^{18,31} .



Potential development	for	4	1	5	Liquid amine technology provides little potential for further development whereas MOF sorbents provide vast potential due to their customisable structure and the number of available MOFs ^{19,25} . Furthermore, MOFs have shown potential for DAC ⁶² .
Current application	successful	5	4	2	Liquid amines are already used in industry but are yet to be rolled out on a wide scale ²⁵ . MOFs for CCS are still in their developmental stages and are a long way from real-world trials ⁵² .
Stability under conditions	service	6	3	3	Both pristine MOF sorbents and liquid-amine sorbents have issues with stability under CCS conditions ^{18,25} . Whilst, amine-doped MOFs have shown improved stability under regeneration and service conditions, they are still mildly affected by the presence of moisture ¹⁸ .
Corrosivity and volatility	and	3	1	5	Liquid amines are shown to be very corrosive and can cause damage to equipment if it has not been given a protective coating ²⁵ . Liquid amines are also very volatile and therefore the process can be subject to high levels of sorbent loss ³³ . There are currently no reported issues with MOF sorbents and corrosion.
Performance score:			93	128	
Recyclability		4	3	3	Recycling prospects for both materials are reasonably poor ^{18,26} .
Toxicity		8	1	4	Liquid amines are toxic ³³ . There is limited research into the toxicity of MOFs however, the literature suggests that some may be toxic when they start to decompose ¹²⁵ .
Production methods		7	3	3	The production of both materials is both complex and reasonably energy-intensive.
Functional requirements	Energy	6	3	4	MOFs have shown potential for CCS at a lower temperature than those used for liquid-amine CCS ⁵² . Furthermore, amine-doped MOF sorbents have a lower regeneration energy requirement compared to liquid-amine sorbents ¹⁸ .
Environmental impact score:			59	89	
Raw material cost		14	3	2	The cost of the MOFs constituent linkers and metal clusters is relatively cheap ¹⁸ . However, pre-synthesised MOFs are expensive due to complex production processes ¹⁸ . Some liquid-

Article Online
DOI: 10.1039/D4TA03877K



				amines like MEA are relatively low-cost ²⁶ .
Usage costs (equipment, temperature/pressure requirements)	15	3	4	MOFs have demonstrated the potential for CCS at lower temperatures ⁵² . Liquid-amine scrubbers have also been shown to reduce the overall efficiency of a power plant to a greater degree than the predicted effects of MOF sorbents ^{18,203} .
Production costs	12	3	2	As previously discussed, MOFs are expensive due to complex production processes. Liquid-amine technology is comparatively well-developed, and processing costs are cheaper ²⁶ .
Cost score:		123	112	
Overall scores:		275	329	

View Article Online
DOI: 10.1039/D4TA03877K

1773 **Note:** All materials were evaluated for each factor using a scale ranging from 1 to 5 (where 1
1774 corresponds to "very bad," 2 to "bad," 3 to "suitable," 4 to "good," and 5 to "very good").

1775 Carbon capture technology stands as one of the most important strategies for mitigating climate
1776 change through the reduction of CO₂ emissions from industrial sources. There are three major
1777 parameters used that express a comparison among the different carbon capture methods: their
1778 cost, efficiency, and environmental impact. Cost means the financial expenditure incurred to
1779 capture, transport, and store CO₂, including capital, operational, and maintenance costs.
1780 Advanced carbon capture methods using MOFs reduce this cost to a large extent. For example,
1781 conventional amine-based capture processes may range between \$40–\$100 per ton of CO₂
1782 captured while advanced materials, such as MOFs, are expected to drop these costs down to
1783 \$20–\$50 per ton by the increase in efficiency and reduction in energy requirements²⁰⁹.
1784 Efficiency is the percentage of CO₂ that can be captured from the sources of emission relative
1785 to the total amount of emissions produced. Traditional methods have efficiencies of 85–90%,
1786 while MOFs and other advanced materials could theoretically be as high as 95–99% according
1787 to the study on 2D MOFs for the reduction of CO₂, where Cu₃(C₁₂N₆S₆)₂ demonstrated very
1788 high activity with small overpotentials, which reflects high efficiency in the processes of
1789 capture and conversion of CO₂²¹⁰. Environmental impact looks at the bigger picture of how
1790 carbon capture affects the environment in general, such as the probable risks associated with
1791



1792 the leakage of CO₂ during storage, the energy used by capture and sequestration, and the net
1793 reduction of GHG emissions. While traditional methods may leave room for a capture process
1794 that is 10–20% more energy-intensive, advanced MOF-based methods can reduce this extra
1795 energy requirement to under 10%, making the process more sustainable. Moreover, according
1796 to the researchers in this study, 2D MOFs showed improved selectivity toward CO₂ reduction
1797 relative to competing reactions, such as hydrogen evolution, which further minimizes unwanted
1798 environmental impacts. The utilization of 2D MOF as an advanced material in carbon capture
1799 technology shows a very promising avenue toward cost-effective, efficient, and
1800 environmentally sustainable processes.

1801 **5.2 Photocatalysis**

1802 Given the very high porosity of the MOFs, the surface area can reach more than 3000 m²/g.
1803 Such high values raise the adsorption and reduction rates of CO₂ in photocatalysis. Furthermore,
1804 their tunable structure provides conditions for the introduction of different metals, increasing
1805 active sites, and enhancing photocatalytic properties. Also, the MOFs exhibit enhanced light
1806 harvesting and photostability, which is very critical in efficient photocatalysis ²¹¹. However,
1807 these materials have low stability in an aqueous/high-temperature environment and poor light
1808 absorption, thereby mostly limiting their application to only the ultraviolet regime, with the
1809 added need for sophisticated and expensive synthesis methods. MOFs demonstrated lower
1810 recombination rates and higher resistance to aggregation compared to titanium dioxide, which,
1811 although highly stable, is prone to aggregation. While titanium dioxide is restricted to UV light,
1812 MOFs can be active in a broader spectrum that includes visible light. Moreover, the MOFs
1813 provide larger surface areas with increased resistance to photo-corrosion. MOFs score 176
1814 while titanium dioxide scores 116, hence superior efficiency for performance evaluation. The
1815 evaluation parameters are weighted as performance, which is efficiency, at 45/100,
1816 environmental impact at 18/100 and cost implications at 37/100. Performance factors include



1817 photostability, the extent of light absorption and recombination rates 180. Environmental
 1818 impact factors include stability of materials in various environments and resistance to photo-
 1819 corrosion. These are, among others, the complexity and cost of the synthesis methods. **Table 6**
 1820 presents the evaluation criteria in the case of photocatalysis, and **Table 7** presents a detailed
 1821 comparison between titanium dioxide and MOFs in photocatalytic applications.

1822 **Table 6.** Photocatalysis factors and the corresponding suggested weighting along with the
 1823 justifications.

Subject	Factor	Weighting	Justification
Performance	Recombination rate	3	Low recombination rates are desirable as it directly effects the efficiency of the photocatalyst.
	Stability under photocatalytic conditions	3	The photocatalytic material must be able to withstand the operating conditions to perform well.
	Level of current development	2	Successful small-scale trials or real-world trials are good indications of the material's suitability.
	Resistance to Aggregation	2	Material aggregation can block the active sites of a material and therefore reduce the effective surface area of the material and consequently reduce its efficiency.
	Photocatalytic activity under Visible light	3	In order to maximise the efficiency of a photocatalyst, ideally it should be photoactive in a wide region of the light spectrum as possible. Most current photocatalysts are only active in the UV region of the spectrum.
	Material morphology	3	This has been shown to greatly influence the efficiency of photocatalysts ²⁰⁶ .
	Resistance to photo corrosion	2	High resistance to photo corrosion is desirable as photo corrosion can lead to a reduction in performance over time.
Environmental impact	Toxicity	3	A toxic material is detrimental to the environment, it can also result in higher costs for disposal at the end of the product's life.
	Energy requirements for processing raw materials	2	Energy-intensive processing methods can be detrimental to the environment. This is an important consideration for technologies with a wide-scale deployment aim.
	End of life outlook	2	For the technology to be "future-proof" it needs to be sustainable.



Cost	Raw material cost	3	Consequently, the option for recycling or safe disposal is very important.
	Production costs	3	This greatly influences the overall cost of a material. It is also important to consider the likelihood of a significant change in the price of a material. High production costs can act as a barrier to wide-scale technology deployment. It is also important to consider if the production costs are likely to reduce when the technology develops further or becomes more mainstream.

1824

1825 **Table 7.** Comparison matrix for titanium dioxide and MOFs for photocatalytic applications.

Factor	Weighting	Material Score		Justification
		TiO ₂	MOFs	
Recombination rate	7	2	4	MOFs have shown reduced recombination rates.
Stability under photocatalytic conditions	8	4	3	Titanium dioxide has shown high stability under photocatalytic conditions ²⁰⁵ . MOFs however, have shown some degradation under these conditions ²³ .
Level of current development	4	5	4	Titanium dioxide has shown issues with aggregation ²⁰⁶ unlike MOFs.
Resistance to Aggregation	5	1	3	ACs are prone to aggregation and therefore often have to be used as a gel suspension, this often limits the reduction of the device size.
Photocatalytic activity under Visible light	9	1	5	Titanium dioxide's photoactivity is restricted to the UV region of the light spectrum (only 5% of available light) ²⁰⁶ . However, some MOFs have shown photoactivity in an extended region of the spectrum.
Material morphology	7	3	4	MOFs can provide a significantly larger surface area ¹²¹ . Furthermore, titanium dioxide is prone to aggregation which reduces its effective surface area ²⁰⁶ .
Resistance to photo corrosion	5	3	4	MOFs have shown increased resistance to photo corrosion ²⁰⁶ . Titanium dioxide has mild difficulty with photo corrosion ¹⁷⁰ .
Performance score:		116	176	
Toxicity	6	5	4	Some MOFs used for this application (such as MILMIL-100(Fe)) are non-toxic ¹²¹ . Titanium dioxide is non-toxic ¹⁷⁰ .
Processing raw materials	6	3	4	The production of both materials is both complex and reasonably energy-intensive. However, due to the novelty of MOFs,



				their production costs remain prohibitively high. ²⁰⁶
End of life outlook	6	2	2	Methods for recycling both materials remain largely unsearched.
Environmental impact score:		60	54	
Raw material costs	17	5	2	Titanium Dioxide is a low-cost material whereas MOFs for this application are high-cost ²⁰⁵ .
Processing costs	20	3	3	MOFs have a significantly higher processing cost ¹⁹¹ .
Cost score:		145	94	
Overall scores:		341	304	

Note: All materials were evaluated for each factor using a scale ranging from 1 to 5 (where 1 corresponds to "very bad," 2 to "bad," 3 to "suitable," 4 to "good," and 5 to "very good").

5.3 Supercapacitors

Supercapacitors, being next-generation energy storage devices, are assessed based on the metrics of specific capacitance, energy density, power density, and cycling stability. The presence of high specific surface areas and porosity contributes to really good electrochemical performance in metal-organic framework materials such as Cu-MOF, Zr-MOF, and Ti-MOF. For example, Cu-MOF showed a specific capacitance of 104.8 F/g with an energy density of 18.2 Wh/kg, greatly outperforming all other materials because of increased ionic transport and charge storage capabilities²¹². Moreover, Ni-DMOF-ADC gave a specific capacitance of 552 F/g and over 98% retention after 16,000 cycles, indicating its excellent cycling stability. Similarly, Ni₃(HITP)₂ tends to be 117 F/g and 90% after 10,000 cycles. For instance, MnOx-MHCF has reached as high as 1200 F/g with 94.7% retention after 10,000 cycles in composite materials, whereas rGO/ZIF-8 has reached 336 F/g with 96% retention²¹³. While these methods could enhance the capacity, the poor intrinsic conductivity of pristine MOFs remains a large problem and needs conductive additives or hybridization with conductive materials like graphene and conductive polymers. Although this composite approach has improved the conductivity and overall performance, it adds complexities in synthesis and possible trade-offs in mechanical stability²¹⁴. Therefore, innovation in design and optimization of electrode



1846 materials remains the key to unlocking the full potential of supercapacitors so that high power
 1847 and long-life energy storage applications are fully satisfied.

1848

1849 However, the complex and rather pricey synthesis processes of MOFs, combined with the fact
 1850 that long-term stability and durability under real conditions is still a topic of research, represent
 1851 major handicaps. On the other hand, non-MOF materials are normally much more stable and
 1852 less expensive but do not offer such high tunability and selectivity as MOFs do. For overall
 1853 performance, MOFs score 173, while activated carbon scores 126. The supercapacitors could
 1854 therefore have evaluation parameters that are weighted at 40/100 for performance, 15/100 for
 1855 environmental impact, and 45/100 for cost implications. Parameters for performance include
 1856 those for cyclic stability, capacitance, energy and power densities; parameters in environmental
 1857 impact include the stability of the materials and their impact on the environment; those in cost
 1858 implication involve the complexity of the methods of synthesis and expenses incurred. The
 1859 evaluation criteria for supercapacitors are summarized in **Table 8**, while **Table 9** presents the
 1860 comparison matrix between AC and MOFs as electrodes of supercapacitors.

1861

1862 **Table 8.** Supercapacitor factors and corresponding suggested weighting along with
 1863 justifications.

Subject	Factor	Weighting	Justification
	Cycle life	3	The electrode's lifespan is very important as it affects which applications the electrode can be used for as well as the level of performance over its lifespan ⁷⁴ .
	Capacitance	3	A poor capacitance can limit an SC's potential applications. A high capacitance is desirable.
	Current application	2	Successful laboratory results or real-world trials are good indications of the material's suitability.
	Size and weight	2	Literature suggests that for most applications, weight and size are not a key consideration, as the systems they would be used in are already
Performance			



		View Article Online DOI: 10.1039/D4TA03877K
Environmental impact	Integrity under service conditions (e.g. thermal stability)	3 very large and packaging space will likely not be an issue ⁸⁰ . This is important as it affects the lifespan of the electrode as well as its performance (including issues with charge leakage) and overall suitability for this application ¹¹⁹ .
	Energy and power densities	3 High energy and power densities are desirable for SCs. High power density would optimise their charging speeds and therefore make the SC an attractive option for electric vehicle charging equipment. A high energy density would increase the number of potential applications of the SC (as it would be able to hold more energy).
	Raw material renewability	3 For the technology to be “future-proof” it needs to be environmentally sustainable. A renewable raw material is desirable as it means the raw material cost is less likely to increase in the future (unlike non-renewable finite resources)
	Toxicity	3 A toxic material is detrimental to the environment, it can also result in higher costs for disposal at the end of the product's life.
	Recyclability	2 For the technology to be “future-proof” it needs to be sustainable.
	Production impacts (e.g. energy use)	2 Energy-intensive processing methods can be detrimental to the environment. This is an important consideration for technologies with a wide-scale deployment aim.
Cost	Material cost	3 Manufacturers want to keep costs low even at the expense of performance. Literature suggests that price is one of the key factors for the material choice of SC electrodes ⁸⁰ .
	Ease of production/ production cost	2 Simple, low-energy production processes are often cheaper. If the production method can be used for bulk production, it also means the cost of the product is likely going to be lower.

1864

1865

Table 9. Comparison matrix for AC and MOFs as SC electrodes.

Factor	Weighting	Material Score		Justification
		Activated carbon	MOFs	
Cycle life	8	3	4	MOFs have exhibited higher cyclic stabilities in both beakers and constructed SC laboratory tests ⁷⁵ . ACs have shown suitable performances for this application ⁸⁰ .
Capacitance	9	3	5	Secondary data suggests that MOFs are able to achieve higher values for capacitance compared to ACs ¹⁰⁶ .
Current successful application	6	4	3	ACs have proven to be successful and are currently used by electrode manufacturers ⁸⁰ . While MOFs have shown success in laboratory tests, there have been not extensive real-life application trials.
Size and weight	7	3	4	ACs are prone to aggregation and therefore often have to be used as a gel suspension, this often limits the reduction of the device size.
Energy and power densities	10	3	5	AC electrodes have shown limited power output due to the device's charge delivery rate ⁸⁴ . Laboratory testing of MOFs has shown improved power densities ¹¹⁹ .
Performance score:		126	173	
Raw material renewability	3	4	3	While ACs can be produced from renewable sources, the majority of commercially available ACs are produced from non-renewable precursors ⁷⁹ . Many MOFs used for this application involved non-renewable materials for their synthesis ⁷⁵ .
Non-toxicity	4	5	3	ACs are environmentally benign ²⁰⁴ . The toxicity of MOFs is not well understood and there is some suggestion that some may be toxic, especially when they begin to degrade ¹²⁵ .
Recyclability	5	4	3	AC electrodes show great recycling potential, with research suggesting processes and promising results from laboratory tests ⁹⁷ . While there is little research available on the recycling of MOF SC electrodes, there is research focused on the synthesis of MOFs using waste PET plastics ¹¹³ .
Production impacts (e.g. energy use)	3	3	4	AC Production is simple and chemical activation requires relatively little energy ⁸⁰ . It is important to note that bulk production of MOFs is largely unresearched and consequently an accurate assessment of this factor is difficult.
Environmental impact score:		61	48	
Material cost	35	4	2	AC is very cheap ⁸⁰ . MOFs are prohibitively expensive ⁷⁴ .



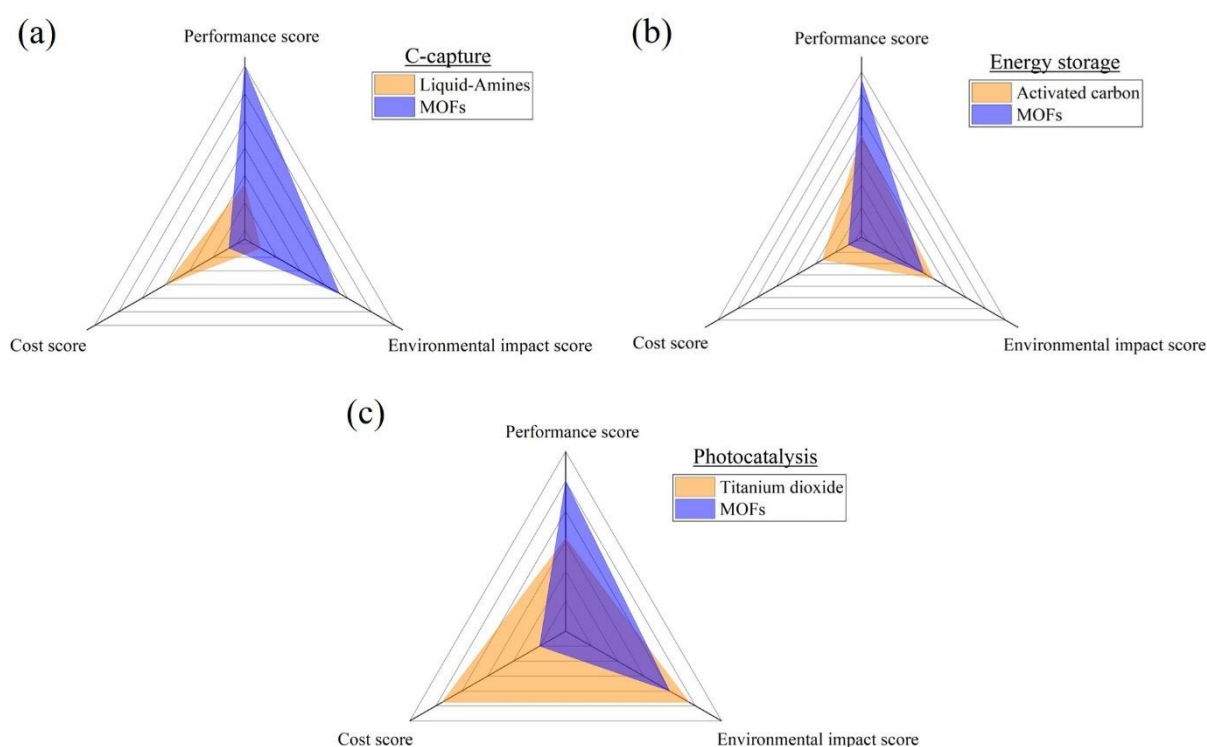
Ease of production/production cost	10	5	4	ACs production process is well-developed and relatively inexpensive ⁸⁰ . Bulk production of MOFs requires further research as the process is often complex and expensive ⁷⁴ .
Cost score:		190	110	
Overall scores:		383	350	

1866 **Note:** All materials were evaluated for each factor using a scale ranging from 1 to 5 (where 1
1867 corresponds to "very bad," 2 to "bad," 3 to "suitable," 4 to "good," and 5 to "very good").
1868

1869 Overall, MOFs score higher than liquid amines for CCS applications despite their poor cost
1870 score (52 compared to 60 for liquid amines) and the high weighting assigned to cost factors. As
1871 the radar graph (**Fig. 10(a)**) shows, the MOFs score considerably better for environmental
1872 impact due to liquid-amines toxicity and environmental harmfulness. Notwithstanding their
1873 relatively modest stage of development, MOFs have a high-performance grade because they
1874 also have the potential to provide considerable performance improvements over liquid amines.
1875 According to the graph, MOFs' performance score gives them the greatest advantage over liquid
1876 amines. In contrast, ACs receive a slightly better rating for SC electrode applications than
1877 MOFs. However, the radar graph (**Fig. 10(b)**) shows that MOFs score considerably better for
1878 performance and their score for environmental impact is only slightly less than that of AC. It is
1879 apparent from **Fig. 10** that this evaluation suggests that the factor preventing the wide-scale use
1880 of MOF electrodes is cost. Literature suggests that the incredibly low price of AC is acting as
1881 a barrier to the entrance of any other material to the SC electrode market⁸⁰, despite the potential
1882 for improved performance. Consequently, further research into the cost-effective synthesis of
1883 MOF electrodes may be beneficial. Regarding photocatalytic application, titanium dioxide
1884 achieved the highest overall score, suggesting that, based on these factors, it provides the most
1885 benefits despite MOFs achieving a considerably higher performance score of 70 (as seen in **Fig.**
1886 **10(c)**). Because of the high weighting of the cost elements, MOFs' cost score was significantly
1887 lower than titanium dioxide's, which is probably what prevents MOFs from being used in this
1888 application. In summary, the cost of MOFs can vary considerably, influenced by factors such



1889 as the specific MOF material, the synthesis method, the production scale, and the purity of the
 1890 final product. It's important to note that while some MOFs may be relatively expensive to
 1891 produce, they can offer unique properties and advantages in various applications, which can
 1892 justify their cost in certain contexts. As research and development in MOFs continue to advance,
 1893 there may be efforts to optimize synthesis methods and reduce production costs, making MOFs
 1894 more accessible for a broader range of applications.



1896
 1897 **Fig. 10.** Radar graph showing 3 factor comparison between MOFs and other conventional
 1898 materials for; (a) C-capture, (b) Energy storage, and (c) Photocatalysis applications.
 1899

1900 6. Limitations and future research directions

1901 6.1 Current MOF technologies

1902 Probably the most stressed limitation of the existing technologies behind MOFs is their poor
 1903 thermal stability. The span in the thermal decomposition temperatures (Td) of MOFs is very
 1904 large, which is the result of inconsistencies in the experimental conditions that include the
 1905 heating rates and atmospheres. As an example, the reported Td values for MOF-5 range from



1906 400 to 500 °C, whereas normally UiO-66 decomposes within the temperature range of 425
1907 500°C, and HKUST-1 shows Td values between 250–300°C. These are some of the factors that
1908 influence the nature and location of functional groups, the hardness of metal ions, and
1909 coordinated solvent molecules ²¹⁵. MOFs with harder metal ions, such as lithium-based UL-
1910 MOF-1, showed the highest stability with Td values as high as about 600 °C due to an increased
1911 ionic character of the metal-oxygen bonds compared to Zn or Zr-based MOFs. For example,
1912 Mg-MOF-74 has extremely high thermal stability with a Td of ca. 400°C under nitrogen
1913 atmosphere ²¹⁵.

1914
1915 Another large problem is their chemical stability, which is easily influenced by moisture and,
1916 therefore, significantly limits their usability for industrial processes. Many MOFs have been
1917 reported to decompose above 300 °C or under humid conditions, which thus bounds their
1918 practical applications. Their syntheses are often complicated, requiring pricey reagents; large-
1919 scale production is economically challenging. For instance, the price for the production of
1920 MOFs can be as high as \$50 per gram, which is very expensive compared with conventional
1921 porous materials like activated carbon with a price of around \$1 per kilogram ²¹⁶. Moreover,
1922 while some MOFs have very high methane storage capacities, for example, HKUST-1,
1923 impurities can reduce their actual performance by a large extent, significantly diminishing real
1924 application.

1925
1926 Another challenge is that it is somehow difficult to scale up the production of MOFs
1927 sustainably. Traditional methods of synthesis typically utilize highly toxic solvents under harsh
1928 conditions, therefore posing associated environmental and health risks, but usually at high
1929 production costs. With more than 99,075 synthetic variants, the enormous number of possible
1930 MOF structures makes it challenging and cumbersome to identify and optimize MOFs for a



1931 given application with certain desired properties. This leads to long experimental cycles and a
1932 high R&D cost ²¹⁷. Even for very promising materials like CALF-20 and MIL-100(Fe), multi-
1933 ton scale syntheses were achieved only recently, which clearly shows the slow transformation
1934 from lab scale to industrial scale production ²¹⁸. This is further frustrated by raw material costs
1935 and synthesis processes, which themselves are costly, often using highly toxic solvents like
1936 DMF that add to the cost and energy requirement of purification methods necessary to maintain
1937 the quality of the MOF product.

1938 **6.2 Future research directions**

1939 Future research in MOF technologies has to be directed toward the enhancement of stability,
1940 precise characterization of catalytic sites, effective regeneration techniques, and controlled
1941 defect engineering. Current MOFs typically show stability up to 300 °C, but future
1942 developments must take it further beyond 500°C through the incorporation of more thermally
1943 stable inorganic components and improvement of the node-linker bonds ²¹⁹. Improvement in
1944 chemical stability to less than 10% degradation in catalytic activity over 100 hours in an
1945 aqueous environment must also be attained. Advanced spectroscopic techniques and
1946 computational modelling shall quantify active catalytic sites with an error margin of less than
1947 5% and predict reaction rates to within 10% accuracy of the experimental values. Effective
1948 regeneration protocols restore at least 90% of the original catalytic activity upon deactivation
1949 cycles; long-term studies. This type of controlled defect synthesis thus should give a standard
1950 deviation of less than 10% in defect concentration from batch to batch, while for defect-free
1951 MOFs it has to be below 1% of total sites ²¹⁹.

1952
1953 One major challenge lies in the naturally very low ionic conductivity of most MOFs, typically
1954 much below the level of 10^{-10} S/cm. Nearly liquid electrolyte conductivities are hard to attain
1955 with solid electrolytes because of the limited carrier mobility and lack of low-energy pathways



1956 for ionic conduction ²²⁰. Future efforts, therefore, need to build on these limitations and focus
1957 on strategies that involve improved density of mobile ions and uninterrupted ionic conduction
1958 pathways. Additionally, it requires the development of MOFs with stable and high ionic
1959 conductivities toward changes in both temperature and humidity. Advancement in synthesis
1960 and functionalization approaches with the design of corresponding theoretical models is highly
1961 imperative for bringing solutions to the above challenges. The inclusion of flexible frameworks
1962 and phase transition mechanisms may yield MOFs with conductivities above 10^{-2} S/cm and
1963 may thus render them applicable in the new class of the next-generation energy storage and
1964 conversion devices ²²⁰.

1965
1966 Critical is the reduction in the number of steps involved in the synthesis process to reduce
1967 production costs to less than \$10 per gram. This can be realized by developing more efficient
1968 and up-scaled synthesis methods where applicability is maximally enhanced, such as solvent-
1969 free synthesis or the adoption of cheaper and more abundant raw materials ²²¹. In the future,
1970 research should also focus on green synthesis methods with non-toxic, biocompatible linking
1971 agents and eco-friendly solvents, along with techniques that apply either no use of solvents at
1972 all or solid-state synthesis. High-throughput computation screening and data mining will greatly
1973 accelerate the assessment of MOF properties to find promising candidates more efficiently ²²².

1974 Separation and recovery processes relating to vacuum filtration and continuous centrifugation,
1975 for example, need to be optimized in the scale-up of production. It may potentially also provide
1976 more sustainable and cost-effective solutions with respect to reduced energy use and
1977 improvement in scalability ²²³. This could provide more sustainable and cost-effective solutions
1978 due to less energy consumption and efficient scaling of microwave-assisted and
1979 mechanochemical synthesis methods.

1980



1981 It is with strategies in creative structural modification and composite material preparation that
1982 finally, such MOF materials could be fabricated with enhanced stability and durability to real-
1983 world working conditions. Comprehensive techno-economic analyses and life cycle assessment
1984 (LCA) are required concerning an evaluation of the feasibility and environmental impact of
1985 large-scale production of MOFs ²²⁴. These assessments will set targets for the development of
1986 green and sustainable economically viable MOF technologies whose industrial applications
1987 would not contradict their environmental benefits. By taking into consideration these points,
1988 there will be a chance for the synthesization of MOFs with improved thermal and chemical
1989 stability, reduced production cost, increased scalability, and finally making them practical in
1990 much more extended temperature range applications and industrial uses ²²⁵.

1991 7. Conclusion

1992 In conclusion, this study provides a comprehensive comparative assessment of Metal-Organic
1993 Frameworks (MOFs) and conventional materials across the domains of energy storage,
1994 environmental remediation, and photocatalysis. The results underscore the remarkable potential
1995 of MOFs as versatile and innovative materials in these critical areas, backed by empirical data.
1996 In energy storage, MOFs consistently outperform conventional activated carbons (ACs) with a
1997 performance score of 128, significantly surpassing them. Their exceptional specific surface
1998 areas, often exceeding 3,000 m²/g, enable efficient charge adsorption, rapid charge transfer, and
1999 easy ion diffusion within their porous structures. These characteristics, along with their
2000 chemical, thermal, and mechanical stability, and the ability to be hybridized with conductive
2001 materials, position MOFs as promising contenders for advanced energy storage devices like
2002 supercapacitors. Regarding environmental concerns, MOFs excel as effective carbon capture
2003 agents, scoring 329 compared to 275 for liquid amines. Exposed surface areas and high pore
2004 volumes further increase their potential for the adsorption capacity toward pollutants.
2005 Additionally, besides the presence of functional groups that act specifically toward interactions



2006 with the contaminants, the stability under environmental conditions and recyclability, underlining
2007 their effectiveness for environmental clean-up and, therefore, in the promotion of
2008 environmental sustainability. In the field of photocatalysis, MOFs exhibit substantial potential
2009 with a total score of 304. They showcase extended light harvesting capabilities into the visible
2010 and near-infrared regions due to their tunable bandgap, allowing for effective utilization of
2011 visible light. They have high surface areas that offer high active sites, while the mechanisms of
2012 charge separation do provide a platform for the prevention of recombination of electron-hole
2013 pairs, therefore enhancing the catalytic activity. Moreover, their photochemical stability and
2014 surface functionalization further enhance their applicability as efficient photocatalysts.
2015 However, it's crucial to acknowledge the cost challenges faced by MOFs, with an overall cost
2016 score of 110 for supercapacitors and 94 for photocatalysis. High production costs due to
2017 complex synthesis processes can act as barriers to widespread technology deployment in these
2018 domains. Some challenges, however, remain, such as stability issues, conductivity, and very
2019 high production costs. It is a problem of stability and poor electrical conductivity that hampers
2020 their potency in energy storage and photocatalysis. Future research should focus on the
2021 development of MOF structures with improved stability and conductivity, integration of MOFs
2022 with other materials to enhance their performance, and expansion of their applications in
2023 environmental remediation. This would have to be supplemented by enhanced environmental
2024 adaptability, low-toxicity development of variants to avoid secondary pollution and a deeper
2025 study of the pathways and kinetics of charge transfer. Computation design of more effective
2026 photocatalysts is probably going to provide the answer. Hence, these issues will be resolved
2027 through focused research and innovative solutions for MOFs to achieve their full potential. This
2028 empirical data underscores MOFs' promising future in energy storage, environmental
2029 remediation, and photocatalysis, showcasing their adaptability and high performance. As the

View Article Online
DOI: 10.1039/D4TA03877K



2030 world seeks sustainable technologies, MOFs emerge as pivotal materials, paving the way for a
2031 more eco-conscious future.

2032 **Acknowledgement**

2033 The authors are grateful to the International Society of Engineering Science and Technology
2034 (ISEST) UK. This research is also supported by “Pioneer” and “Leading Goose” R&D Program
2035 of Zhejiang (2024C04049), China. The authors are also thankful for financial support from the
2036 Ministry of Research, Innovation and Digitalization (MCID) under Romanian National Core
2037 Program LAPLAS VII-Contract No. 30N/2023.

2038



2039 **Reference**View Article Online
DOI: 10.1039/D4TA03877K

- 2040 1 A. Maghfirah, M. M. Ilmi, A. T. N. Fajar and G. T. M. Kadja, *Mater Today Chem*, 2020,
2041 **17**, 100348.
- 2042 2 A. El Guerraf, W. Zeng, A. Mantel, E. Benhsina, J. M. Chin and H. Shiozawa, *Adv*
2043 *Electron Mater*, 2024, 2300854.
- 2044 3 M. Ding, X. Cai and H.-L. Jiang, *Chem Sci*, 2019, **10**, 10209–10230.
- 2045 4 H. C. J. Zhou and S. Kitagawa, *Chem Soc Rev*, 2014, **43**, 5415–5418.
- 2046 5 S. Akhtar, P. Singha, A. De, K. S. Das, S. Saha, S. Bala and R. Mondal, *New Journal of*
2047 *Chemistry*, 2021, **45**, 6438–6449.
- 2048 6 L. R. Redfern and O. K. Farha, *Chem Sci*, 2019, **10**, 10666–10679.
- 2049 7 C. Yue, L. Wu, Y. Lin, Y. Lu, C. Shang, R. Ma, X. Zhang, X. Wang, W. D. Wu and X.
2050 D. Chen, *ACS Appl Mater Interfaces*, 2021, **13**, 26264–26277.
- 2051 8 R. Shah, S. Ali, F. Raziq, S. Ali, P. M. Ismail, S. Shah, R. Iqbal, X. Wu, W. He and X.
2052 Zu, *Coord Chem Rev*, 2023, **477**, 214968.
- 2053 9 G. Song, Y. Shi, S. Jiang and H. Pang, *Adv Funct Mater*, 2023, **33**, 2303121.
- 2054 10 N. F. Suremann, B. D. McCarthy, W. Gschwind, A. Kumar, B. A. Johnson, L.
2055 Hammarström and S. Ott, *Chem Rev*, 2023, **123**, 6545–6611.
- 2056 11 J. Chen and Y. Li, *The Chemical Record*, 2016, **16**, 1456–1476.
- 2057 12 M. U. Shahid, T. Najam, M. H. Helal, I. Hossain, S. M. El-Bahy, Z. M. El-Bahy, A. ur
2058 Rehman, S. S. A. Shah and M. A. Nazir, *Int J Hydrogen Energy*, 2024, **62**, 1113–1138.
- 2059 13 T. Wu, X. Liu, Y. Liu, M. Cheng, Z. Liu, G. Zeng, B. Shao, Q. Liang, W. Zhang, Q. He
2060 and W. Zhang, *Coord Chem Rev*, 2020, **403**, 213097.
- 2061 14 N. C. Burtch, J. Heinen, T. D. Bennett, D. Dubbeldam and M. D. Allendorf, *Advanced*
2062 *materials*, 2018, **30**, 1704124.
- 2063 15 D. Senthil Raja and D.-H. Tsai, *Chemical Communications*, 2024.
- 2064 16 C. Lamiel, I. Hussain, H. Rabiee, O. R. Ogunsakin and K. Zhang, *Coord Chem Rev*,
2065 **2023**, **480**, 215030.
- 2066 17 L. Zhang and Y. Hou, *Adv Energy Mater*, 2023, **13**, 2204378.
- 2067 18 A. Mukherjee, J. A. Okolie, A. Abdelrasoul, C. Niu and A. K. Dalai, *Journal of*
2068 *Environmental Sciences*, 2019, **83**, 46–63.
- 2069 19 S. Ghosh, *Metal-organic frameworks (MOFs) for environmental applications*, 2019.
- 2070 20 S. Horike, S. Shimomura and S. Kitagawa, *Nat Chem*, 2009, **1**, 695–704.



- 2071 21 T. Ghanbari, F. Abnisa and W. M. A. Wan Daud, *Science of The Total Environment*,
 2072 2020, **707**, 135090. View Article Online
DOI: 10.1039/D4TA03877K
- 2073 22 Y. Zhao, Z. Song, X. Li, Q. Sun, N. Cheng, S. Lawes and X. Sun, *Energy Storage Mater*,
 2074 2016, **2**, 35–62.
- 2075 23 Y. Li, H. Xu, S. Ouyang and J. Ye, *Physical Chemistry Chemical Physics*, 2016, **18**,
 2076 7563–7572.
- 2077 24 H. Furukawa, K. E. Cordova, M. O’Keeffe and O. M. Yaghi, *Science (1979)*, ,
 2078 DOI:10.1126/science.1230444.
- 2079 25 F. Vega, M. Cano, S. Camino, L. M. G. Fernández, E. Portillo and B. Navarrete, *Carbon
 2080 Dioxide Chemistry, Capture and Oil Recovery*, , DOI:10.5772/INTECHOPEN.71443.
- 2081 26 M. Bui, C. S. Adjiman, A. Bardow, E. J. Anthony, A. Boston, S. Brown, P. S. Fennell,
 2082 S. Fuss, A. Galindo, L. A. Hackett, J. P. Hallett, H. J. Herzog, G. Jackson, J. Kemper, S.
 2083 Krevor, G. C. Maitland, M. Matuszewski, I. S. Metcalfe, C. Petit, G. Puxty, J. Reimer,
 2084 D. M. Reiner, E. S. Rubin, S. A. Scott, N. Shah, B. Smit, J. P. M. Trusler, P. Webley, J.
 2085 Wilcox and N. Mac Dowell, *Energy Environ Sci*, 2018, **11**, 1062–1176.
- 2086 27 J. J. Vericella, S. E. Baker, J. K. Stolaroff, E. B. Duoss, J. O. Hardin, J. Lewicki, E.
 2087 Glogowski, W. C. Floyd, C. A. Valdez, W. L. Smith, J. H. Satcher, W. L. Bourcier, C.
 2088 M. Spadaccini, J. A. Lewis and R. D. Aines, *Nat Commun*, 2015, **6**, 6124.
- 2089 28 A. I. Osman, M. Hefny, M. I. A. Abdel Maksoud, A. M. Elgarahy and D. W. Rooney,
 2090 *Environ Chem Lett*, 2021, **19**, 797–849.
- 2091 29 X. Li, X. Zhou, J. Wei, Y. Fan, L. Liao and H. Wang, *Sep Purif Technol*, 2021, **265**,
 2092 118481.
- 2093 30 M. Stec, A. Tatarczuk, L. Więclaw-Solny, A. Krótki, T. Spietz, A. Wilk and D. Śpiewak,
 2094 *Clean Technol Environ Policy*, 2016, **18**, 151–160.
- 2095 31 C. A. Grande, R. Blom, A. Spjelkavik, V. Moreau and J. Payet, *Sustainable Materials
 2096 and Technologies*, 2017, **14**, 11–18.
- 2097 32 Z. Zhang, Z.-Z. Yao, S. Xiang and B. Chen, *Energy Environ Sci*, 2014, **7**, 2868.
- 2098 33 N. Williams, R. C.-C. C. Journal and undefined 2019, *osti.gov* NJ Williams, R
 2099 *CustelceanCarbon Capture Journal*, 2019•*osti.gov*.
- 2100 34 Energy technologies Institute, *Reducing the cost of CCS developments in capture plant
 2101 technology*, 2016.
- 2102 35 S. Budinis, S. Krevor, N. Mac Dowell, N. Brandon and A. Hawkes, *Energy Strategy
 2103 Reviews*, 2018, **22**, 61–81.



- 2104 36 A. Andersen, S. Divekar, S. Dasgupta, J. H. Cavka, Aarti, A. Nanoti, A. Spjelkavik, A. View Article Online
DOI: 10.1039/D4TA03877K
2105 N. Goswami, M. O. Garg and R. Blom, *Energy Procedia*, 2013, **37**, 33–39.
- 2106 37 B. L. Huang, Z. Ni, A. Millward, A. J. H. McGaughey, C. Uher, M. Kaviany and O.
2107 Yaghi, *Int J Heat Mass Transf*, 2007, **50**, 405–411.
- 2108 38 N. Iqbal, X. Wang, J. Yu and B. Ding, *Adv Sustain Syst*, 2017, **1**, 1600028.
- 2109 39 Y. Lin, C. Kong, Q. Zhang and L. Chen, *Adv Energy Mater*, 2017, **7**, 1601296.
- 2110 40 H. R. Khan, Z. Jahan, M. B. Khan Niazi, T. Noor, H. Hou and S. Rafiq, *Carbon Capture
2111 Science & Technology*, 2022, **3**, 100048.
- 2112 41 P. M. Bhatt, Y. Belmabkhout, A. Cadiou, K. Adil, O. Shekhah, A. Shkurenko, L. J.
2113 Barbour and M. Eddaoudi, *J Am Chem Soc*, 2016, **138**, 9301–9307.
- 2114 42 L. Hu, W. Wu, L. Jiang, M. Hu, H. Zhu, L. Gong, J. Yang, D. Lin and K. Yang, *ACS
2115 Appl Mater Interfaces*, 2023, **15**, 43925–43932.
- 2116 43 G. Greene-Diniz, D. Z. Manrique, W. Sennane, Y. Magnin, E. Shishenina, P. Cordier, P.
2117 Llewellyn, M. Krompiec, M. J. Rančić and D. Muñoz Ramo, *EPJ Quantum Technol*,
2118 2022, **9**, 37.
- 2119 44 T. Zurrer, K. Wong, J. Horlyck, E. C. Lovell, J. Wright, N. M. Bedford, Z. Han, K. Liang,
2120 J. Scott and R. Amal, *Adv Funct Mater*, , DOI:10.1002/adfm.202007624.
- 2121 45 A. S. Palakkal and R. S. Pillai, *Sep Purif Technol*, 2022, **295**, 121298.
- 2122 46 L. Lei, Y. Cheng, C. Chen, M. Kosari, Z. Jiang and C. He, *J Colloid Interface Sci*, 2022,
2123 **612**, 132–145.
- 2124 47 H. An, W. Tian, X. Lu, H. Yuan, L. Yang, H. Zhang, H. Shen and H. Bai, *Chemical
2125 Engineering Journal*, 2023, **469**, 144052.
- 2126 48 T.-H. Bae, M. R. Hudson, J. A. Mason, W. L. Queen, J. J. Dutton, K. Sumida, K. J.
2127 Micklash, S. S. Kaye, C. M. Brown and J. R. Long, *Energy Environ. Sci.*, 2013, **6**, 128–
2128 138.
- 2129 49 D. Bahamon and L. F. Vega, *Chemical Engineering Journal*, 2016, **284**, 438–447.
- 2130 50 H. Li, K. Wang, Y. Sun, C. T. Lollar, J. Li and H.-C. Zhou, *Materials Today*, 2018, **21**,
2131 108–121.
- 2132 51 Y. He, W. Zhou, G. Qian and B. Chen, *Chem. Soc. Rev.*, 2014, **43**, 5657–5678.
- 2133 52 E. J. Kim, R. L. Siegelman, H. Z. H. Jiang, A. C. Forse, J.-H. Lee, J. D. Martell, P. J.
2134 Milner, J. M. Falkowski, J. B. Neaton, J. A. Reimer, S. C. Weston and J. R. Long, *Science
2135 (1979)*, 2020, **369**, 392–396.
- 2136 53 T. M. McDonald, J. A. Mason, X. Kong, E. D. Bloch, D. Gygi, A. Dani, V. Crocellà, F.
2137 Giordanino, S. O. Odoh, W. S. Drisdell, B. Vlasisavljevich, A. L. Dzubak, R. Poloni, S.



- 2138 K. Schnell, N. Planas, K. Lee, T. Pascal, L. F. Wan, D. Prendergast, J. B. Neaton, B. Smit, J. B. Kortright, L. Gagliardi, S. Bordiga, J. A. Reimer and J. R. Long, *Nature*, 2015, **519**, 303–308. View Article Online
DOI: 10.1039/D4TA03877K
- 2139
- 2140
- 2141 54 Y. Huang, W. Qin, Z. Li and Y. Li, *Dalton Transactions*, 2012, **41**, 9283.
- 2142 55 T. M. McDonald, W. R. Lee, J. A. Mason, B. M. Wiers, C. S. Hong and J. R. Long, *J Am Chem Soc*, 2012, **134**, 7056–7065.
- 2143
- 2144 56 P.-Q. Liao, X.-W. Chen, S.-Y. Liu, X.-Y. Li, Y.-T. Xu, M. Tang, Z. Rui, H. Ji, J.-P. Zhang and X.-M. Chen, *Chem Sci*, 2016, **7**, 6528–6533.
- 2145
- 2146 57 D. Saha, Z. Bao, F. Jia and S. Deng, *Environ Sci Technol*, 2010, **44**, 1820–1826.
- 2147 58 M. Mazaj, N. Z. Logar, E. Žagar and S. Kovačič, *J Mater Chem A Mater*, 2017, **5**, 1967–1971.
- 2148
- 2149 59 J. Liu, Y. Wang, A. I. Benin, P. Jakubczak, R. R. Willis and M. D. LeVan, *Langmuir*, 2010, **26**, 14301–14307.
- 2150
- 2151 60 G. W. Peterson, J. B. DeCoste, T. G. Glover, Y. Huang, H. Jasuja and K. S. Walton, *Microporous and Mesoporous Materials*, 2013, **179**, 48–53.
- 2152
- 2153 61 T. Asadi, M. R. Ehsani, A. M. Ribeiro, J. M. Loureiro and A. E. Rodrigues, *Chem Eng Technol*, 2013, **36**, 1231–1239.
- 2154
- 2155 62 Z. Hu, Y. Wang, B. B. Shah and D. Zhao, *Adv Sustain Syst*, , DOI:10.1002/adsu.201800080.
- 2156
- 2157 63 P. J. Milner, R. L. Siegelman, A. C. Forse, M. I. Gonzalez, T. Runčevski, J. D. Martell, J. A. Reimer and J. R. Long, *J Am Chem Soc*, 2017, **139**, 13541–13553.
- 2158
- 2159 64 V. H. Dalvi and P. J. Rossky, *Proceedings of the National Academy of Sciences*, 2010, **107**, 13603–13607.
- 2160
- 2161 65 A. H. Valekar, K.-H. Cho, U.-H. Lee, J. S. Lee, J. W. Yoon, Y. K. Hwang, S. G. Lee, S. J. Cho and J.-S. Chang, *RSC Adv*, 2017, **7**, 55767–55777.
- 2162
- 2163 66 R. Das, D. Muthukumar, R. S. Pillai and C. M. Nagaraja, *Chemistry – A European Journal*, 2020, **26**, 17445–17454.
- 2164
- 2165 67 J. Yan, Y. Sun, T. Ji, Y. Liu, N. Zhang, B. Sun, S. Meng, B. H. Yin, M. Wu, H. Hu and Y. Liu, *Ind Eng Chem Res*, 2023, **62**, 5973–5983.
- 2166
- 2167 68 M. R. Abdul Hamid, Y. Qian, R. Wei, Z. Li, Y. Pan, Z. Lai and H.-K. Jeong, *J Memb Sci*, 2021, **640**, 119802.
- 2168
- 2169 69 F. Yang, T. Ge, X. Zhu, J. Wu and R. Wang, *Sep Purif Technol*, 2022, **287**, 120535.
- 2170 70 J. M. Park, D. K. Yoo and S. H. Jhung, *Chemical Engineering Journal*, 2020, **402**, 126254.
- 2171



- 2172 71 Y. Liu, Z. Ng, E. A. Khan, H.-K. Jeong, C. Ching and Z. Lai, *Microporous and*
2173 *Mesoporous Materials*, 2009, **118**, 296–301. View Article Online
DOI: 10.1039/D4TA03877K
- 2174 72 C. R. Groom, I. J. Bruno, M. P. Lightfoot and S. C. Ward, *Acta Crystallogr B Struct Sci*
2175 *Cryst Eng Mater*, 2016, **72**, 171–179.
- 2176 73 S. Huang, X.-R. Shi, C. Sun, Z. Duan, P. Ma and S. Xu, *Nanomaterials*, 2020, **10**, 2268.
- 2177 74 S. Sundriyal, H. Kaur, S. K. Bhardwaj, S. Mishra, K.-H. Kim and A. Deep, *Coord Chem*
2178 *Rev*, 2018, **369**, 15–38.
- 2179 75 P. Forouzandeh, V. Kumaravel and S. C. Pillai, *Catalysts*, 2020, **10**, 969.
- 2180 76 A. C. Forse, C. Merlet, J. M. Griffin and C. P. Grey, *J Am Chem Soc*, 2016, **138**, 5731–
2181 5744.
- 2182 77 Y. Wu and C. Cao, *Sci China Mater*, 2018, **61**, 1517–1526.
- 2183 78 S. Kumar, G. Saeed, L. Zhu, K. N. Hui, N. H. Kim and J. H. Lee, *Chemical Engineering*
2184 *Journal*, 2021, **403**, 126352.
- 2185 79 J. Phiri, J. Dou, T. Vuorinen, P. A. C. Gane and T. C. Maloney, *ACS Omega*, 2019, **4**,
2186 18108–18117.
- 2187 80 L. Weinstein and R. Dash, *Materials Today*, 2013, **16**, 356–357.
- 2188 81 P. Pongprayoon and A. Chaimanatsakun, *Acta Mechanica Solida Sinica*, 2019, **32**, 81–
2189 92.
- 2190 82 A. Gitipour, A. El Badawy, M. Arambewela, B. Miller, K. Scheckel, M. Elk, H. Ryu, V.
2191 Gomez-Alvarez, J. Santo Domingo, S. Thiel and T. Tolaymat, *Environ Sci Technol*,
2192 2013, **47**, 14385–14393.
- 2193 83 L. Li, X. Wang, S. Wang, Z. Cao, Z. Wu, H. Wang, Y. Gao and J. Liu, *Electroanalysis*,
2194 2016, **28**, 243–248.
- 2195 84 M. Cossutta, V. Vretenar, T. A. Centeno, P. Kotrusz, J. McKechnie and S. J. Pickering,
2196 *J Clean Prod*, 2020, **242**, 118468.
- 2197 85 K. M. Ajay and M. N. Dinesh, *IOP Conf Ser Mater Sci Eng*, 2018, **310**, 012083.
- 2198 86 M. Karnan, A. G. K. Raj, K. Subramani, S. Santhoshkumar and M. Sathish, *Sustain*
2199 *Energy Fuels*, 2020, **4**, 3029–3041.
- 2200 87 S. Breitenbach, A. Lumetzberger, M. A. Hobisch, C. Unterweger, S. Spirk, D. Stifter, C.
2201 Fürst and A. W. Hassel, *C — Journal of Carbon Research*, 2020, **6**, 17.
- 2202 88 A. Arenillas, J. A. Menéndez, G. Reichenauer, A. Celzard, V. Fierro, F. J. Maldonado
2203 Hodar, E. Bailón-García and N. Job, 2019, pp. 1–26.
- 2204 89 Z. S. Iro, C. Subramani and S. S. Dash, *Int J Electrochem Sci*, 2016, **11**, 10628–10643.



- 2205 90 I. I. G. Inal, S. M. Holmes, E. Yagmur, N. Ermumcu, A. Banford and Z. Aktas, *Journal*
 2206 *of industrial and engineering chemistry*, 2018, **61**, 124–132. View Article Online
DOI:10.1039/D4TA03877K
- 2207 91 J. Chen, J. Xie, C. Q. Jia, C. Song, J. Hu and H. Li, *Chemical Engineering Journal*, 2022,
 2208 **450**, 137938.
- 2209 92 X. Li, Y. Tang, J. Song, W. Yang, M. Wang, C. Zhu, W. Zhao, J. Zheng and Y. Lin,
 2210 *Carbon N Y*, 2018, **129**, 236–244.
- 2211 93 F. Ma, S. Ding, H. Ren and Y. Liu, *RSC Adv*, 2019, **9**, 2474–2483.
- 2212 94 R. Mehdi, S. R. Naqvi, A. H. Khoja and R. Hussain, *Fuel*, 2023, **348**, 128529.
- 2213 95 S. Bhat, U. T. Uthappa, T. Sadhasivam, T. Altalhi, S. Soo Han and M. D. Kurkuri,
 2214 *Chemical Engineering Journal*, 2023, **459**, 141577.
- 2215 96 Y.-P. Gao, Z.-B. Zhai, K.-J. Huang and Y.-Y. Zhang, *New Journal of Chemistry*, 2017,
 2216 **41**, 11456–11470.
- 2217 97 G. Jiang and S. J. Pickering, *Waste Management*, 2016, **48**, 465–470.
- 2218 98 Q. Ke and J. Wang, *Journal of Materiomics*, 2016, **2**, 37–54.
- 2219 99 V. Ntuli, I. H.-S. A. J. of Science and undefined 2013, *journals.co.za V Ntuli, I*
 2220 *Hapazari South African Journal of Science*, 2013, *journals.co.za*, ,
 2221 DOI:10.1590/sajs.2013/1077.
- 2222 100 E. Glogic, A. K. Kamali, N. M. Keppetipola, B. Alonge, G. R. A. Kumara, G.
 2223 Sonnemann, T. Toupance and L. Cojocar, *ACS Sustain Chem Eng*, 2022, **10**, 15025–
 2224 15034.
- 2225 101 Z. Jiang, Y. Zou, Y. Li, F. Kong and D. Yang, *Biochar*, 2021, **3**, 701–714.
- 2226 102 V. Ruiz, C. Blanco, M. Granda and R. Santamaría, *Electrochim Acta*, 2008, **54**, 305–
 2227 310.
- 2228 103 C. Li, W. Wu, P. Wang, W. Zhou, J. Wang, Y. Chen, L. Fu, Y. Zhu, Y. Wu and W.
 2229 Huang, *Advanced Science*, 2019, **6**, 1801665.
- 2230 104 D. Dong and Y. Xiao, *Chemical Engineering Journal*, 2023, 144441.
- 2231 105 L. M. Grishchenko, G. G. Tsapyuk, M. Ricco, V. E. Diyuk, O. Yu. Boldyrieva, R.
 2232 Mariychuk, I. P. Matushko, D. Pontiroli, V. V. Lisnyak and S. Scaravonati, in *2020 IEEE*
 2233 *40th International Conference on Electronics and Nanotechnology (ELNANO)*, IEEE,
 2234 2020, pp. 173–177.
- 2235 106 F. Cheng, X. Yang, S. Zhang and W. Lu, *J Power Sources*, 2020, **450**, 227678.
- 2236 107 L.-H. Tseng, W.-C. Li and T.-C. Wen, *J Taiwan Inst Chem Eng*, 2023, **143**, 104684.
- 2237 108 G. Dhakal, D. R. Kumar, S. Sahoo and J.-J. Shim, *Carbon N Y*, 2023, **208**, 277–289.



- 2238 109 I. Bordun, V. Pohrebennyk, M. Sadowa, V. Ptashnyk, A. Klos-Witkowska and V. Martsenyuk, in *2017 9th IEEE International Conference on Intelligent Data Acquisition and Advanced Computing Systems: Technology and Applications (IDAACS)*, IEEE, 2017, pp. 86–90.
- 2242 110 F. R. Maria Sundar Raj, N. V. Jaya, G. Boopathi, D. Kalpana and A. Pandurangan, *Mater Chem Phys*, 2020, **240**, 122151.
- 2244 111 I. I. G. Inal, Y. Gokce and Z. Aktas, in *2016 IEEE International Conference on Renewable Energy Research and Applications (ICRERA)*, IEEE, 2016, pp. 458–462.
- 2246 112 M. A. Yahya, Z. Al-Qodah and C. W. Z. Ngah, *Renewable and Sustainable Energy Reviews*, 2015, **46**, 218–235.
- 2248 113 A. M. Al-Enizi, M. Ubaidullah, J. Ahmed, T. Ahamad, T. Ahmad, S. F. Shaikh and Mu. Naushad, *Compos B Eng*, 2020, **183**, 107655.
- 2250 114 M. K. Sahoo, P. Mane, B. Chakraborty and J. N. Behera, *Inorg Chem*, 2024, **63**, 6383–6395.
- 2252 115 B. Ramasubramanian, C. Chinglenthobai, X. Huiqing, N. Xiping, H. K. Hui, S. Valiyaveetil, S. Ramakrishna and V. Chellappan, *Surfaces and Interfaces*, 2022, **34**, 102397.
- 2255 116 S. Xiong, S. Jiang, J. Wang, H. Lin, M. Lin, S. Weng, S. Liu, Y. Jiao, Y. Xu and J. Chen, *Electrochim Acta*, 2020, **340**, 135956.
- 2257 117 M. Shaheen, M. Z. Iqbal, M. W. Khan, S. Siddique, S. Aftab and S. M. Wabaidur, *Energy & Fuels*, 2023, **37**, 4000–4009.
- 2259 118 F. Yi, R. Zhang, H. Wang, L. Chen, L. Han, H. Jiang and Q. Xu, *Small Methods*, , DOI:10.1002/smt.201700187.
- 2261 119 M. Gu, M. Wu, S.-C. Wang, C. Chen, D. Xiong and F.-Y. Yi, *Electrochim Acta*, 2020, **343**, 135617.
- 2263 120 N. Campagnol, R. Romero-Vara, W. Deleu, L. Stappers, K. Binnemans, D. E. De Vos and J. Fransaer, *ChemElectroChem*, 2014, **1**, 1182–1188.
- 2265 121 L. Wang, Y. Han, X. Feng, J. Zhou, P. Qi and B. Wang, *Coord Chem Rev*, 2016, **307**, 361–381.
- 2267 122 R. Ramachandran, W. Xuan, C. Zhao, X. Leng, D. Sun, D. Luo and F. Wang, *RSC Adv*, 2018, **8**, 3462–3469.
- 2269 123 D. Y. Lee, S. J. Yoon, N. K. Shrestha, S.-H. Lee, H. Ahn and S.-H. Han, *Microporous and Mesoporous Materials*, 2012, **153**, 163–165.
- 2271 124 Y. Tan, W. Zhang, Y. Gao, J. Wu and B. Tang, *RSC Adv*, 2015, **5**, 17601–17605.



- 2272 125 P. Kumar, B. Anand, Y. F. Tsang, K.-H. Kim, S. Khullar and B. Wang, *Environ Res*,
 2273 2019, **176**, 108488. View Article Online
DOI: 10.1039/D4TA03877K
- 2274 126 Y. Yan, P. Gu, S. Zheng, M. Zheng, H. Pang and H. Xue, *J Mater Chem A Mater*, 2016,
 2275 **4**, 19078–19085.
- 2276 127 J. Yang, P. Xiong, C. Zheng, H. Qiu and M. Wei, *J. Mater. Chem. A*, 2014, **2**, 16640–
 2277 16644.
- 2278 128 M. S. Rahmanifar, H. Hesari, A. Noori, M. Y. Masoomi, A. Morsali and M. F. Mousavi,
 2279 *Electrochim Acta*, 2018, **275**, 76–86.
- 2280 129 G. Li, H. Cai, X. Li, J. Zhang, D. Zhang, Y. Yang and J. Xiong, *ACS Appl Mater*
 2281 *Interfaces*, 2019, **11**, 37675–37684.
- 2282 130 Q. Yang, R. Song, Y. Wang, X. Hu, Z. Chen, Z. Li and W. Tan, *Colloids Surf A*
 2283 *Physicochem Eng Asp*, 2021, **631**, 127665.
- 2284 131 R. Sahoo, S. Ghosh, S. Chand, S. Chand Pal, T. Kuila and M. C. Das, *Compos B Eng*,
 2285 2022, **245**, 110174.
- 2286 132 Y.-L. Chang, M.-D. Tsai, C.-H. Shen, C.-W. Huang, Y.-C. Wang and C.-W. Kung,
 2287 *Materials Today Sustainability*, 2023, **23**, 100449.
- 2288 133 S. C. Wechsler and F. Z. Amir, *ChemSusChem*, 2020, **13**, 1491–1495.
- 2289 134 H. S. Kim, M. S. Kang and W. C. Yoo, *J Mater Chem A Mater*, 2019, **7**, 5561–5574.
- 2290 135 K. M. Choi, H. M. Jeong, J. H. Park, Y.-B. Zhang, J. K. Kang and O. M. Yaghi, *ACS*
 2291 *Nano*, 2014, **8**, 7451–7457.
- 2292 136 D. Sheberla, L. Sun, M. A. Blood-Forsythe, S. Er, C. R. Wade, C. K. Brozek, A. Aspuru-
 2293 Guzik and M. Dincă, *J Am Chem Soc*, 2014, **136**, 8859–8862.
- 2294 137 M. G. Campbell, D. Sheberla, S. F. Liu, T. M. Swager and M. Dincă, *Angewandte*
 2295 *Chemie International Edition*, 2015, **54**, 4349–4352.
- 2296 138 D. Feng, W. Sun and W. Hu, *Optical Switching and Networking*, 2018, **29**, 1–14.
- 2297 139 M. Sajid, *Environmental Science and Pollution Research*, 2016, **23**, 14805–14807.
- 2298 140 K. M. Choi, H. M. Jeong, J. H. Park, Y.-B. Zhang, J. K. Kang and O. M. Yaghi, *ACS*
 2299 *Nano*, 2014, **8**, 7451–7457.
- 2300 141 T. N. Tu, M. V Nguyen, H. L. Nguyen, B. Yulianto, K. E. Cordova and S. Demir, *Coord*
 2301 *Chem Rev*, 2018, **364**, 33–50.
- 2302 142 H. Luo, F. Cheng, L. Huelsenbeck and N. Smith, *J Environ Chem Eng*, 2021, **9**, 105159.
- 2303 143 M. Mon, R. Bruno, J. Ferrando-Soria, D. Armentano and E. Pardo, *J Mater Chem A*
 2304 *Mater*, 2018, **6**, 4912–4947.



- 2305 144 Y. Zhao, J. Peng, K. Chen, L. Luo, H. Chen, H. Zhang, S. Chou, X. Feng, W. Chen and
2306 R. Cao, *Sci China Chem*, 2023, **66**, 3154–3160. View Article Online
DOI: 10.1039/D4TA03877K
- 2307 145 Y. Fang, Y. Zeng, Q. Jin, X. F. Lu, D. Luan, X. Zhang and X. W. Lou, *Angewandte*
2308 *Chemie International Edition*, 2021, **60**, 8515–8520.
- 2309 146 J. Du, J. Chai, Q. Li, W. Zhang and B. Tang, *Colloids Surf A Physicochem Eng Asp*,
2310 2022, **632**, 127810.
- 2311 147 J.-G. Zhao, H.-Y. Zhou, Z. Hu, Y.-W. Wu, H. Jia and X.-M. Liu, *Rare Metals*, 2022, **41**,
2312 1504–1511.
- 2313 148 Y. Fang, D. Luan, Y. Chen, S. Gao and X. W. Lou, *Angewandte Chemie International*
2314 *Edition*, 2020, **59**, 2644–2648.
- 2315 149 S. Bibi, S. S. A. Shah, M. A. Nazir, M. H. Helal, S. M. El-Bahy, Z. M. El-Bahy, S. Ullah,
2316 M. A. Wattoo and A. ur Rehman, *Adv Sustain Syst*, 2024, 2400011.
- 2317 150 X.-Y. Dao, J.-H. Guo, Y.-P. Wei, F. Guo, Y. Liu and W.-Y. Sun, *Inorg Chem*, 2019, **58**,
2318 8517–8524.
- 2319 151 Y. Wang, Y. Pan, L. Zhu, H. Yu, B. Duan, R. Wang, Z. Zhang and S. Qiu, *Carbon N Y*,
2320 2019, **146**, 671–679.
- 2321 152 K.-S. Lin, A. K. Adhikari, C.-N. Ku, C.-L. Chiang and H. Kuo, *Int J Hydrogen Energy*,
2322 2012, **37**, 13865–13871.
- 2323 153 M. Y. Zorainy, M. G. Alalm, S. Kaliaguine and D. C. Boffito, *J Mater Chem A Mater*,
2324 2021, **9**, 22159–22217.
- 2325 154 Q. Zhao, W. Yuan, J. Liang and J. Li, *Int J Hydrogen Energy*, 2013, **38**, 13104–13109.
- 2326 155 Z. Yin, Y.-L. Zhou, M.-H. Zeng and M. Kurmoo, *Dalton Transactions*, 2015, **44**, 5258–
2327 5275.
- 2328 156 T.-H. Chen, I. Popov, W. Kaveevivitchai and O. Š. Miljanić, *Chemistry of Materials*,
2329 2014, **26**, 4322–4325.
- 2330 157 K.-S. Lin, A. K. Adhikari, C.-N. Ku, C.-L. Chiang and H. Kuo, *Int J Hydrogen Energy*,
2331 2012, **37**, 13865–13871.
- 2332 158 Z. Mai and D. Liu, *Cryst Growth Des*, 2019, **19**, 7439–7462.
- 2333 159 M. A. Mohamud and A. B. Yurtcan, *Int J Hydrogen Energy*, 2021, **46**, 33782–33800.
- 2334 160 S. Bibi, S. S. A. Shah, M. A. Nazir, M. H. Helal, S. M. El-Bahy, Z. M. El-Bahy, S. Ullah,
2335 M. A. Wattoo and A. ur Rehman, *Adv Sustain Syst*, 2024, 2400011.
- 2336 161 Z. Hu, Y. Peng, Z. Kang, Y. Qian and D. Zhao, *Inorg Chem*, 2015, **54**, 4862–4868.
- 2337 162 E. M. C. Morales, M. A. Méndez-Rojas, L. M. Torres-Martínez, L. F. Garay-Rodríguez,
2338 I. López, I. E. Uflyand and B. I. Kharisov, *Polyhedron*, 2021, **210**, 115517.



- 2339 163 S. Bibi, S. S. A. Shah, M. A. Nazir, M. H. Helal, S. M. El-Bahy, Z. M. El-Bahy, S. Ullah, M. A. Wattoo and A. ur Rehman, *Adv Sustain Syst*, 2024, 2400011. Article Online
DOI: 10.1039/D4TA03877K
- 2340
- 2341 164 A. Al Obeidli, H. Ben Salah, M. Al Murisi and R. Sabouni, *Int J Hydrogen Energy*, 2022,
- 2342 **47**, 2561–2593.
- 2343 165 M. Safaei, M. M. Foroughi, N. Ebrahimpoor, S. Jahani, A. Omid and M. Khatami, *TrAC*
- 2344 *Trends in Analytical Chemistry*, 2019, **118**, 401–425.
- 2345 166 A. FUJISHIMA and K. HONDA, *Nature*, 1972, **238**, 37–38.
- 2346 167 A. B. Djurišić, Y. He and A. M. C. Ng, *APL Mater*, , DOI:10.1063/1.5140497.
- 2347 168 S. R. Shanmugham, G. B. Jegadeesan and V. Ponnusami, in *Nanotechnology in the*
- 2348 *Beverage Industry*, Elsevier, 2020, pp. 25–49.
- 2349 169 A. Dhakshinamoorthy, Z. Li and H. Garcia, *Chem Soc Rev*, 2018, **47**, 8134–8172.
- 2350 170 M. Pawar, S. Topcu Sendoğdular and P. Gouma, *J Nanomater*, 2018, **2018**, 1–13.
- 2351 171 S. Peiris, H. B. de Silva, K. N. Ranasinghe, S. V. Bandara and I. R. Perera, *Journal of*
- 2352 *the Chinese Chemical Society*, 2021, **68**, 738–769.
- 2353 172 S.-N. Zhao, G. Wang, D. Poelman and P. Van Der Voort, *Molecules*, 2018, **23**, 2947.
- 2354 173 J. Moma and J. Baloyi, *Photocatalysts-Applications and Attributes*.
- 2355 174 S. Higashimoto, *Catalysts*, 2019, **9**, 201.
- 2356 175 Z. Li, S. Wang, J. Wu and W. Zhou, *Renewable and Sustainable Energy Reviews*, 2022,
- 2357 **156**, 111980.
- 2358 176 F. Li, G. Liu, F. Liu, J. Wu and S. Yang, *J Hazard Mater*, 2023, **452**, 131237.
- 2359 177 Y. Jin, W. Tang, J. Wang, F. Ren, Z. Chen, Z. Sun and P.-G. Ren, *J Alloys Compd*, 2023,
- 2360 **932**, 167627.
- 2361 178 A. Meng, L. Zhang, B. Cheng and J. Yu, *Advanced Materials*, ,
- 2362 DOI:10.1002/adma.201807660.
- 2363 179 S.-Y. Lee and S.-J. Park, *Journal of Industrial and Engineering Chemistry*, 2013, **19**,
- 2364 1761–1769.
- 2365 180 S. Higashimoto, *Catalysts*, 2019, **9**, 201.
- 2366 181 X. Chen, S. Shen, L. Guo and S. S. Mao, *Chem Rev*, 2010, **110**, 6503–6570.
- 2367 182 M. Skocaj, M. Filipic, J. Petkovic and S. Novak, *Radiol Oncol*, , DOI:10.2478/v10019-
- 2368 011-0037-0.
- 2369 183 F. Wu, Z. Zhou and A. L. Hicks, *Environ Sci Technol*, 2019, **53**, 4078–4087.
- 2370 184 A.-I. Gopalan, J.-C. Lee, G. Saianand, K.-P. Lee, W.-Y. Chun, Y. Hou, V. Kannan, S.-
- 2371 S. Park and W.-J. Kim, *Materials*, 2020, **13**, 5072.



- 2372 185 T. Sansenya, N. Masri, T. Chankhanittha, T. Senasu, J. Piriyanon, S. Mukdasai and S. Nanan, *Journal of Physics and Chemistry of Solids*, 2022, **160**, 110353.
- 2373
- 2374 186 T. Chankhanittha, N. Komchoo, T. Senasu, J. Piriyanon, S. Youngme, K. Hemavibool and S. Nanan, *Colloids Surf A Physicochem Eng Asp*, 2021, **626**, 127034.
- 2375
- 2376 187 D. Kim and K. Yong, *Appl Catal B*, 2021, **282**, 119538.
- 2377 188 Z. Li, R. Li, H. Jing, J. Xiao, H. Xie, F. Hong, N. Ta, X. Zhang, J. Zhu and C. Li, *Nat Catal*, 2023, **6**, 80–88.
- 2378
- 2379 189 N. A. F. Al-Rawashdeh, O. Allabadi and M. T. Aljarrah, *ACS Omega*, 2020, **5**, 28046–28055.
- 2380
- 2381 190 K. Chaudhary, M. Aadil, S. Zulfiqar, S. Ullah, S. Haider, P. O. Agboola, M. F. Warsi and I. Shakir, *Fullerenes, Nanotubes and Carbon Nanostructures*, 2021, **29**, 915–928.
- 2382
- 2383 191 A. Alshammari, Z. Jiang and K. E. Cordova, in *Semiconductor Photocatalysis - Materials, Mechanisms and Applications*, InTech, 2016.
- 2384
- 2385 192 V. García-Salcido, P. Mercado-Oliva, J. L. Guzmán-Mar, B. I. Kharisov and L. Hinojosa-Reyes, *J Solid State Chem*, 2022, **307**, 122801.
- 2386
- 2387 193 Y. Gao, X.-H. Yi, C.-C. Wang, F. Wang and P. Wang, *Mater Res Bull*, 2023, **158**, 112072.
- 2388
- 2389 194 C. Jing, Y. Zhang, J. Zheng, S. Ge, J. Lin, D. Pan, N. Naik and Z. Guo, *Particuology*, 2022, **69**, 111–122.
- 2390
- 2391 195 H. Sepehrmansourie, H. Alamgholiloo, N. Noroozi Pesyan and M. A. Zolfigol, *Appl Catal B*, 2023, **321**, 122082.
- 2392
- 2393 196 L. Wang, P. Jin, S. Duan, H. She, J. Huang and Q. Wang, *Sci Bull (Beijing)*, 2019, **64**, 926–933.
- 2394
- 2395 197 M. Xu, C. Sun, X. Zhao, H. Jiang, H. Wang and P. Huo, *Appl Surf Sci*, 2022, **576**, 151792.
- 2396
- 2397 198 F. Drache, V. Bon, I. Senkovska, C. Marschelke, A. Synytska and S. Kaskel, *Inorg Chem*, 2016, **55**, 7206–7213.
- 2398
- 2399 199 A. J. Howarth, Y. Liu, P. Li, Z. Li, T. C. Wang, J. T. Hupp and O. K. Farha, *Nat Rev Mater*, 2016, **1**, 15018.
- 2400
- 2401 200 G. Paille, M. Gomez-Mingot, C. Roch-Marchal, B. Lassalle-Kaiser, P. Mialane, M. Fontecave, C. Mellot-Draznieks and A. Dolbecq, *J Am Chem Soc*, 2018, **140**, 3613–3618.
- 2402
- 2403
- 2404 201 S. S. A. Shah, M. A. Nazir, K. Khan, I. Hussain, M. Tayyab, S. S. Alarfaji, A. M. Hassan, M. Sohail, M. S. Javed and T. Najam, *J Energy Storage*, 2024, **75**, 109725.
- 2405



- 2406 202 D. Crawford, J. Casaban, R. Haydon, N. Giri, T. McNally and S. L. James, *Chem Sci*,
 2407 2015, **6**, 1645–1649. View Article Online
DOI: 10.1039/D4TA03877K
- 2408 203 J. C. Glier and E. S. Rubin, *Energy Procedia*, 2013, **37**, 65–72.
- 2409 204 M. Karnan, A. G. K. Raj, K. Subramani, S. Santhoshkumar and M. Sathish, *Sustain
 2410 Energy Fuels*, 2020, **4**, 3029–3041.
- 2411 205 J. Moma and J. Baloyi, in *Photocatalysts - Applications and Attributes*, IntechOpen,
 2412 2019.
- 2413 206 S.-N. Zhao, G. Wang, D. Poelman and P. Van Der Voort, *Molecules*, 2018, **23**, 2947.
- 2414 207 R. Asahi, T. Morikawa, T. Ohwaki, K. Aoki and Y. Taga, *Science (1979)*, 2001, **293**,
 2415 269–271.
- 2416 208 H. Demir, G. O. Aksu, H. C. Gulbalkan and S. Keskin, *Carbon Capture Science and
 2417 Technology*, , DOI:10.1016/j.ccst.2021.100026.
- 2418 209 S. Ali, P. M. Ismail, F. Wahid, A. Kumar, M. Haneef, F. Raziq, S. Ali, M. Javed, R. U.
 2419 Khan and X. Wu, *Fuel Processing Technology*, 2022, **236**, 107427.
- 2420 210 S. Ali, P. M. Ismail, M. Humayun, M. Bououdina and L. Qiao, *Fuel Processing
 2421 Technology*, 2024, **255**, 108049.
- 2422 211 M. Khan, Z. Akmal, M. Tayyab, S. Mansoor, A. Zeb, Z. Ye, J. Zhang, S. Wu and L.
 2423 Wang, *Carbon Capture Science and Technology*, , DOI:10.1016/j.ccst.2024.100191.
- 2424 212 P. Dubey, V. Shrivastav, P. H. Maheshwari, M. Hołdyński, A. Krawczyńska and S.
 2425 Sundriyal, *J Energy Storage*, , DOI:10.1016/j.est.2023.107828.
- 2426 213 Y. Cao, W. Yang, M. Wang, N. Wu, L. Zhang, Q. Guan and H. Guo, *Int J Hydrogen
 2427 Energy*, 2021, **46**, 18179–18206.
- 2428 214 J. Khan, A. Khan, B. Rubab, F. Jamshaid, A. A. Al-Kahtani and A. Dahshan, *Appl Mater
 2429 Today*, 2023, **34**, 101906.
- 2430 215 C. Healy, K. M. Patil, B. H. Wilson, L. Hermanspahn, N. C. Harvey-Reid, B. I. Howard,
 2431 C. Kleinjan, J. Kolien, F. Payet and S. G. Telfer, *Coord Chem Rev*, 2020, **419**, 213388.
- 2432 216 S. Bhattacharyya and T. K. Maji, *Coord Chem Rev*, 2022, **469**, 214645.
- 2433 217 Q. He, F. Zhan, H. Wang, W. Xu, H. Wang and L. Chen, *Materials Today Sustainability*,
 2434 2022, **17**, 100104.
- 2435 218 D. Chakraborty, A. Yurdusen, G. Mouchaham, F. Nouar and C. Serre, *Adv Funct Mater*,
 2436 2023, 2309089.
- 2437 219 D. Yang and B. C. Gates, *ACS Catal*, 2019, **9**, 1779–1798.
- 2438 220 W. Xue, C. D. Sewell, Q. Zhou and Z. Lin, *Angewandte Chemie International Edition*,
 2439 2022, **61**, e202206512.



- 2440 221 R. Freund, O. Zaremba, G. Arnauts, R. Ameloot, G. Skorupskii, M. Dincă, A. Bavykina, J. Gascon, A. Ejsmont and J. Goscianska, *Angewandte Chemie International Edition*, 2021, **60**, 23975–24001.
- 2443 222 A. Bavykina, N. Kolobov, I. S. Khan, J. A. Bau, A. Ramirez and J. Gascon, *Chem Rev*, 2020, **120**, 8468–8535.
- 2445 223 P. Falcaro, R. Ricco, C. M. Doherty, K. Liang, A. J. Hill and M. J. Styles, *Chem Soc Rev*, 2014, **43**, 5513–5560.
- 2447 224 E.-S. M. El-Sayed and D. Yuan, *Green Chemistry*, 2020, **22**, 4082–4104.
- 2448 225 X. Song, Y. Wang, C. Wang, D. Wang, G. Zhuang, K. O. Kirlikovali, P. Li and O. K. Farha, *J Am Chem Soc*, 2022, **144**, 10663–10687.

View Article Online
DOI: 10.1039/D4TA03877K



Data availability statement

The data that support the findings of this study are available from the corresponding author, upon reasonable request.

